Master's thesis

NTNU
Norwegian University of Science and Technology
Faculty of Natural Sciences
Department of Chemical Engineering

Anders Runningen

Fischer-Tropsch reaction kinetics: Mathematical modeling and model fitting

Master's thesis in Chemical Engineering and Biotechnology
Supervisor: Magne Hillestad, IKP and Erling Rytter, IKP
June 2019

NTNU
Norwegian University of
Science and Technology

Anders Runningen

Fischer-Tropsch reaction kinetics: Mathematical modeling and model fitting

Master's thesis in Chemical Engineering and Biotechnology
Supervisor: Magne Hillestad, IKP and Erling Rytter, IKP
June 2019

Norwegian University of Science and Technology
Faculty of Natural Sciences
Department of Chemical Engineering

Preface

This thesis is written as part of the course 'TKP4900 - Chemical Process Technology, Master's Thesis' and is a continuation of a previous project carried out by the same author in the fall of 2018. The thesis work was carried out over a time period of 20 weeks and culminates in this final thesis report where the results of the work done are presented. All work in this thesis was carried out at the Department of Chemical Engineering at the Norwegian University of Science and Technology (NTNU).

Firstly, I would like to extend my sincere gratitude to my supervisors, professor Magne Hillestad and adjunct professor Erling Rytter, whose guidance and mentoring have been invaluable, and whose vast knowledge have been admirable.
I would also like to thank professor Edd Anders Blekkan, post-doc Ljubisa Gavrilovic, and master student Erik Andreas Jørgensen for great discussions, and for sharing their experimental results with me, allowing for a deeper understanding of the proposed model. Thanks to research scientist Kumar R. Rout, post-doc Koteswara Rao Putta, and Ph.D. candidate Umesh Pandey for insightful discussions and suggestions in my work.
Lastly, I would like to thank friends and family for their continued encouragement and support throughout all the years.

Abstract

In this thesis, a model for the Fischer-Tropsch synthesis is proposed, including the effects of water on reaction kinetics, product selectivities, and catalyst deactivation. The proposed model is based on the consorted vinylene mechanism [1]. Four catalysts with different catalyst characterizations were considered; three corresponding to three different Co/Re/γ-Al_2O_3 catalysts, and one corresponding to a Co/Re/α-Al_2O_3 catalyst. These catalysts were considered at P = 20 bar, T = 210 °C, and H_2/CO = 2.1. Additionally, a commercial type catalyst was also considered at P = 20-22 bar, T = 210 °C, and H_2/CO = 1.12, 1.72, and 2.1.

It is concluded that the proposed model is quite capable of describing the main responses of the system. However, particularly for the commercial type catalyst, a methane formation model where the partial pressure of water is actively a part of the model seems to explain the CH_4-selectivities better, as such suggesting that the effect of water is kinetic by nature. A second order deactivation model including the partial pressure of water was found to adequately describe the catalyst deactivation over time. The model also accounts for the expected effect of water, namely that water increases the catalyst deactivation. By studying how different catalyst characterizations affect the estimated model parameters, it was observed that most model parameters follow linear trends when plotted as functions of the cobalt dispersion. The proposed chain growth model was found to explain the C_{5+}-selectivities very well, and is also able to correctly account for the effect of water on the responses. Interestingly, the chain growth model does not include the partial pressure of hydrogen.

Sammendrag

I denne masteroppgaven er en matematisk modell for Fischer-Tropsch syntesen foreslått. Modellen inkluderer effektene av vann på reaksjonskinetikk, selektiviteter, og deaktivering av katalysator. Modellen er basert på 'consorted vinylene'-mekanismen. Fire katalysatorer med ulike karakteriseringer ble testet; tre av katalysatorene svarer til tre ulike $Co/Re/\gamma$-Al_2O_3 katalysatorer, og den fjerde svarer til en $Co/Re/\alpha$-Al_2O_3 katalysator. Disse katalysatorene ble testet ved P = 20 bar, T = 210 °C, og H_2/CO = 2.1. Videre ble en kommersiell katalysator også testet ved P = 22-22 bar, T = 210 °C, og H_2/CO = 1.12, 1.72, og 2.1.

Det konkluderes at den foreslåtte modellen klarer å beskrive hovedresponsene generelt veldig bra. Spesielt for den kommersielle katalysatoren ble metanselektivitetene i perioder hvor vann tilsettes bedre forklart med en modell for metandannelsen der vann er en aktiv del av dannelsesuttrykket. En andre ordens deaktiveringsmodell som inkluderer effekten av vann ble funnet til å beskrive katalysatorens deaktivering over tid på en tilfredsstillende måte. Modellen beskriver også den forventede effekten av vann, nærmere bestemt at vann øker katalysatorens deaktivering. Ved å studere hvordan ulike katalysator karakteriseringer påvirker de estimerte modellparameterne ble det observert at de fleste parameterne følger lineære trender når de plottes mot kobalt dispersjonene til katalysatorene. Den foreslåtte modellen for kjedevekst beskriver selektiviteten til C_{5+} veldig bra, og modellen fanger også opp effekten av vann på riktig måte. Denne kjedevekstmodellen inkluderer ikke partialtrykket av hydrogen.

Table of Content

List of Figures

List of Tables

List of Abbreviations

FTS	Fischer-Tropsch synthesis
BTL	Biomass-to-liquid
ASF	Anderson-Schultz-Flory
LHHW	Langmuir-Hinshelwood-Hougen-Watson
FBR	Fixed bed reactor
WGS	Water-gas shift
PFR	Plug flow reactor
ODR	Orthogonal distance regression
MSE	Mean squared error
TOS	Time on stream
CSTR	Continuously stirred tank reactor

1 Introduction

This thesis is a continuation of a previous project by the same author where a model for the Fischer-Tropsch kinetics and product selectivities was proposed. The basis for this project is the model obtained in that project, and the goal of this thesis is to improve the performance of the model.

The Fischer-Tropsch synthesis (FTS) is a complex synthesis in which a wide range of linear hydrocarbons [2], in the form of paraffins and olefins, are produced from a synthesis gas (syngas), consisting of CO and H_2 [3, 4]. Other products in the Fischer-Tropsch synthesis include oxygenated products such as alcohols and carbonyls, although these particular products are often neglected as only small amounts are produced [3, 5, 6, 7].

Over the recent years, the world's dependency on fossil fuels, a non-renewable fuel source, and the resulting climate changes by global warming, have been motivating the world toward finding better, more environmentally friendly options to replace the fossil fuels [4, 8, 9]. One such viable replacement has been identified to be biomass, and this has sparked a new-found interest in the Fischer-Tropsch synthesis. Using biomass as a way of producing liquid fuels is attractive as the emissions (measured in carbon) related to converting biomass is about equal to the amount of carbon taken up producing the biomass, assuming that the biomass is produced in a sustainable manner [10]. Further, the availability of biomass derived from different sources worldwide [10, 11], paired with the fact that the FTS does not discriminate against the quality of the biomass from which the synthesis gas is produced, as long as the synthesis gas is free of any impurities [4], makes biomass-to-liquid fuels (BTL) through the FTS a viable option.

Before such a biomass-to-liquid fuels plant using the Fischer-Tropsch synthesis can be built, it is critical to simulate the process to design and optimize the plant, as well as carrying out an economic analysis. Saxena identifies that this is problematic without a proper kinetic model available [12, 13]. A model describing the product selectivities will also be of significant importance. Proper models for the reaction kinetics and product selectivities must be capable of predicting the reaction rates as well as the product selectivities with varying operating conditions, such as temperature, pressure, inlet H_2/CO-ratio, and addition of water to the feed flow [14, 15, 16].
Additionally, it is well known that the type of catalyst and support used in the Fischer-Tropsch synthesis will have a profound effect on the kinetics and

product selectivities [4, 13, 17]. Commercially, Co or Fe catalysts are used, and certain promoters, such as Pt or Re, are added to improve the performance of the catalyst [18].
In the literature, several different kinetic models have been proposed for various commercially-used catalysts. Ma et al. [19], and Ostadi et al. [14], both present several kinetic models proposed for Co catalysts. Although several kinetic models have been proposed by various authors, no consensus regarding one particular FTS kinetic model has been reached as of today [19].

Today, the effect of water on the Fischer-Tropsch product selectivities is well understood, and a consensus has been reached, at least for one particular type of catalyst [14, 18, 19, 20, 21]; for Co catalysts, the selectivity of higher hydrocarbons, C_{5+}, increases as water is added or indigenous water is produced in the synthesis, while the selectivity of CH_4 is decreasing under the same conditions. Further, in a paper by Rytter et al. [18] it is also observed that, for Co catalysts, water will impact the kinetics of the FTS, though the effect can be positive or negative depending on the characterization of the catalyst. Specifically, the pore size distribution is identified to influence the performance of the catalyst [18].
Another important effect that should be taken into account when developing a kinetic model is catalyst deactivation. Catalyst deactivation is an inevitability and causes difficulties when carrying out kinetic studies [19]. In the literature, several mechanisms for Co catalyst deactivation have been put forth, including sintering of cobalt crystallites, poisoning from sulphur and nitrogen compounds, and re-oxidation of the cobalt metal [21, 22, 23, 24]. Rytter et al. [18] also report that water causes significant deactivation of the catalyst. Here, it is believed that the addition of water enhances the effect of sintering.
As the effects of water on selectivities, kinetics, and catalyst deactivation are as profound as they are, it is important that these effects are properly accounted for in an eventual model.

This thesis aims to obtain a consistent model capable of predicting the reaction rates and product selectivities of the Fischer-Tropsch synthesis over Co catalysts. The obtained model should also be able to accurately account for the effect of water on reaction rates and selectivities, as well as on deactivation. Catalysts with different characterizations are considered to also study how the pore sizes impact the estimated parameters in the model. The water-gas shift reaction is also to be included in the model to account for the (typically small) production of CO_2 observed experimentally.

2 Theory

The Fischer-Tropsch synthesis (FTS) is a polymerization reaction converting synthesis gas made up of H_2 and CO, to linear hydrocarbons mainly in the form of paraffins and olefins [2, 25]. The polymerization reaction occurs as CH_x-monomers are inserted into the growing carbon chain in a stepwise fashion [15, 26]. At every step in the chain growth, there is a probability, denoted α, that the monomer is incorporated and thus allowing the chain to grow. However, at every step, there is also the possibility that the chain will terminate to form the final product [15]. The chain growth propagation probability, α, is described in Section 2.1. It is commonly believed that primarily olefins are produced, but that through readsorption and secondary reactions, the olefins are hydrogenated to paraffins [1]. Further, it is believed that longer hydrocarbons have a greater chance of hydrogenation than shorter hydrocarbons [27].
The growth process in the Fischer-Tropsch synthesis is illustrated in Figure 2.1 below.

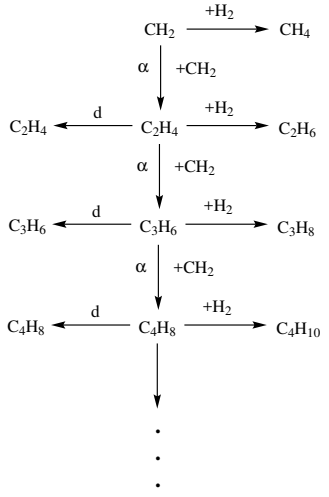

Figure 2.1: Illustration of the stepwise chain growth in the Fischer-Tropsch synthesis. It is to be pointed out that this illustration is not implying a specific chemical mechanism. The illustration is adapted from Dry [15] with permission from Elsevier.

For modeling purposes, as the main products of the Fischer-Tropsch synthesis are linear paraffins and olefins, the synthesis can be described by two different net reactions. Each net reaction will, in this case, have its own chain growth factor to describe the product distributions. The two net reactions describing the Fisher-Tropsch synthesis are shown in Equation (2.1) and Equation (2.2) below [5].

$$\mathrm{CO} + \mathrm{U_1H_2} \xrightarrow{r_1} \sum_{i=1}^{\infty} \nu_{i,1}\mathrm{C}_i\mathrm{H}_{2i+2} + \mathrm{H_2O} \tag{2.1}$$

$$\mathrm{CO} + \mathrm{U_2H_2} \xrightarrow{r_2} \nu_{1,2}\mathrm{CH_4} + \sum_{i=2}^{\infty} \nu_{i,2}\mathrm{C}_i\mathrm{H}_{2i} + \mathrm{H_2O} \tag{2.2}$$

Here, $\mathrm{U_1}$ and $\mathrm{U_2}$ are the stoichiometric coefficient for the hydrogen consumptions, while $\nu_{i,1}$ and $\nu_{i,2}$ are the stoichiometric coefficients for the paraffin and olefin products, respectively.

2.1 Fischer-Tropsch product distribution

The parameter α, as introduced in the beginning of Section 2, is called the *chain growth propagation probability*. It describes the rate at which the carbon chain is propagating relative to the total turnover rate of the chain [28]. In general, the chain growth propagation probability can be defined as shown in Equation (2.3) below [29],

$$\alpha = \frac{r_{p,n}}{r_{p,n} + r_{t,n}} \tag{2.3}$$

where $r_{p,n}$ is the rate of propagation, and $r_{t,n}$ is the rate of termination. As indicated in Equation (2.3), the rate of propagation and termination can be dependent on the chain length [28].

As the Fischer-Tropsch synthesis is a polymerization reaction where a $\mathrm{CH_x}$-monomer is added to a growing hydrocarbon chain, a product distribution can be used to predict the selectivities of various products based on α and the chain length, n [7, 30, 31]. Assuming that α is independent of the chain length, the product distribution can be calculated according to the Anderson-Schultz-Flory (ASF) distribution [30, 32],

$$y_n = (1-\alpha)\alpha^{n-1} \tag{2.4}$$

where y_n is the molar fraction of a hydrocarbon with chain length n.
Alternatively, the ASF distribution can be expressed in terms of a mass fraction, as shown in Equation (2.5) below [33, 34].

$$\frac{\omega_n}{n} = (1-\alpha)^2 \alpha^{n-1} \tag{2.5}$$

Experimentally, it is observed that the Fischer-Tropsch product distribution generally follows an ideal ASF distribution for paraffins and olefins separately [30]. Further, by considering the distribution of the total hydrocarbons, it can be observed that, seemingly, the product distribution is a linear combination of two distributions [3, 5, 27, 30]. Additionally, some deviations from the ideal ASF distributions are also to be noted. Specifically, it is observed a higher-than-expected production of methane, and a lower-than-expected production of ethene [30]. The individual distributions of paraffins and olefins, as well as the total hydrocarbon distribution, are illustrated (for constant values of α) in Figure 2.2 shown below.

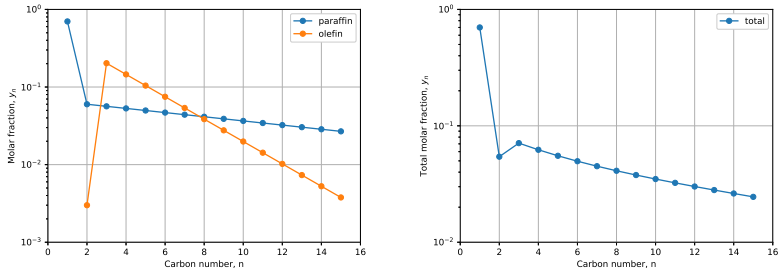

(a) Illustration of the product distributions of paraffin and olefin products.

(b) Illustration of the total product distribution in the Fischer-Tropsch synthesis.

Figure 2.2: Illustration of the Fischer-Tropsch product distributions. Two values of α are used; $\alpha_1 = 0.94$ for the paraffins, and $\alpha_2 = 0.72$ for the olefins.

Though there are still uncertainties regarding the specifics, the deviations from the ideal ASF behavior are mainly attributed to secondary reactions taking place. Some of the proposed secondary reactions include separate methane

formation pathways [30], hydrogenolytic cleavage of olefins, or olefins initiating new chains [3].

2.1.1 Fischer-Tropsch stoichiometry

Using the chain growth propagation probability as described Section 2.1, and choosing CO as the key component, the stoichiometric coefficients for the products must be defined according to the ASF distribution in the following way:

$$\nu_{i,1} = (1-\alpha_1)^2 \alpha_1^{i-1} \tag{2.6}$$

$$\nu_{i,2} = (1-\alpha_2)^2 \alpha_2^{i-1} \tag{2.7}$$

where α_1 and α_2 are the chain growth propagation probabilities for the paraffins and the olefins, respectively.
By defining the stoichiometric coefficients as in Equation (2.6) and Equation (2.7), the reactions are balanced, as the following will hold true [5]:

$$\sum_{i=1}^{\infty} i \cdot \nu_{i,1} = \sum_{i=1}^{\infty} i \cdot \nu_{i,2} = 1 \tag{2.8}$$

Now, it is also possible to define the stoichiometric coefficients for hydrogen, U_1 and U_2, in Equation (2.1) and Equation (2.2) using Equation (2.6) and Equation (2.7) [5].

$$U_1 = 1 + \sum_{i=1}^{\infty} \nu_{i,1}(i+1) = 3 - \alpha_1 \tag{2.9}$$

$$U_2 = 1 + 2\nu_{1,2} + \sum_{i=2}^{\infty} \nu_{i,2} \cdot i = (1-\alpha_2)^2 + 2 \tag{2.10}$$

2.2 Component lumping

While the product distribution accounts for an infinite number of products, a model must consider a finite number of components due to limiting computational power. A way to overcome this hindrance is to introduce lumping of components. For a lumped component, it will be necessary to be able to calculate the stoichiometric coefficient, along with the average carbon number of the lump [5].

Consider a lumped component with carbon atoms in the closed interval of N to M. The molar fraction of the lump is calculated according to Equation (2.11).

$$y_{[N,M]} = \sum_{i=N}^{M} (1-\alpha) \cdot \alpha^{i-1} = y_{[1,M]} - y_{[1,N-1]} = \alpha^{N-1} - \alpha^{M} \tag{2.11}$$

The stoichiometric coefficient of a lumped component, in the same interval as above, can be calculated according to Equation (2.12) by using the stoichiometric coefficients of the products as defined by Equation (2.6) and Equation (2.7).

$$\nu_{[N,M]} = \sum_{i=N}^{M} \nu_i = (1-\alpha)(\alpha^{N-1} - \alpha^{M}) \tag{2.12}$$

Further, the average carbon number of a lumped component with carbon atoms in the closed interval of N to M is calculated as shown in Equation (2.13) below [5].

$$\begin{aligned} \bar{n}_{n,[N,M]} &= \frac{\sum_{i=N}^{M} i \cdot \alpha^{i-1}}{\sum_{i=N}^{M} \alpha^{i-1}} \\ &= \frac{N\alpha^{N-1} - (N-1)\alpha^{N} - (M+1)\alpha^{M} + M\alpha^{M+1}}{(1-\alpha)(\alpha^{N-1} - \alpha^{M})} \end{aligned} \tag{2.13}$$

Furthermore, the weight average carbon number of the same lumped component is calculated according to Equation (2.14) [5].

$$\bar{n}_{w,[N,M]} = \frac{\sum_{i=N}^{M} i^2 \cdot \alpha^{i-1}}{\sum_{i=N}^{M} i \cdot \alpha^{i-1}} \tag{2.14}$$

2.3 Fischer-Tropsch kinetic model

As described earlier, the two main chemical reactions in consideration are shown in Equation (2.1) and Equation (2.2). Describing the reactions rates accurately will be critical for the development of a kinetic model of the synthesis. Additionally, it will be important to model the chain growth propagation probabilities, as well as to account for the non-ASF behavior of the FTS.

2.3.1 Modeling the reaction rates

In the literature, several different kinetic expressions for the Fischer-Tropsch synthesis have been proposed [2, 14, 19]. While there are some structural differences between the various expressions, and different coefficients, several of them are based on the Langmuir-Hinshelwood-Hougen-Watson (LHHW) adsorption theory [35, 36, 37], and generally, have a structure as shown in Equation (2.15) below,

$$r_1 = \frac{k(T)P_{\mathrm{CO}}^{a}P_{\mathrm{H_2}}^{b}}{\left(1 + K_1 P_{\mathrm{CO}}\right)^2} \tag{2.15}$$

where a and b are empirical exponents fitted to experimental data.
Yates and Satterfield [35] propose $a = b = 1.0$, Zennaro et al. [38] propose $a = 0.74, b = 1.0$, and Mansouri et al. [39] propose $a = 1.0, b = 0$.
It should be noted that while it is generally understood that water will affect the reaction rate of the synthesis, most proposed kinetic expressions are not including this effect.

In a recent paper, Rytter et al. [1] propose the consorted vinylene mechanism encompassing water assisted CO-activation for the Fischer-Tropsch synthesis over Co catalysts. Here, a kinetic expression is derived for the proposed mechanism. For the purposes of this thesis, the final kinetic expression is shown in Equation (2.16) below, though the derivation is left out.

$$r_1 = \frac{k_1(T)P_{\mathrm{CO}}P_{\mathrm{H_2}}^{0.5}P_{\mathrm{H_2O}}}{\left(1 + aP_{\mathrm{CO}} + bP_{\mathrm{H_2}}^{0.5} + cP_{\mathrm{CO}}P_{\mathrm{H_2}}^{0.5} + dP_{\mathrm{CO}}P_{\mathrm{H_2O}} + eP_{\mathrm{H_2O}}/P_{\mathrm{H_2}}^{0.5} + fP_{\mathrm{H_2O}}\right)^2} \tag{2.16}$$

a, b, c, d, e, and f correspond to the coverage of the various surface species. As these coefficients are functions of equilibrium and rate constants, they are expected to be positive. To reduce the complexity of the model, it can be assumed the surface sites on the catalyst are primarily occupied by CO, H_2, and H_2O, namely the main components. This reduces the kinetic expression to the following:

$$r_1 = \frac{k_1(T)P_{\mathrm{CO}}P_{\mathrm{H_2}}^{0.5}P_{\mathrm{H_2O}}}{\left(1 + aP_{\mathrm{CO}} + bP_{\mathrm{H_2}}^{0.5} + fP_{\mathrm{H_2O}}\right)^2} \tag{2.17}$$

From a modeling perspective, the kinetic expression in Equation (2.17) proposes one potential issue, namely that the synthesis gas must contain water in order to initiate the reaction. To circumvent this problem, a modification can be made to the model, similarly to what was done for Temkin-Pyzhev rate expression for

the ammonia synthesis [40, 41]. The modified kinetic expression for the FTS is obtained by replacing the partial pressure of water in the numerator with the factor $(1 + gP_{\mathrm{H_2O}})$ in Equation (2.17). The newly obtained kinetic expression is shown in Equation (2.18) below.

$$r_1 = \frac{k_1'(T)P_{\mathrm{CO}}P_{\mathrm{H_2}}^{0.5}\left(P^o + P_{\mathrm{H_2O}}\right)}{\left(1 + aP_{\mathrm{CO}} + bP_{\mathrm{H_2}}^{0.5} + fP_{\mathrm{H_2O}}\right)^2}, \quad k_1' = k_1 g,\ P^o = g^{-1} \tag{2.18}$$

This modification can be made assuming some water is present on the Co catalyst, for instance following a reduction of cobalt oxide with hydrogen. Here, g is a positive coefficient.

The reaction rate expression for the olefin production, r_2, as shown in Equation (2.2), is set to a percentage of the paraffin reaction rate as shown in Equation (2.19) [14].

$$r_2 = \beta_o r_1 \tag{2.19}$$

As the measured production rate of methane, given as $r_{\mathrm{CH_4}}$, is greater than the methane production rate predicted from the two net reactions given in Equation (2.1) and Equation (2.2), this discrepancy can be accounted for by the introduction of a secondary reaction producing methane, such as a methanation reaction shown below [5],

$$\mathrm{CO} + 3\mathrm{H_2} \xrightarrow{r_3} \mathrm{CH_4} + \mathrm{H_2O} \tag{2.20}$$

where the reaction rate r_3 is modeled as simply being the difference between the observed production rate of methane and the production rates of methane according to the two net reactions.

$$r_3 = r_{\mathrm{CH_4}} - \nu_{1,1}r_1 - \nu_{1,2}r_2 \tag{2.21}$$

In the paper describing the consorted vinylene mechanism, Rytter et al. [1] point out that the methane formation is not described in the mechanism. However, the methane formation could be derived from the same $\mathrm{CH_x}$-pool [1]. One possible methane formation rate expression is shown below,

$$r_{\mathrm{CH_4}} = k_{\mathrm{CH_4}}(T)r_1 P_{\mathrm{H_2}}^x \tag{2.22}$$

where x is a parameter accounting for the variance of the catalyst support on the methane formation [42, 43]. It is expected that larger Co-particles on

the catalytic surface have more H_2-coverage, and as such the value of x should increase with the Co-particle size. Furthermore, it is expected that the methane formation rate above captures the main effects with respect to water, as an increased partial pressure of water will cause a decrease to the partial pressure of hydrogen.

By combining Equation (2.21) and Equation (2.22), and introducing the stoichiometric coefficients for methane, the final rate expression for the methanation reaction is obtained.

$$r_3 = k_{\mathrm{CH_4}}(T) r_1 P_{\mathrm{H_2}}^x - (1-\alpha_1)^2 r_1 - (1-\alpha_2)^2 r_2 \tag{2.23}$$

Ma et al. [20] suggest that the effect of water on the selectivity of methane is kinetic by nature, and as such water should actively be a part of the methane formation rate expression. One alternative methane formation rate expression is shown below

$$r_{\mathrm{CH_4}} = k_{\mathrm{CH_4}}(T) r_1 \left(\frac{P_{\mathrm{H_2}}}{P_{\mathrm{H_2O}}} \right)^x \tag{2.24}$$

where x is as described above. When using this rate expression shown in Equation (2.24) a numerical problem arises in the modeling of fixed bed reactors (FBRs) with dry synthesis gas at the reactor inlet; namely that the reaction rate, $r_{\mathrm{CH_4}}$, tends to become infinitely large. This issue is very reminiscent of an issue faced in the Temkin-Pyzhev rate expression [40, 41]. The modified methane formation rate expression is obtained by multiplying Equation (2.24) with the factor $\left(\frac{P_{\mathrm{H_2O}}}{1+K_{\mathrm{CH_4}} P_{\mathrm{H_2O}}} \right)^x$ and the final rate expression is shown in Equation (2.25).

$$r_{\mathrm{CH_4}} = k'_{\mathrm{CH_4}} r_1 \left(\frac{P_{\mathrm{H_2}}}{1 + K_{\mathrm{CH_4}} P_{\mathrm{H_2O}}} \right)^x, \quad k'_{\mathrm{CH_4}} = k_{\mathrm{CH_4}} K_{\mathrm{CH_4}}^x \tag{2.25}$$

Lastly, to account for the lower-than-expected production of ethene, another secondary reaction can be included in the reaction set. The proposed secondary reaction, in this case, is a further polymerization reaction of ethene, and is given by Equation (2.26) below.

$$(1-\alpha_4)\mathrm{C_2H_4} + 2\mathrm{H_2} + \mathrm{CO} \xrightarrow{r_4} \sum_{i=1}^{\infty} \nu_{i,4} \mathrm{C_{2i+1}H_{2i+4}} + \mathrm{H_2O} \tag{2.26}$$

In Equation (2.26), it is assumed that the product distribution of the reaction follows an ASF distribution with a chain growth propagation probability α_4.

Lastly, the reaction rate in Equation (2.26) is modeled as according to Equation (2.27).

$$r_4 = k_4(T) P_{C_2H_4} P_{CO} P_{H_2}^2 \tag{2.27}$$

At this point, it should be stressed that the chemical reactions shown in Equation (2.20) and Equation (2.26) are introduced to help explain the observed non-ASF behavior, and not to justify a particular mechanism [5].

Experimentally, small amounts of CO_2 are produced in the FTS from the water-gas shift (WGS) reaction. This despite the fact that the Co catalyst is WGS inactive. One potential explanation is that Co(II)O is formed when the catalyst deactivates through re-oxidation, and the produced Co(II)O is WGS active [44]. The water-gas shift reaction is given by the following equilibrium reaction:

$$CO + H_2O \underset{k_{-wgs}}{\overset{k_{wgs}}{\rightleftharpoons}} CO_2 + H_2 \tag{2.28}$$

and can be modelled according to Equation (2.29) shown below.

$$r_5 = k_{wgs}(T) \left(P_{CO} P_{H_2O} - \frac{1}{K_{eq}} P_{CO_2} P_{H_2} \right) \tag{2.29}$$

K_{eq} is the equilibrium constant, and can be estimated in the temperature range of operation by Equation (2.30),

$$K_{eq} = \exp\left(\frac{4577.8}{T} - 4.33 \right) \tag{2.30}$$

where T is the temperature in K [45].

2.3.2 Modeling of chain growth propagation probabilities

As outlined in section 2.1, the chain growth propagation probability can be defined according to Equation (2.3). Most proposed chain growth models all depend on the partial pressures of both H_2 and CO [2, 5, 14, 15], but not on the partial pressure of H_2O, even though the effect of water on the product selectivities is well understood [14, 18, 19, 20]. Ostadi et al. [14] propose a chain growth model in which the effect of water is included:

$$\alpha = \frac{1}{1 + k_\alpha(T) \frac{P_{H_2}^x}{P_{CO}^z P_{H_2O}^y}} \tag{2.31}$$

where x, y, and z are empirical exponents fitted to experimental data. As the H_2/CO-ratio is increasing, the value of α should decrease, as is also observed experimentally. Further, this model is also capable of reflecting the observed behavior, as described earlier, concerning water.

For the consorted vinyene mechanism encompassing water assisted CO-activation, Rytter et al. [1] also derive an expression for the chain growth propagation probability, α.

$$\alpha = \frac{1}{1 + \frac{k_\alpha(T)}{P_{\mathrm{CO}} P_{\mathrm{H_2O}}}} \tag{2.32}$$

Curiously enough, the derived expression for α is not including the partial pressure of hydrogen [1]. This is explained by the proposed mechanism as both the rate of propagation and termination are hydrogen dependent, and as such this effect will cancel out. It is further pointed out that, even with a lack of hydrogen in the α expression, a lower H_2/CO-ratio should also correspond to a higher value of α. This is rationalized by the fact that a lower partial pressure of hydrogen will cause the partial pressures of CO and water to increase, and thus accounting for the observed responses [1].
In practice, a model with modified dependency of H_2O is adopted as shown in Equation (2.33) below,

$$\alpha = \frac{1}{1 + k_\alpha(T) \left(\frac{1}{P_{\mathrm{CO}}}\right) \left(\frac{1}{P_{\mathrm{H_2O}}}\right)^y}, \qquad 0 < y \leq 1 \tag{2.33}$$

where x and y are empirical exponents fitted to experimental data.

For simplicity, the chain growth propagation probability for the olefin products, α_2, can be modeled as proposed by Todic et al. [37, 46].

$$\alpha_2 = \alpha_1 \cdot e^{-0.27} \tag{2.34}$$

In a similar fashion, the chain growth propagation probability for the further polymerization reaction can be modeled according to Equation (2.35).

$$\alpha_4 = c_{\alpha_4} \cdot \alpha_1 \tag{2.35}$$

where c_{α_4} is a constant fitted to experimental data.

2.3.3 Modeling of catalyst deactivation

To accurately model the Fischer-Tropsch synthesis, a model for the catalyst deactivation must also be constructed. As pointed out by Rytter et al. [18], water has a significant impact on the deactivation of the catalyst. As such, it is important that a deactivation model is capable of reflecting this behavior.
To incorporate this effect on the deactivation, a proposed model is shown in Equation (2.36),

$$\frac{\mathrm{d}D}{\mathrm{d}t} = -k_d D^n P_{\mathrm{H_2O}}^{\gamma} \tag{2.36}$$

where D is the deactivation of the catalyst corresponding to the relative number of active sites on the catalyst. n is the deactivation order, and γ is an empirical exponent. Evidently, different catalyst can deactivate at different rates and can also respond differently to water [18]. As such, n and γ could differ between catalysts.

2.4 Reactor model

For this thesis, a simple plug flow reactor (PFR) model is used for the reactor model. This model can be derived from a generalized mass balance, assuming steady-state conditions,

$$W_{tot} \cdot \frac{d\omega_i}{dV} = \tilde{R}_i \tag{2.37}$$

where W_{tot} is the total mass flow, ω_i is the mass fraction of component i, and $\tilde{R}_i$ is total reaction rate of component i. It should be noted that an energy balance is not included as the temperature remains nearly constant along the experimental rig. Further, as the pressure drop along the reactor is small, the pressure is assumed to be constant along the axial direction. The mass balance is a pseudo-homogeneous model and as such the catalytic particles are not modeled here.

The reaction rates can also be calculated from the reaction rates on molar basis, $\hat{R}_i$,

$$\tilde{R}_i = \rho_{cat} M_i \hat{R}_i \tag{2.38}$$

where ρ_{cat} is the density of the catalyst, and M_i is the molar mass of component i. Furthermore, the reaction rates can be expressed in terms of the reactions

r_1-r_5 [5].

$$\hat{R}_i = \sum_{j=1}^{n_{rx}} \nu_{i,j} r_j \tag{2.39}$$

Lastly, the PFR model defined in Equation (2.37) can be put on dimensionless form by introducing a dimensionless variable for the volume of the reactor:

$$\xi = \frac{V}{V_R} \tag{2.40}$$

where V_R is the total volume of the reactor. Introducing this variable to Equation (2.37) gives the final dimensionless form of the PFR model:

$$\frac{\mathrm{d}\omega_i}{\mathrm{d}\xi} = \frac{m_{cat}}{W_{tot}} \cdot M_i \hat{R}_i \tag{2.41}$$

2.5 Lumped Fischer-Tropsch model

In this thesis, when lumping products from the Fischer-Tropsch synthesis, all hydrocarbons with five and more carbon atoms are lumped together. Here, two lumps are created, one for the paraffin products (lumped as C_{5+}^{P}) and one for olefin the products (lumped as C_{5+}^{O}). Equation (2.1), Equation (2.2), Equation (2.20), Equation (2.26), and Equation (2.28) become the following:

$$\begin{aligned} \mathrm{CO} + \mathrm{H_2} \xrightarrow{r_1} \nu_{1,1}\mathrm{CH_4} + \nu_{2,1}\mathrm{C_2H_6} + \nu_{3,1}\mathrm{C_3H_8} + \\ \nu_{5,1}\mathrm{C_4H_{10}} + \nu_{[5,\infty],1}\mathrm{C}_{5+}^{P} + \mathrm{H_2O} \end{aligned} \tag{2.42}$$

$$\begin{aligned} \mathrm{CO} + \mathrm{H_2} \xrightarrow{r_2} \nu_{1,2}\mathrm{CH_4} + \nu_{2,2}\mathrm{C_2H_4} + \nu_{3,2}\mathrm{C_3H_6} + \\ \nu_{4,2}\mathrm{C_4H_8} + \nu_{[5,\infty],2}\mathrm{C}_{5+}^{O} + \mathrm{H_2O} \end{aligned} \tag{2.43}$$

$$\mathrm{CO} + 3\mathrm{H_2} \xrightarrow{r_3} \mathrm{CH_4} + \mathrm{H_2O} \tag{2.44}$$

$$\begin{aligned} (1-\alpha_4)\mathrm{C_2H_4} + 2\mathrm{H_2} + \mathrm{CO} \xrightarrow{r_4} \nu_{1,4}\mathrm{C_3H_6} + \nu_{2,4}\mathrm{C_4H_8} + \\ \nu_{[5,\infty],4}\mathrm{C}_{5+}^{O} + \mathrm{H_2O} \end{aligned} \tag{2.45}$$

$$\mathrm{CO} + \mathrm{H_2O} \underset{\mathrm{k_{-wgs}}}{\overset{\mathrm{k_{wgs}}}{\rightleftharpoons}} \mathrm{CO_2} + \mathrm{H_2} \tag{2.46}$$

For the lumps defined in the equations above, their stoichiometric coefficients are calculated according to Equation (2.12).

$$\nu_{[5,\infty],1} = (1-\alpha_1)\alpha_1^4 \tag{2.47}$$

$$\nu_{[5,\infty],2} = (1-\alpha_2)\alpha_2^4 \tag{2.48}$$

$$\nu_{[5,\infty],4} = (1-\alpha_4)\alpha_4^2 \tag{2.49}$$

The average carbon number is calculated from Equation (2.13) by letting $M \to \infty$.

$$\bar{n}_{n,[5,\infty]} = \frac{5\alpha^4 - 4\alpha^5}{(1-\alpha)\alpha^4} = 5 + \frac{\alpha}{1-\alpha} \tag{2.50}$$

Lastly, the weight average carbon number of the lump reduces to the following [5]:

$$\bar{n}_{w,[5,\infty]} = \frac{\left(4 + \frac{1+\alpha}{1-\alpha}\right) 5 + \frac{(1+\alpha)\alpha}{(1-\alpha)^2}}{4 + \frac{\alpha}{1-\alpha}} \tag{2.51}$$

From the average carbon number defined in Equation (2.50), the molar masses of the lumped components, C_{5+}^P and C_{5+}^O, can be calculated as shown in Equation (2.52) and Equation (2.53) below.

$$M_{w,\mathrm{C}_{5+}^P} = 14\left(5 + \frac{\alpha}{1-\alpha}\right) + 2 \tag{2.52}$$

$$M_{w,\mathrm{C}_{5+}^O} = 14\left(5 + \frac{\alpha}{1-\alpha}\right) \tag{2.53}$$

Table 2.1 shows the stoichiometric coefficients, $\nu_{i,j}$, for the lumped Fischer-Tropsch synthesis model as defined in Equation (2.42)-Equation (2.46). The reaction rates are given in $\mathrm{kmol\,kg^{-1}\,h^{-1}}$.

Component	r_1	r_2	r_3	r_4	r_5
CO	-1	-1	-1	-1	-1
H_2	$-(3-\alpha_1)$	$-2-(1-\alpha_2)^2$	-3	-2	1
H_2O	1	1	1	1	-1
CH_4	$(1-\alpha_1)^2$	$(1-\alpha_2)^2$	1	0	0
C_2H_6	$(1-\alpha_1)^2\alpha_1$	0	0	0	0
C_3H_8	$(1-\alpha_1)^2\alpha_1^2$	0	0	0	0
C_4H_{10}	$(1-\alpha_1)^2\alpha_3$	0	0	0	0
C_{5+}^P	$(1-\alpha_1)\alpha_1^4$	0	0	0	0
C_2H_4	0	$(1-\alpha_2)^2\alpha_2$	0	$-(1-\alpha_4)$	0
C_3H_6	0	$(1-\alpha_2)^2\alpha_2^2$	0	$(1-\alpha_4)^2$	0
C_4H_8	0	$(1-\alpha_2)^2\alpha_2^3$	0	$(1-\alpha_4)^2\alpha_4$	0
C_{5+}^0	0	$(1-\alpha_2)\alpha_2^4$	0	$(1-\alpha_4)\alpha_4^2$	0
CO_2	0	0	0	0	1

Table 2.1: Stoichiometric coefficients, $\nu_{i,j}$ for the reactions r_1-r_5 defined in Equation (2.42)-Equation (2.46).

2.5.1 Selectivity

The product selectivities can be calculated for each individual component through Equation (2.54),

$$S_{\mathrm{C}_i} = \frac{M_{\mathrm{CO}}}{M_{\mathrm{C}_i}} \frac{i(\omega_{\mathrm{C}_i}^{\mathrm{out}} - \omega_{\mathrm{C}_i}^{\mathrm{in}})}{\omega_{\mathrm{CO}}^{\mathrm{in}} - \omega_{\mathrm{CO}}^{\mathrm{out}}} \cdot 100\%, \qquad i = 1, \cdots, 4 \tag{2.54}$$

where S_{C_i} is the selectivity of a hydrocarbon with i carbon atoms in its chain, M is the molar mass of the component, and ω is the weight fraction.
As the selectivities must sum to unity or 100%, the selectivity of the lump, C_{5+} is simply calculated as the following:

$$S_{\mathrm{C}_{5+}} = 100\% - S_{\mathrm{CO}_2} - \sum_{i=1}^{4} S_{\mathrm{C}_i} \tag{2.55}$$

2.6 Parameter estimation

When doing parameter estimation, a set of parameters in a mathematical model are estimated by using measured data obtained experimentally. The measured data are said to have some inherent noise such that for each observation the following will hold true, [47, 48]:

$$Y_i = y_i + \varepsilon_i, \qquad i = 1, \cdots, n \tag{2.56}$$

where Y_i is the observed measurement i, y_i is the true, underlying observed measurement, and ε_i is the inherent noise associated with measurement i.
Additionally, it is also possible to have some error or inherent noise associated with the independent variable X_i, such that

$$X_i = x_i + \delta_i, \qquad i = 1, \cdots, n \tag{2.57}$$

where δ_i denote the error associated with the true, underlying value x_i.

From this point on, let boldface symbols denote vectors.
The set of responses $\boldsymbol{Y}$ can be expressed in terms of a function f being dependent on $\boldsymbol{X}$ and a set of parameters, $\boldsymbol{\beta}$, as shown in Equation (2.58) below. The method for estimating a set of parameters in which there are measurement

errors associated with both the dependent and independent variables is called *Orthogonal Distance Regression* (ODR) [49].

$$\boldsymbol{Y} = f\left(\boldsymbol{X} + \boldsymbol{\delta}; \boldsymbol{\beta}\right) + \boldsymbol{\varepsilon} \tag{2.58}$$

In this case, when estimating the parameters $\boldsymbol{\beta}$, we are interested in evaluating, and minimizing, the residual as defined in Equation (2.59) [47, 49],

$$\begin{aligned} r_i^2 = \quad & \min_{\varepsilon_i, \delta_i} \left[\varepsilon_i^2 + \delta_i^2\right] \\ \text{s.t.} \quad & Y_i = f(X_i + \delta_i; \boldsymbol{\beta}) + \varepsilon_i \end{aligned} \tag{2.59}$$

which can be simplified somewhat by using the constraint to eliminate the term ε_i^2. Now, the optimization problem is formulated in terms of finding a set of parameters that minimized the objective function as defined below.

$$\min_{\boldsymbol{\beta}, \boldsymbol{\delta}} \sum_{i=1}^{n} \{[f(X_i + \delta_i; \boldsymbol{\beta}) - Y_i]^2 + \delta_i^2\} \tag{2.60}$$

Lastly, by allowing weights to be associated with each response, the *weighted Orthogonal Distance Regression* is defined [47, 50].

$$\min_{\boldsymbol{\beta}, \boldsymbol{\delta}} \sum_{i=1}^{n} \omega_i^2 \{[f(X_i + \delta_i; \boldsymbol{\beta}) - Y_i]^2 + d_i^2 \delta_i^2\} \tag{2.61}$$

where the weights, ω_i and d_i, are defined according to Equation (2.62) and Equation (2.63)

$$w_i = \frac{1}{\sigma_{\varepsilon_i}} \tag{2.62}$$

$$d_i = \frac{\sigma_{\varepsilon_i}}{\sigma_{\delta_i}} \tag{2.63}$$

where σ_ε is the standard deviation of the error or noise associated with the responses, and σ_δ is the standard deviation of the error or noise associated with the independent variables.

To see if the estimated parameters fit the measured responses, the confidence interval of each estimated parameter can be calculated from its estimated standard deviation, $s_{\hat{\beta}_i}$, as shown in Equation (2.64) [51, p. 403],

$$\hat{\beta}_i \pm t_{0.975, n-p} \cdot s_{\hat{\beta}_i} \tag{2.64}$$

where $t_{0.975,n-p}$ correspond to the t-value for a 95%-confidence interval with $n-p$ degrees of freedom. If the confidence interval of a particular parameter does not contain zero, the parameter is considered to be statistically important, and as such it should be kept in the model.
To evaluate the overall quality of the model, the *mean squared error* (MSE) is calculated. The MSE is calculated according to the following:

$$MSE = \frac{1}{n-p} \sum_{i=1}^{n} \left(Y_i - \hat{Y}_i \right)^2 \tag{2.65}$$

where p is the number of parameters in the model, and $\hat{Y}_i$ is the response i predicted by the model. The MSE will be a positive number, and an MSE closer to zero will indicate a higher quality of the model.

3 Model implementation

The reactor, kinetic, and selectivity models are all implemented in `Python` as shown in Appendix F. A set of optimal parameters, including their respective uncertainties, are estimated using ODR as described in Section 2.6. `objfun` is the objective function in which the reactor model is solved numerically using the `odeint`-function. It should be noted that only two points along the reactor are used when solving the reactor model; one at the inlet and one at the outlet of the reactor, the outlet of the reactor is the main point of interest.
Further, the product selectivities and partial pressures of the gaseous components are calculated. When calculating the partial pressures, all components, except for C_{5+}, are assumed to be gaseous.

The reactor model itself is implemented as a plug flow reactor as described in Section 2.4 and is assumed to be a reasonably good model for the experimental setup. The reactor model is implemented in a user-defined function `rate`. Here, the five reaction rates, r_1-r_5, are calculated, as well as all the stoichiometric coefficients. Note that the reaction rates are dimensionless as the reactor model is defined on dimensionless form. It should also be noted that, experimentally, small amounts of CO_2 (typically below 1%) are produced. However, the inclusion of the WGS reaction can be particularly important when low H_2/CO-ratios (and addition of water) are used, as under these conditions the production of CO_2 can be significant. The molar masses of the C_{5+} lumps are also calculated in `rate`.
Additionally, the model for the deactivation of the catalyst is solved using the `odeint`-function. The deactivation model is solved using two points in time; one at the previous Time-On-Stream and one at the current Time-On-Stream (TOS). The initial condition is set to be the previously calculated deactivation. This is done so that the calculated deactivation at a particular TOS takes into account how the catalyst has previously deactivated at earlier TOS. The deactivation model itself, as described in Section 2.3.3, is implemented in the user-defined function `catalyst_deactivation`.

Lastly, the user-defined function `xlread` extracts experimental data from a defined spreadsheet. `alpha` calculates the α-value based on the partial pressures of CO and H_2O as defined in Equation (2.33). `coeff` calculates the stoichiometric coefficient for a particular hydrocarbon with i carbons in its chain.

For the uncertainties, the independent variables are assumed to be measured quite accurately, and as such their respective relative uncertainties are small.

For the measured responses, the uncertainties of the conversion of CO, the selectivity of C_{5+}, and selectivity of CH_4 are set such that their respective relative uncertainties are small as these particular responses are considered as the main responses (i.e. these responses are the most important to be explained well by the model). The uncertainties of the C_2-C_4 paraffin and olefin responses, as well as the CO_2 responses, are set such that their respective relative uncertainties are quite high as these responses are considered as secondary responses, and accurately estimating these particular responses are not as important.
Table 3.1 shows the absolute uncertainties used for both the independent variables as well as for the measured responses.

Independent variables		Measured responses	
Variable	Uncertainty	Response	Uncertainty
TOS	$1 \cdot 10^{-2}$	χ_{CO}	0.3
T	1.0	$S_{\mathrm{CH_4}}$	0.3
P_{tot}	$1 \cdot 10^{-2}$	$S_{\mathrm{C_2^O}}$	0.3
$\omega_{\mathrm{H_2}}$	$1 \cdot 10^{-5}$	$S_{\mathrm{C_2^P}}$	1.5
ω_{CO}	$1 \cdot 10^{-4}$	$S_{\mathrm{C_3^O}}$	3.0
$\omega_{\mathrm{N_2}}$	$1 \cdot 10^{-4}$	$S_{\mathrm{C_3^P}}$	2.0
$\omega_{\mathrm{H_2O}}$	$1 \cdot 10^{-4}$	$S_{\mathrm{C_4^O}}$	3.3
m_{cat}	$1 \cdot 10^{-4}$	$S_{\mathrm{C_4^P}}$	3.0
W_{tot}	$1 \cdot 10^{-8}$	$S_{\mathrm{C_{5+}}}$	0.3
		$S_{\mathrm{CO_2}}$	0.3

Table 3.1: Absolute uncertainties of all independent variables (X_i), and measured responses (Y_i).

4 Experimental data

A model accounting for the reaction kinetics, product selectivities, and catalyst deactivation including the effect of water is proposed and fitted to experimental data obtained from Borg [25]. Four different datasets; three corresponding to three different Co/Re/γ-Al_2O_3 catalysts and one corresponding to a Co/Re/α-Al_2O_3 catalyst, were used. Table 1 in the paper by Rytter et al. [18] shows an overview of 13 different catalysts from Borg [25], of which the catalysts labeled C3, C10, and C11 were considered. A more detailed characterization of the relevant catalysts can be found in the paper by Borg et al. [16]. Additionally, the fourth catalyst under consideration (for simplicity labeled as C14) is the Co/Re/α-Al_2O_3. All catalysts have catalyst loadings of 0.5 wt% and 20 wt% Re and Co, respectively. Catalyst C14 is not shown in Table 1 in [18], though this catalyst has a significantly higher pore diameter than the others. The experimental run for each catalyst can be split into five periods as follows [18]:

A. Dry syngas with a flow rate of 250 NmL/min.

B. Dry syngas with a reduced flow rate such that the conversion of CO is 50%.

C. Flow rate of dry syngas remains as in period B, water is added to get 21% water pressure at the inlet of the reactor. The total pressure remains at 20 bar.

D. Water pressure increased to 35%.

E. Same conditions as in period B.

For catalysts C3, C10, C11, and C14, the temperature, pressure, and H_2/CO-ratio are kept constant at 210°C, 20 bar, and 2.1 respectively. For each catalyst, a catalyst mass of approximately 1.0 grams is used. For each of the catalysts, the model is fitted to the experimental data, and a set of optimal parameters is obtained. As the catalysts have different pore diameters and pore size distributions it is also possible to study how the different catalyst characterizations affect the estimated parameters.
When considering the experimental data for these catalysts, period A is removed from the datasets as an unusually large deactivation is observed experimentally in this period. It is believed that the experimental observations related to periods B-E are better representing the catalysts.
The model parameters obtained for a previously fitted model (using data from

Lillebø [52]) were used to obtain a set of initial guesses for the model parameters. The initial guesses, though having large uncertainties, were used further and adjusted to better fit the model. Due to a lack of information about the system in the experiments carried out, some of the model parameters had to be estimated manually through a trial-and-error process. These manually estimated parameters were fitted such as to best explain the experimental data, and such that the uncertainties of the remaining parameters were as low as possible. To evaluate the quality of the parameters, their respective estimated uncertainties were considered.

Additionally, a fifth catalyst is considered. This catalyst is a commercial type catalyst and is a variant of catalyst C10 investigated by Borg [25], though the performance of the catalyst will differ slightly due to different productions. For this catalyst, the temperature is kept constant at 210°C, the pressure is varied between 20 and 22 bar (20 bar for runs with dry syngas, and 22 bar for runs with approximately 10% water pressure). Different H_2/CO-ratios between 2.1 and 1.12 are investigated. At different H_2/CO-ratios, slightly different catalyst masses are used. In a similar fashion as above, for one particular H_2/CO-ratio, the experimental run can be split into different periods. The different periods for the experimental run at $H_2/CO = 2.1$ is shown below:

A. Dry syngas with a flow rate of 250 NmL/min.

B. Dry syngas with a reduced flow rate such that the conversion of CO is approximately 50%.

C. Dry syngas with a reduced flow rate such that the conversion of CO is approximately 75%.

D. Dry syngas with a flow rate of 250 NmL/min as in period A.

E. Flow rate of dry syngas remains as in period D, water is added to get approximately 10% water pressure at the reactor inlet.

F. Syngas flow rate is reduced such that the conversion of CO is approximately 50%. Water pressure remains at approximately 10%.

G. Same conditions as in period A.

It should be noted that, for the commercial type catalyst, the experimental runs do not always follow the periods as described above. Most notably, for the experiment using $H_2/CO = 1.12$, the flow rate of the dry syngas is varied more than shown in periods A-C above. Further, for this particular H_2/CO-ratio, the

periods corresponding to the periods E-G are not used for the model fitting as the experimental data show that the C_{5+}-selectivities drop when water is first added to the system.
As the commercial type catalyst is a variant of the C10 catalyst, the model parameters obtained for this catalyst were used as initial guesses. As the performance is slightly different, some small changes to the initial guesses were required to better fit the model. As before, to evaluate the quality of the estimated parameters, their respective estimated uncertainties were considered.

5 Results

The chemical reactions presented in Equation (2.42) - Equation (2.46) were found to adequately describe the Fischer-Tropsch synthesis. The mathematical model encompassing reaction kinetics, product selectivities, and catalyst deactivation is summarized below.

$$r_1 = \frac{D(t, P_{H_2O}) k_1' P_{CO} P_{H_2}^{0.5} \left(P^o + P_{H_2O}\right)}{\left(1 + aP_{CO} + bP_{H_2}^{0.5} + fP_{H_2O}\right)^2}, \qquad k_1' = k_1 g, \quad P^o = g^{-1} \tag{5.1}$$

$$r_2 = \beta_o r_1 \tag{5.2}$$

$$r_3 = k_{CH_4} r_1 P_{H_2}^x - (1-\alpha_1)^2 r_1 - (1-\alpha_2)^2 r_2 \tag{5.3}$$

$$r_4 = k_4 P_{C_2H_4} P_{CO} P_{H_2}^2 \tag{5.4}$$

$$r_5 = k_{wgs} \left(P_{CO} P_{H_2O} - \frac{1}{K_{eq}} P_{CO_2} P_{H_2} \right) \tag{5.5}$$

$$K_{eq} = \exp\left(\frac{4577.8}{T} - 4.33\right) \tag{5.6}$$

$$\frac{\mathrm{d}D}{\mathrm{d}t} = -k_d D^n P_{H_2O}^{\gamma}, \quad n = 2, \ \gamma = 1 \tag{5.7}$$

$$\alpha_1 = \frac{1}{1 + k_\alpha \left(\frac{1}{P_{CO}}\right) \left(\frac{1}{P_{H_2O}}\right)^y} \tag{5.8}$$

$$\alpha_2 = \alpha_1 \cdot e^{-0.27} \tag{5.9}$$

$$\alpha_4 = c_{\alpha_4} \cdot \alpha_1 \tag{5.10}$$

For each catalyst, the model was fitted to a corresponding set of experimental data. The results for each catalyst are presented in the following subsections.

5.1 Catalyst C3

For catalyst C3, the estimated parameters by the ODR and their respective absolute uncertainties are shown in Table 5.1. Estimated parameters with no given uncertainty have been estimated manually.

Parameter	Estimated value [a.u.]	Uncertainty [a.u.]
k_1	1.928	$\pm$ 0.05904
a	3.50	-
b	1.889	-
f	0.676	$\pm$ 0.104
g	1.428	-
β_o	0.10	-
k_{CH_4}	0.1067	$\pm$ 0.004676
x	1.0	$\pm$ 0.20
k_4	1.20	-
k_{wgs}	0.0025	-
k_d	0.00850	$\pm$ 0.00105
k_α	0.05792	$\pm$ 0.004015
y	0.09700	$\pm$ 0.004676
c_{α_4}	0.70	-

Table 5.1: Estimated parameters and their respective absolute uncertainties for catalyst C3. Parameters with no given uncertainty have been estimated manually.

To evaluate the quality of the model, parity plots of all the responses are constructed. The parity plots show the performance of each period as described in Section 4. As mentioned, period A for this catalyst is removed as unusually large catalyst deactivation is observed specifically for this period, and it is believed that periods B-E better represent the catalyst.
Further, trend plots of the main responses (i.e. conversion of CO, selectivity of C_{5+}, and selectivity of CH_4) are also generated. Lastly, residual plots of the main responses are constructed. The residual plots can be found in Appendix A.1.

Figure 5.1 shows the parity plots of the conversion of CO, C_{5+}-selectivity, and CH_4-selectivity for catalyst C3. Periods B-E are shown in each parity plot. Here, the responses of the model are plotted against the responses measured experimentally. A reference line is also included to see how well the model is able to describe the experimental data. Only periods B-E are considered when doing the model fitting.

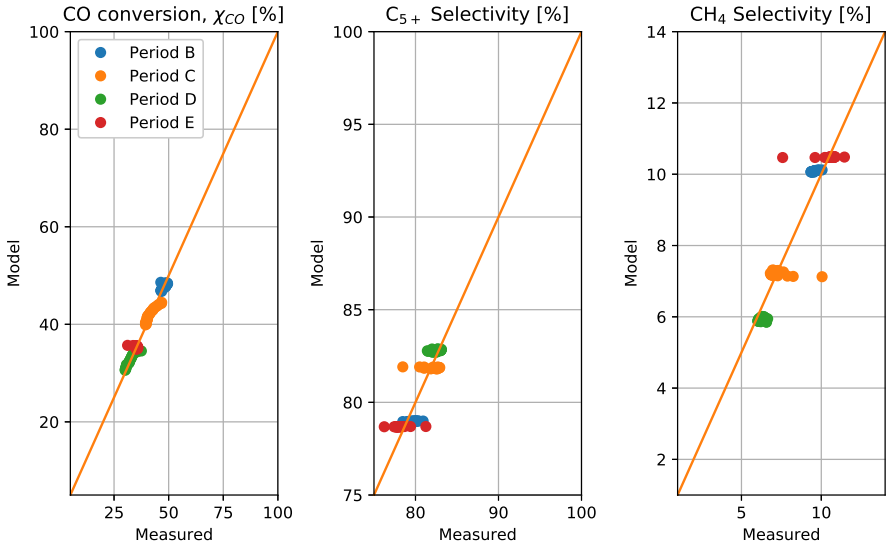

Figure 5.1: Parity plots of the conversion of CO, C_{5+}-selectivity, and CH_4-selectivity for catalyst C3. The periods B-E are shown in the plot. Only these are considered when doing the model fitting.

Figure 5.2 shows the parity plots of the C_2-C_4 paraffin and olefin selectivities, as well as the CO_2-selectivity. The periods B-E are shown in each parity plot. The responses of the model are plotted against the responses measured experimentally. A reference line is also included to see how well the model can describe the experimental data. Only the periods B-E are considered when doing the model fitting.

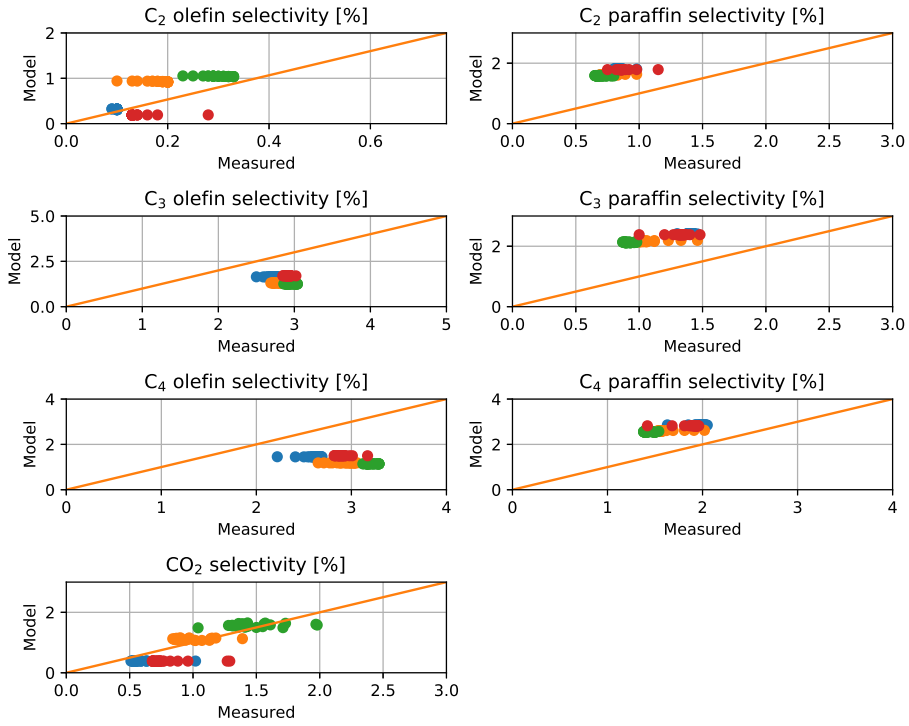

Figure 5.2: Parity plots of the C_2-C_4 paraffin and olefin selectivities, and the CO_2-selectivity for catalyst C3. The blue dots correspond to period B, the orange dots correspond to period C, the green dots correspond to period D, and the red dots correspond to period E.

Figure 5.3 shows the trend plots of the conversion of CO, C_{5+}-selectivity, and CH_4-selectivity for catalyst C3. Here, a H_2/CO-ratio of 2.1 is used. As mentioned, period A removed from the dataset due to unusual catalyst deactivation, and as such, only periods B-E are considered when doing the model fitting. Only periods B-E are shown in the trend plots.

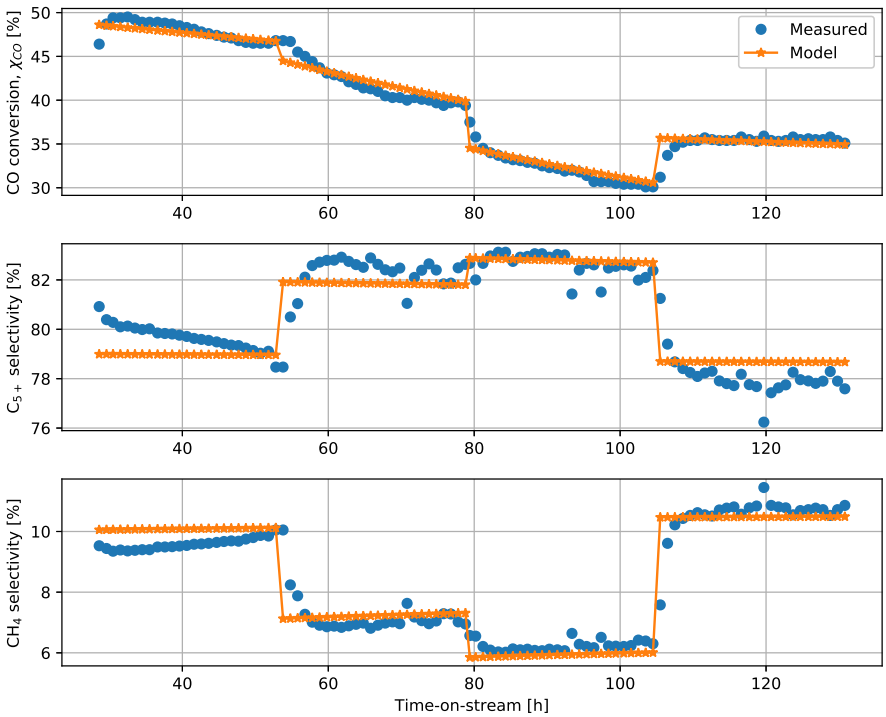

Figure 5.3: Trend plots of the conversion of CO, C_{5+}-selectivity, and CH_4-selectivity for periods B-E for catalyst C3. Each period is run for approximately 30 hours.

5.2 Catalyst C10

For catalyst C10, the estimated parameters and their respective absolute uncertainties are shown in Table 5.2. Estimated parameters with no given uncertainty have been estimated manually.

Parameter	Estimated value [a.u.]	Uncertainty [a.u.]
k_1	1.815	$\pm$ 0.5217
a	3.50	-
b	1.504	-
f	1.364	$\pm$ 0.7708
g	1.523	-
β_o	0.10	-
k_{CH_4}	0.08613	$\pm$ 0.009037
x	1.7	$\pm$ 0.66
k_4	1.00	-
k_{wgs}	0.002155	-
k_d	0.01692	$\pm$ 0.004575
k_α	0.02940	$\pm$ 0.005481
y	0.358	$\pm$ 0.0809
c_{α_4}	0.70	-

Table 5.2: Estimated parameters and their respective absolute uncertainties for catalyst C10. Parameters with no given uncertainty have been estimated manually.

To evaluate how well the model fits the experimental data, parity plots of all the responses are constructed. The parity plots show the performance of each period as described in Section 4. As mentioned, period A for this catalyst is removed as unusually large catalyst deactivation is observed specifically for the period, and it is believed that periods B-E better represent the catalyst.
Further, trend plots of the main responses (i.e. conversion of CO, C_{5+}-selectivity, and CH_4-selectivity) are generated. Lastly, the residual plots of the main responses are also constructed. The residual plots can be found in Appendix A.2.

Figure 5.4 shows the parity plots of the conversion of CO, C_{5+}-selectivity, and CH_4-selectivity for catalyst C10. The periods B-E are shown in each parity plot. The responses of the model are plotted against the responses measured experimentally. A reference line is also included to see how well the model is able to describe the experimental data. Only the periods B-E are considered when doing the model fitting.

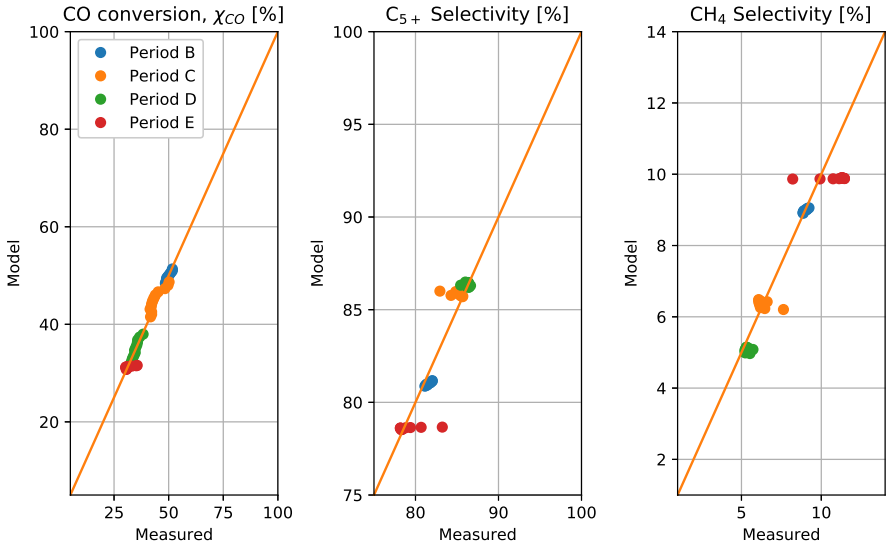

Figure 5.4: Parity plots of the conversion of CO, C_{5+}-selectivity, and CH_4-selectivity for catalyst C10. The periods B-E are shown in the plot. These are the only periods considered when doing the model fitting.

Figure 5.5 shows the parity plots of the C_2-C_4 paraffin and olefin selectivities, as well as the CO_2-selectivity. The periods B-E are shown in each parity plot. The responses of the model are plotted against the responses measured experimentally. A reference line is also included to see how well the model is able to describe the experimental data. Only the periods B-E are considered when doing the model fitting.

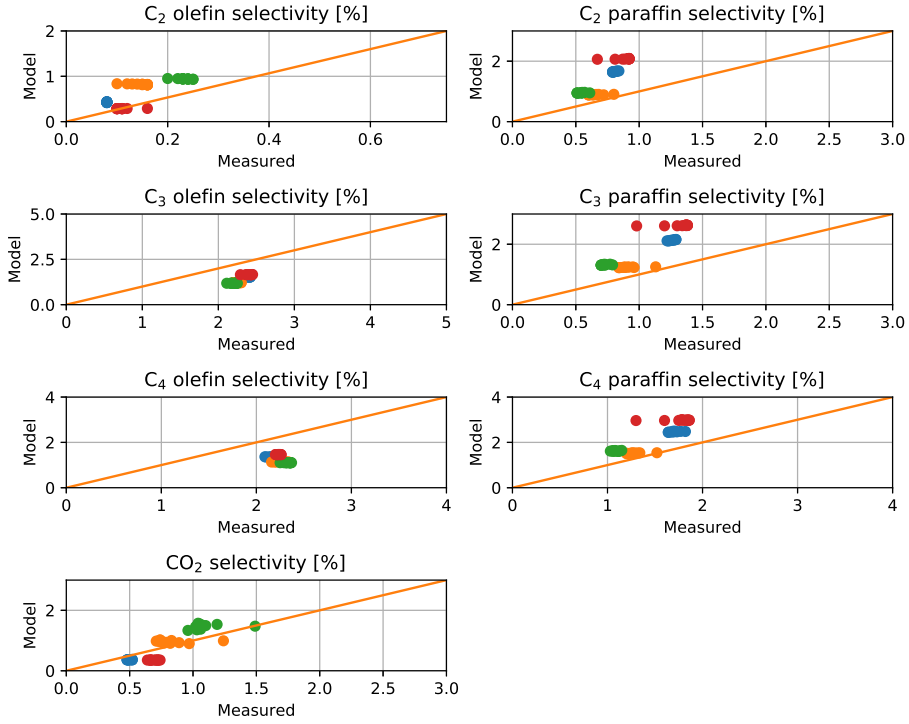

Figure 5.5: Parity plots of the C_2-C_4 paraffin and olefin selectivities, and the CO_2-selectivity for catalyst C10. The blue dots correspond to period B, the orange dots correspond to period C, the green dots correspond to period D, and the red dots correspond to period E.

Figure 5.6 shows the trend plots of the conversion of CO, C_{5+}-selectivity, and CH_4-selectivity for catalyst C10. Here, a H_2/CO-ratio of 2.1 is used. As outlined earlier, period A is removed from the dataset when doing the model fitting due to unusual catalyst deactivation in this period. As such, only the periods B-E are considered when doing the model fitting. Only the periods B-E are shown in the trend plots.

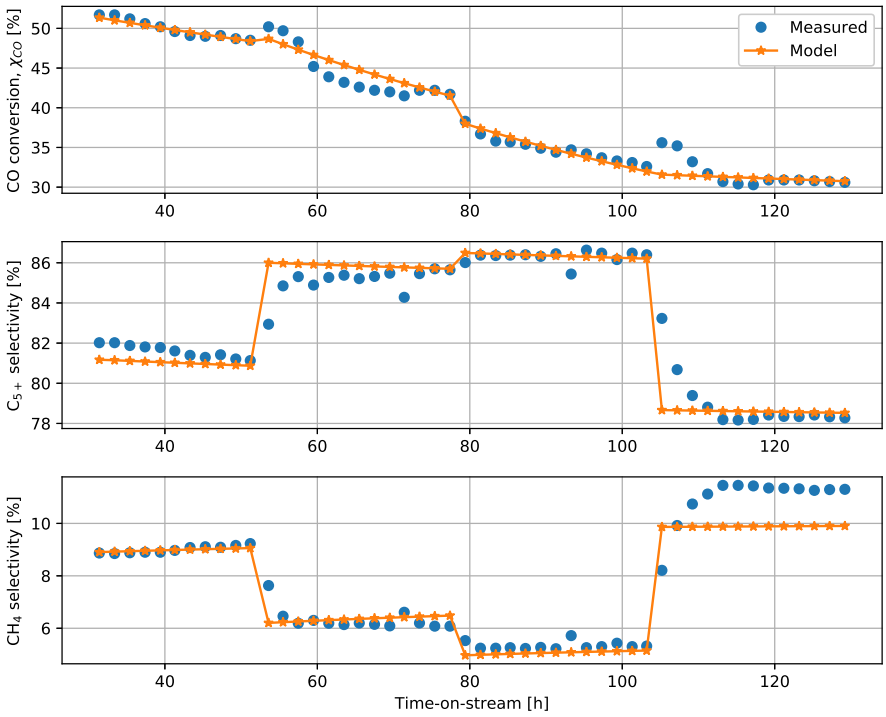

Figure 5.6: Trend plots of the conversion of CO, C_{5+}-selectivity and CH_4-selectivity for periods B-E for catalyst C10. Each period is run for approximately 30 hours.

5.3 Catalyst C11

For catalyst C11, the estimated parameters and their respective absolute uncertainties are shown in Table 5.3. Estimated parameters with no given uncertainty have been estimated manually.

Parameter	Estimated value [a.u.]	Uncertainty [a.u.]
k_1	1.448	$\pm$ 0.2275
a	3.50	-
b	1.152	-
f	1.897	$\pm$ 0.7498
g	1.0696	-
β_o	0.10	-
k_{CH_4}	0.09017	$\pm$ 0.01289
x	1.10	$\pm$ 0.930
k_4	1.00	-
k_{wgs}	0.002155	-
k_d	0.01456	$\pm$ 0.007765
k_α	0.0309	$\pm$ 0.00768
y	0.31	$\pm$ 0.12
c_{α_4}	0.70	-

Table 5.3: Estimated parameters and their respective absolute uncertainties for catalyst C11. Parameters with no given uncertainty have been estimated manually.

To evaluate how well the model fits to the experimental data, parity plots of all the responses are constructed. The parity plots show the performance of each period as described in Section 4. As mentioned, period A for this catalyst is removed as unusually large catalyst deactivation is observed specifically for this period, and it is believed that periods B-E are better representations of the catalyst. Further, trend plots of the main responses (i.e. the conversion of CO, C_{5+}-selectivity, and CH_4-selectivity) are constructed. Lastly, residual plots of the main responses are also constructed. The residual plots can be found in Appendix A.3.

Figure 5.7 shows the parity plots of the conversion of CO, C_{5+}-selectivity, and CH_4-selectivity for catalyst C11. Periods B-E are shown in each parity plot. The responses of the model are plotted against the responses measured experimentally. A reference line is also included to see how well the model is able to describe the experimental data. Only periods B-E are considered when doing the model fitting.

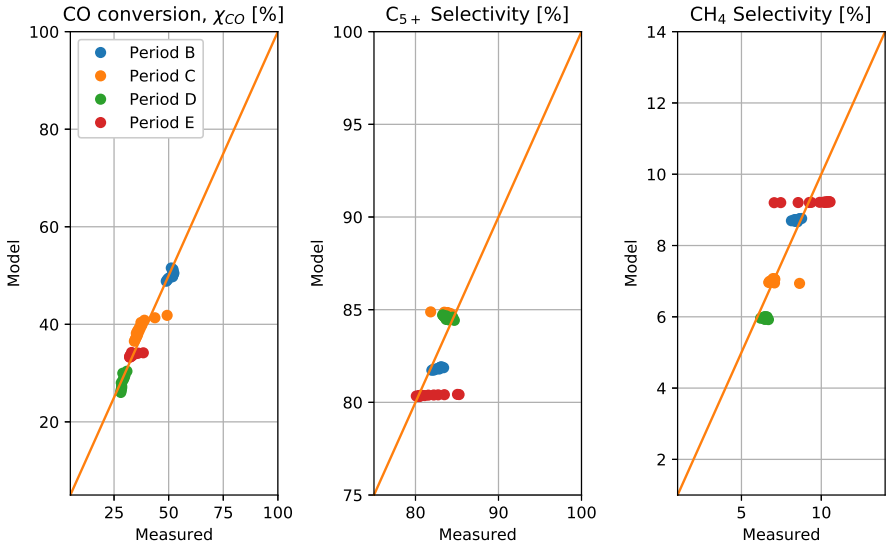

Figure 5.7: Parity plots of the conversion of CO, C_{5+}-selectivity, and CH_4-selectivity for catalyst C11. The periods B-E are shown in the plot. These are the only periods considered when doing the model fitting.

Figure 5.8 shows the parity plots of the C_2-C_4 paraffin and olefin selectivities, as well as the CO_2-selectivity. The periods B-E are shown in each parity plot. The responses of the model are plotted against the responses measured experimentally. A reference line is also included to see how well the model is able to describe the experimental data. Only the periods B-E are considered when doing the model fitting.

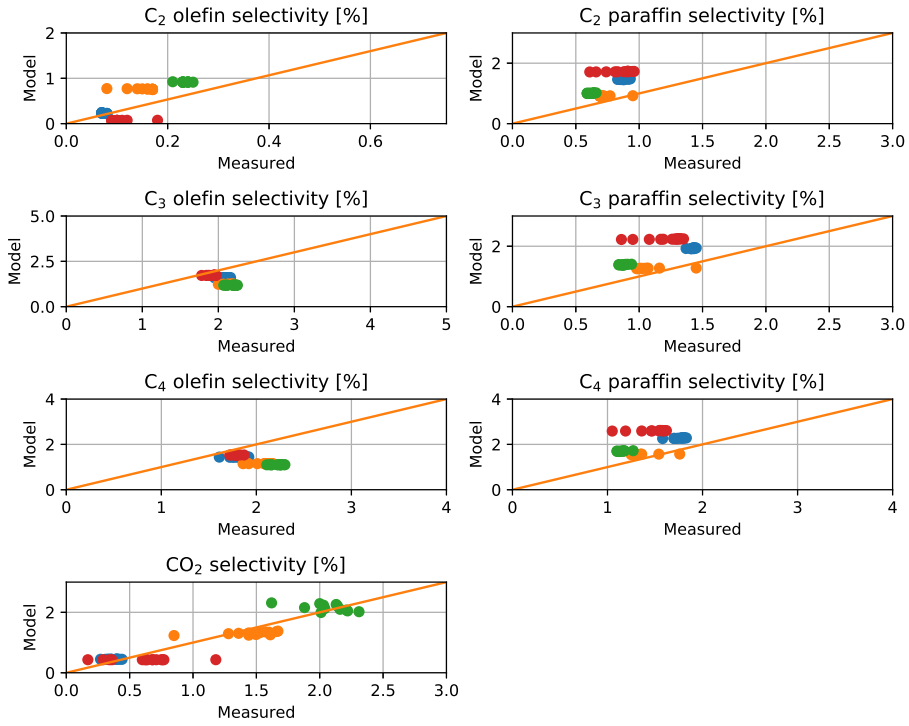

Figure 5.8: Parity plots of the C_2-C_4 paraffin and olefin selectivities, as well as the CO_2-selectivity for catalyst C11. The blue dots correspond to period B, the orange dots correspond to period C, the green dots correspond to period D, and the red dots correspond to period E.

Figure 5.9 shows the trend plots of the conversion of CO, C_{5+}-selectivity, and the CH_4-selectivity for catalyst C11. A H_2/CO-ratio of 2.1 is used in this case. As described earlier, period A is removed from the dataset when doing the model fitting due to unusual catalyst deactivation in this particular period. As such, only the periods B-E are considered when doing the model fitting. Only the periods B-E are shown in the trend plots.

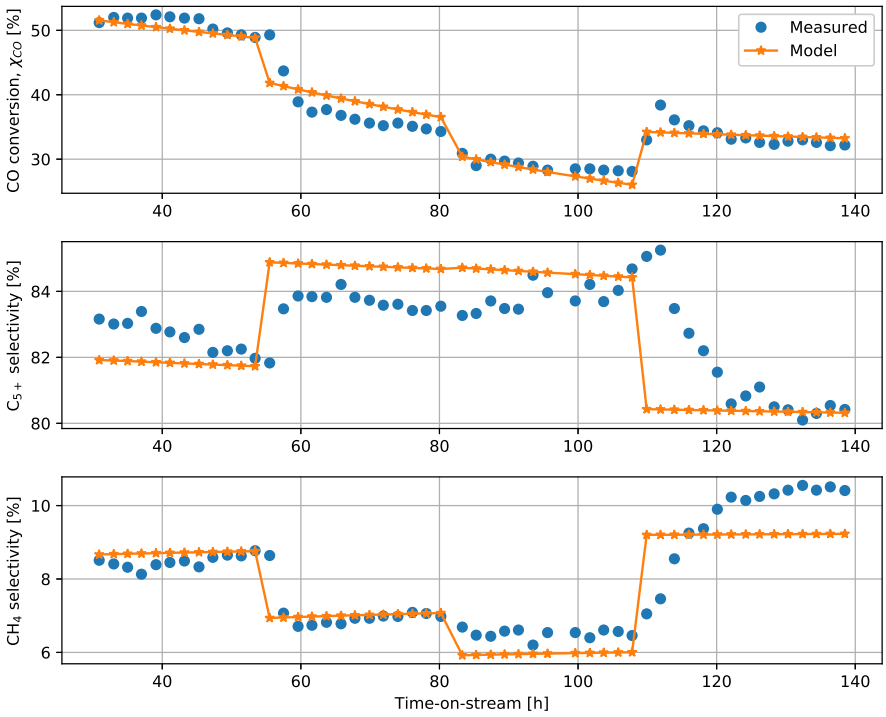

Figure 5.9: Trend plots of the conversion of CO, C_{5+}-selectivity, and CH_4-selectivity for periods B-E for catalyst C11. Each period is run for approximately 30 hours.

5.4 Catalyst C14

For catalyst C14, the estimated parameters and their respective absolute uncertainties are shown in Table 5.4. Estimated parameters with no given uncertainty have been estimated manually.

Parameter	Estimated value [a.u.]	Uncertainty [a.u.]
k_1	0.5820	± 0.07306
a	3.50	-
b	1.669	-
f	1.170	± 0.3710
g	2.233	-
β_o	0.10	-
k_{CH_4}	0.06600	± 0.01006
x	2.0	± 0.8638
k_4	0.45	-
k_{wgs}	0.000045	-
k_d	0.008141	± 0.003747
k_α	0.01413	± 0.007921
y	0.46	± 0.20
c_{α_4}	0.70	-

Table 5.4: Estimated parameters and their respective absolute uncertainties for catalyst C14. Parameters with no given uncertainty have been estimated manually.

To evaluate the performance of the model, several parity plots are constructed: one for each of the responses. The parity plots help to show the quality of the model, and the parity plots show the performance of each period as described in Section 4. As mentioned, period A for this catalyst (as for the others) is removed due to the observation of unusually large catalyst deactivation specifically for this period. It is believed that the periods B-E are better representations of the catalyst. Additionally, trend plots of the main responses (i.e. the conversion of CO, C_{5+}-selectivity, and CH_4-selectivity) are generated. Further, residual plots of the main responses are constructed. The residual plots can be found in Appendix A.4.

In Figure 5.10, the parity plots of the conversion of CO, C_{5+}-selectivity, and CH_4-selectivity for catalyst C14. Only periods B-E are considered when doing the model fitting, and as such only these periods are shown in the parity plots. In each parity plot, the responses of the model are plotted against the responses measured experimentally. A reference line is also included to see how well the model is able to describe the experimental data.

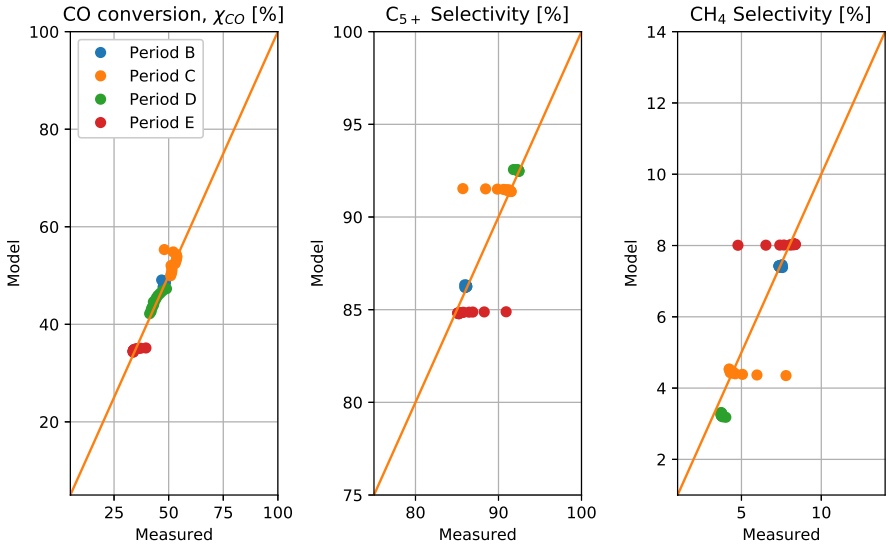

Figure 5.10: Parity plots of the conversion of CO, C_{5+}-selectivity, and CH_4-selectivity for catalyst C14. Periods B-E are shown in the plot. Only these are considered when doing the model fitting.

Figure 5.11 shows the parity plots of the C_2-C_4 paraffin and olefin selectivities, as well as the CO_2-selectivity. As only the periods B-E are considered when doing the model fitting, these periods are shown in each of the parity plots. The model responses are plotted against the responses measured experimentally. Additionally, a reference line is included to see how well the model is capable of describing the experimental data.

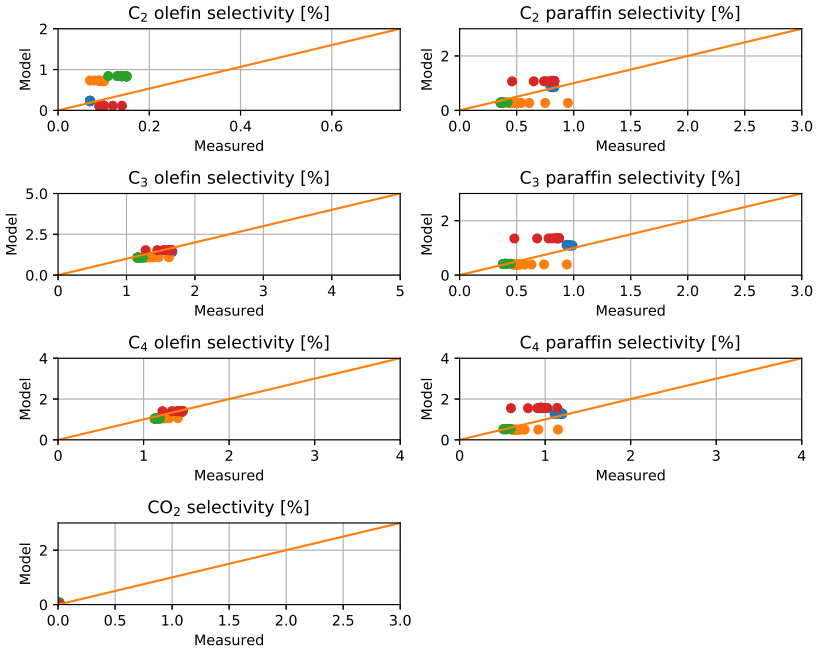

Figure 5.11: Parity plots of the C_2-C_4 paraffin and olefin selectivities, as well as the CO_2-selectivity for catalyst C14. The blue dots correspond to period B, the orange dots correspond to period C, the green dots correspond to period D, and the red dots correspond to period E.

In Figure 5.12, the trend plots of the CO-conversion, C_{5+}-selectivity, and CH_4-selectivity are shown for catalyst C14. A H_2/CO-ratio of 2.1 is used for this catalyst. As mentioned, period A is removed from the dataset when doing the model fitting due to unusual catalyst deactivation observed in this period. As such, only the periods B-E are considered when doing the model fitting. Only the periods B-E are shown in the trend plots.

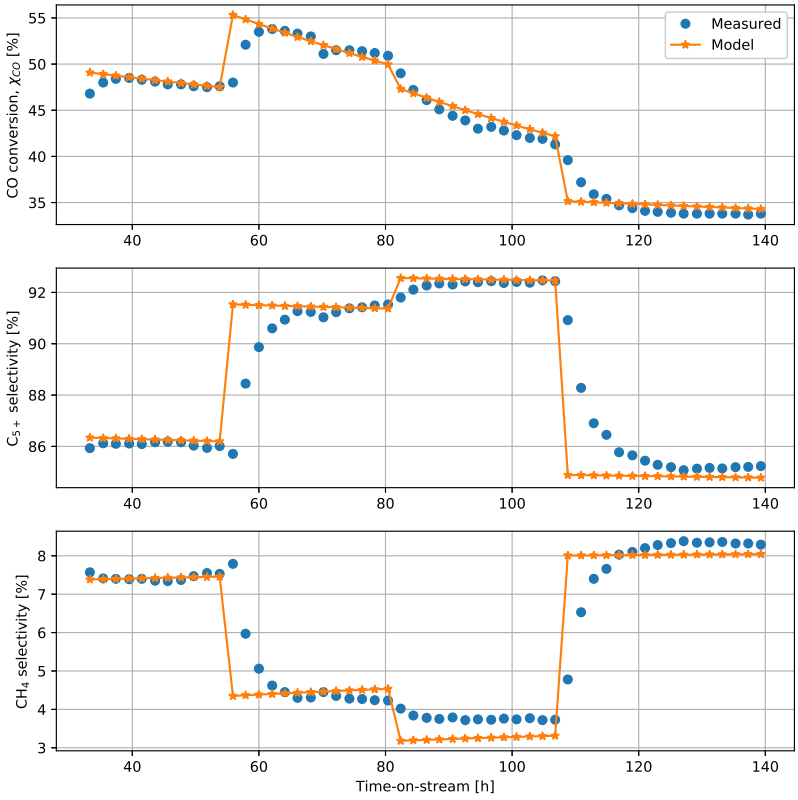

Figure 5.12: Trend plots of the conversion of CO, C_{5+}-selectivity, and CH_4-selectivity for periods B-E for catalyst C14. Each period is run for approximately 30 hours.

5.5 Impact of catalyst characterization on model parameters

As pointed out by Borg et al. [16], the product selectivities, as well as the kinetics are linked to the characterization of the catalyst. As the catalysts C3, C10, C11, and C14 all have different catalyst characterizations, several of the model parameters are plotted against the cobalt dispersions of the catalysts. A linear trend line is drawn for each model parameter to show how a particular parameter changes with the cobalt dispersion. Under the assumption of uniform, spherical Co-particles, the cobalt dispersion becomes inversely proportional to the cobalt particle size [16]. In most cases, the model parameters follow linear trends concerning the cobalt dispersion.
Figure 5.13 shows the model parameters k_1, g, f, y, and x plotted against the cobalt dispersions. Cobalt dispersions of 5.05 %, 7.3 %, 7.9 %, and 8.7 % correspond to catalyst C14, C10, C11, and C3 respectively.

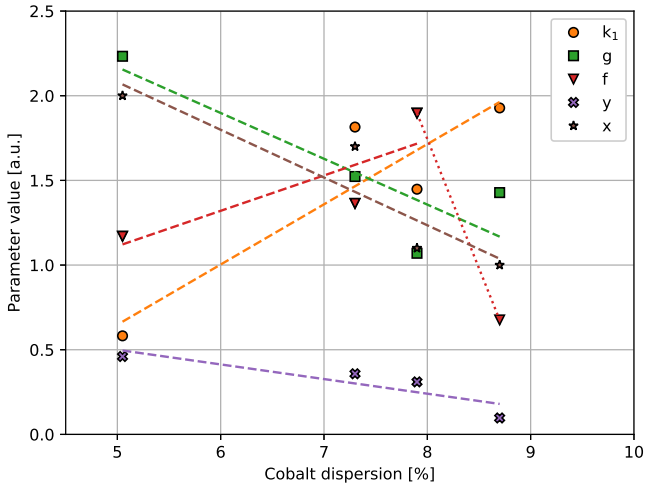

Figure 5.13: A set of model parameters (k_1, g, f, y, and x) as functions of cobalt dispersion. Cobalt dispersions of 5.05 %, 7.3 %, 7.9 %, and 8.7 % correspond to catalyst C14, C10, C11, and C3 respectively. Linear trend lines are also drawn for each model parameter. In most cases the model parameters follows a linear trend with respect to the cobalt dispersion.

In Figure 5.14, the model parameters k_{CH_4}, k_α, and k_{deac} are plotted against the colbalt dispersions. Cobalt dispersions of 5.05 %, 7.3 %, 7.9 %, and 8.7 % correspond to catalyst C14, C10, C11, and C3 respectively.

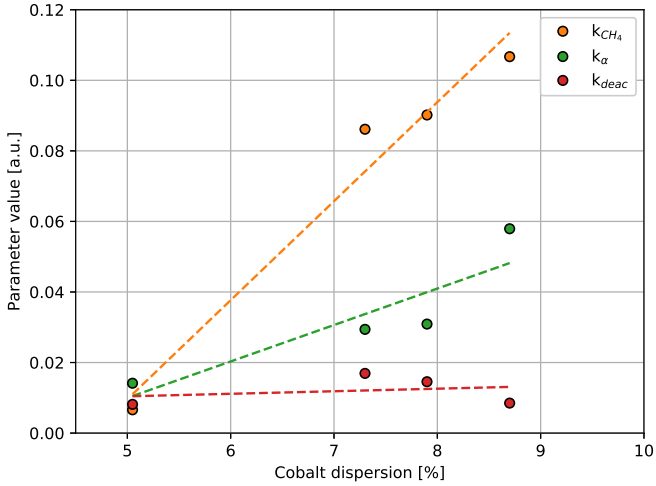

Figure 5.14: A set of model parameters (k_{CH_4}, k_α, and k_{deac}) as functions of cobalt dispersion. Cobalt dispersions of 5.05 %, 7.3 %, 7.9 %, and 8.7 % correspond to catalyst C14, C10, C11, C3 respectively. Linear trend lines are also drawn for each model parameter. The model parameters seem to follow a linear trend with respect to the cobalt dispersion.

In Figure 5.15, the model parameter b is plotted as a function of the cobalt dispersion. Cobalt dispersions of 5.05 %, 7.3 %, 7.9 %, and 8.7 % correspond to catalyst C14, C10, C11, and C3 respectively. The average C_3 olefin/paraffin ratio for each period B-E are also shown for each catalyst. It can appear as if the parameter b generally follows the same trends as the olefin/paraffin ratios. This is shown in the plot for periods D and E. The periods B and C are also, in general, following the same trends.

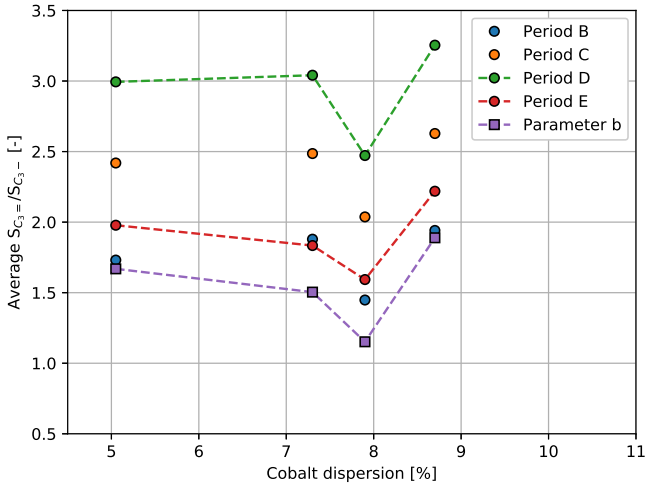

Figure 5.15: The model parameter b plotted as a function of the cobalt dispersion. Cobalt dispersions of 5.05 %, 7.3 %, 7.9 %, and 8.7 % correspond to catalyst C14, C10, C11, and C3 respectively. The average C_3 olefin/paraffin ratio for the periods B-E are also shown in the same plot. The trends in the olefin/paraffin ratios of periods D and E are also indicated by a line. The periods B and C also follow the same trends.

5.6 Commercial type catalyst, $H_2/CO = 2.1$

For the commercial type catalyst with $H_2/CO = 2.1$, the estimated parameters and their respective absolute uncertainties are shown in Table 5.5. The parameters with no given uncertainty have been estimated manually. As the commercial type catalyst is a variant of catalyst C10, several of the estimated parameters remain the same between this catalyst and catalyst C10. Some variations could be expected in terms of catalyst performance due to different productions. Further, the temperature is set to the reported 483 K for all periods in the experimental run. A case where the temperatures in periods B and C are changed is shown in Appendix B.

Parameter	Estimated value [a.u.]	Uncertainty [a.u.]
k_1	1.464	± 0.1553
a	3.50	-
b	1.504	-
f	1.364	± 1.152
g	1.523	-
β_o	0.10	-
k_{CH_4}	0.09013	± 0.01055
x	1.70	± 2.24
k_4	1.0	-
k_{wgs}	0.0010	-
k_d	0.01756	± 0.009759
k_α	0.03442	± 0.01295
y	0.278	± 0.126
c_{α_4}	0.70	-

Table 5.5: Estimated parameters and their respective absolute uncertainties for the commercial type catalyst with $H_2/CO = 2.1$. Parameters with no given uncertainty have been estimated manually.

To evaluate the quality of the model, several parity plots are constructed; one for each response. The parity plots show the performance of each period as described in Section 4. Further, trend plots of the main responses (i.e. the conversion of CO, C_{5+}-selectivity, and CH_4-selectivity) are also constructed. Furthermore, the residual plots of the main responses are constructed. The residual plots can be found in Appendix A.5.

Figure 5.16 shows the parity plots of the CO-conversion, C_{5+}-selectivity, and CH_4-selectivity for the commercial type catalyst with $H_2/CO = 2.1$. In each parity plot, the responses predicted by the model in each period are plotted against the same responses measured experimentally. A reference line is also included to see how well the model fits the experimental data. The temperature is kept at 483 K in all the periods in this case.

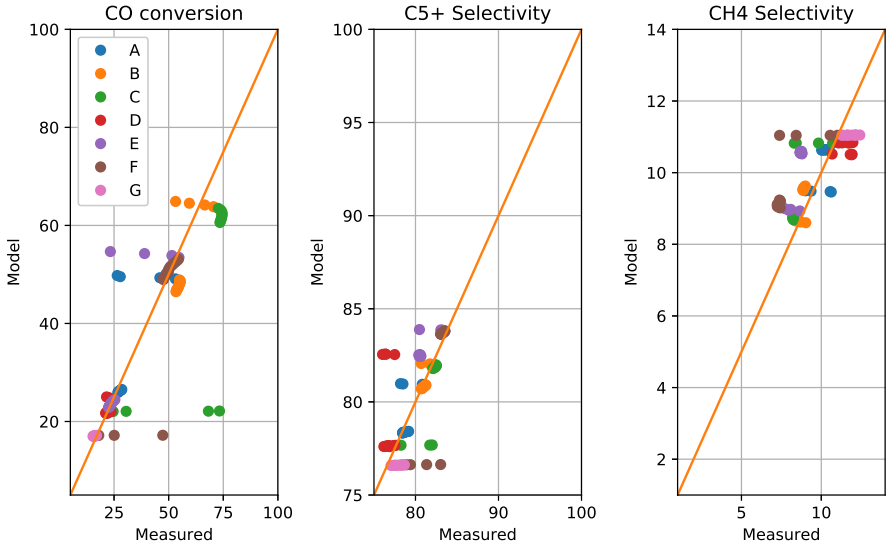

Figure 5.16: Parity plots of the conversion of CO, C_{5+}-selectivity, and CH_4-selectivity for the commercial type catalyst with $H_2/CO = 2.1$. All periods A-G are shown in the plot.

In Figure 5.17, the parity plots of the C_2-C_4 paraffin and olefin selectivities, as well as the CO_2-selectivity, are shown. In each parity plot, the responses predicted by the model in each period are plotted against the same responses measured experimentally. A reference line is included to show how well the model fits the experimental data. The temperature is kept at 483 K across all the periods.

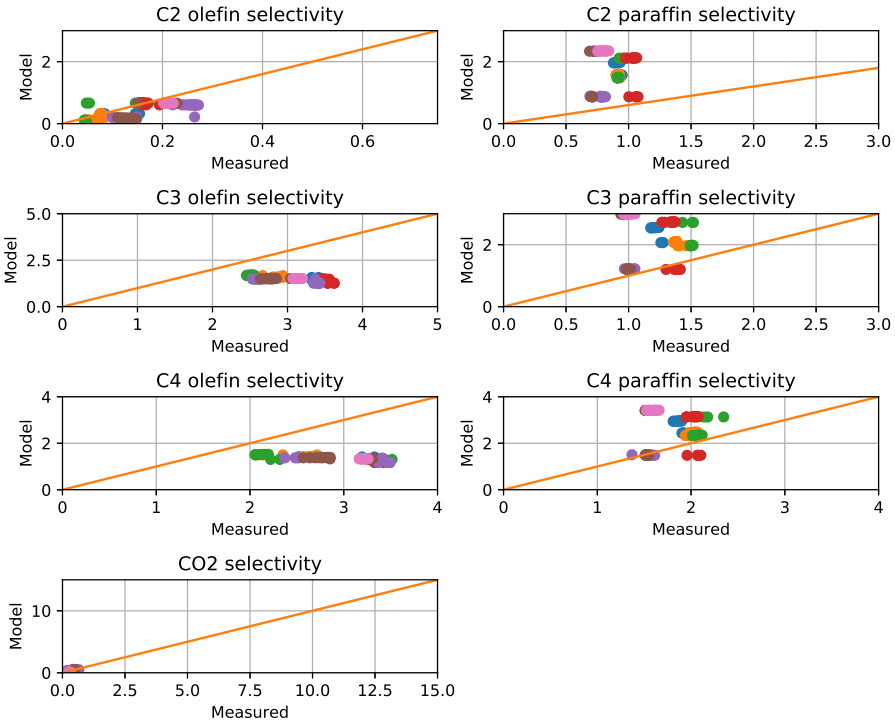

Figure 5.17: Parity plots of the C_2-C_4 paraffin and olefin selectivities, as well as the CO_2-selectivity for the commercial type catalyst with H_2/CO = 2.1. The blue dots correspond to period A, the orange to period B, the green to period C, the red to period D, the purple to period E, the brown to period F, and the pink to the period G.

In Figure 5.18, the trend plots of the main responses are shown for the commercial type catalyst with $H_2/CO = 2.1$. In the trend plots, an alternative model (labeled simply as *Model 2*) is also included. The model structure remains the same for both models, with the exception of the methane formation rate expression, which for Model 2 is replaced by the methane formation rate expression defined in Equation (2.25). The notable differences between the models are observed in the CH_4-selectivities in periods E and F. It should be noted that the estimated parameters and their uncertainties as shown in Table 5.5 are for Model 1. Model 2 is shown in its entirety in Appendix D. The model parameters and respective absolute uncertainties for Model 2 are also shown in Appendix D.5.

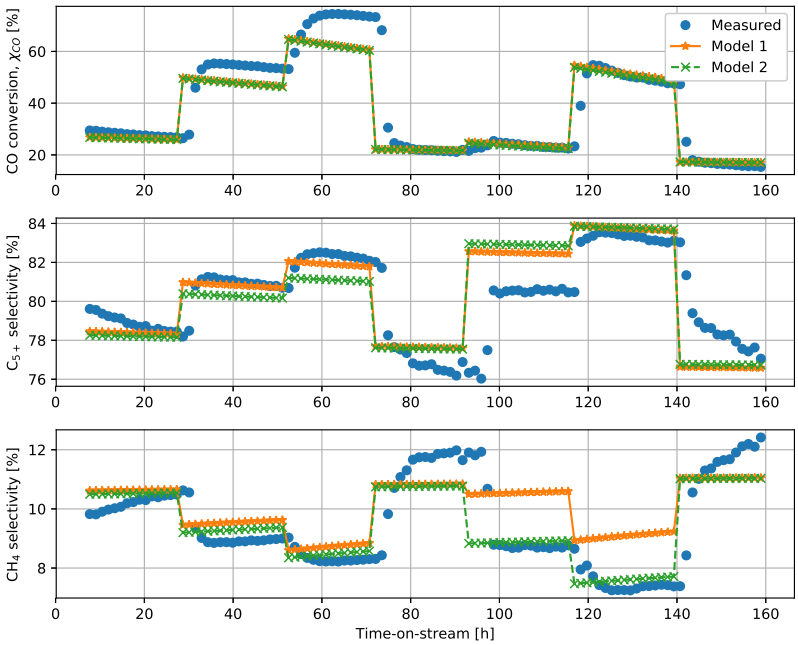

Figure 5.18: Trend plots of the CO-conversion, C_{5+}-selectivity, and CH_4-selectivity for the commercial type catalyst with $H_2/CO = 2.1$. Two models are shown in the trend plots. Both models (the alternative model being labeled as 'Model 2') have mostly the same model structure, with the only difference being in the methane formation rate expression. Model 2 uses a methane formation rate expression as shown in Equation (2.25).

5.7 Commercial type catalyst, $H_2/CO = 1.12$

For the commercial type catalyst with $H_2/CO = 1.12$, the estimated parameters and their respective absolute uncertainties are shown in Table 5.6. The parameters with no given uncertainty have been estimated manually. As the commercial type catalyst is a variant of catalyst C10, several of the estimated parameters remain the same between this catalyst and catalyst C10. Some variations could be expected in terms of catalyst performance due to different productions. When doing the model fitting, no periods with addition of water are considered due to some odd behavior of the experimental data, including a drop in C_{5+}-selectivity when water is added. As such, the effect of water on conversion and selectivities are not well estimated in this case.

Parameter	Estimated value [a.u.]	Uncertainty [a.u.]
k_1	0.6226	± 0.2090
a	3.50	-
b	1.504	-
f	1.364	± 3.175
g	1.523	-
β_o	0.10	-
k_{CH_4}	0.09013	±0.08978
x	1.70	± 5.89
k_4	0.50	-
k_{wgs}	0.0010	-
k_d	0.01756	± 0.01662
k_α	0.05581	± 0.09131
y	0.278	± 0.614
c_{α_4}	0.70	-

Table 5.6: Estimated parameters and their respective absolute uncertainties for the commercial type catalyst with $H_2/CO = 1.12$. Parameters with no given uncertainty have been estimated manually. As the periods with water addition are not included due to odd behavior of the experimental data, the effect of water is not well accounted for in this case.

To evaluate the performance of the model, several parity plots are constructed; one for each response. Further, trend plots of the main responses (i.e. the CO-conversion, C_{5+}-selectivity, and CH_4-selectivity) are generated. Furthermore, residual plots of the main responses are also constructed. These residual plots

can be found in Appendix A.6.

Figure 5.19 shows the parity plot of the main responses for the commercial type catalyst with $H_2/CO = 1.12$. In each parity plot, the predicted responses by the model are plotted against the experimentally measured responses. A reference line is also included to see how well the model is fitted to the experimental data. It should be mentioned that the periods A-F shown in the plots are without the addition of water, as the experimental data showed some quite unusual behavior when water is added.

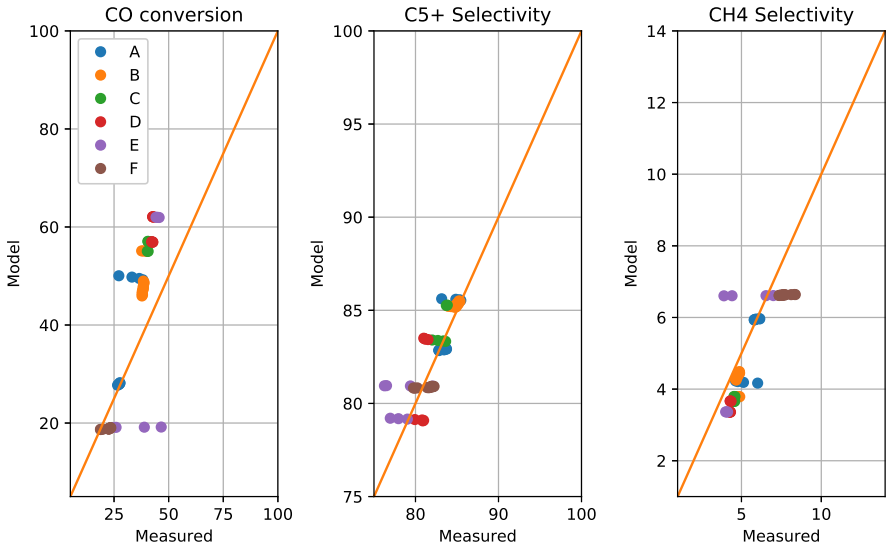

Figure 5.19: Parity plots of the CO-conversion, C_{5+}-selectivity, and CH_4-selectivity for the commercial type catalyst with $H_2/CO = 1.12$. No period with water addition is included when doing the model fitting since the experimental data show some unusual behavior when water is fed to the system.

In Figure 5.20, the parity plots for the C_2-C_4 paraffin and olefin selectivities, as well as the CO_2-selectivity, are shown for the commercial type catalyst with $H_2/CO = 1.12$. In each parity plot, the responses predicted by the model are plotted against the experimentally measured responses. A reference line is also included to see how well the model fits the experimental data. All periods shown, A-F, are without water addition. Further, periods B-E have reduced flow to give higher conversion. The periods with water addition are excluded as the corresponding experimental data show some significant, unusual behavior when water was added to the system, included a drop of C_{5+}-selectivity.

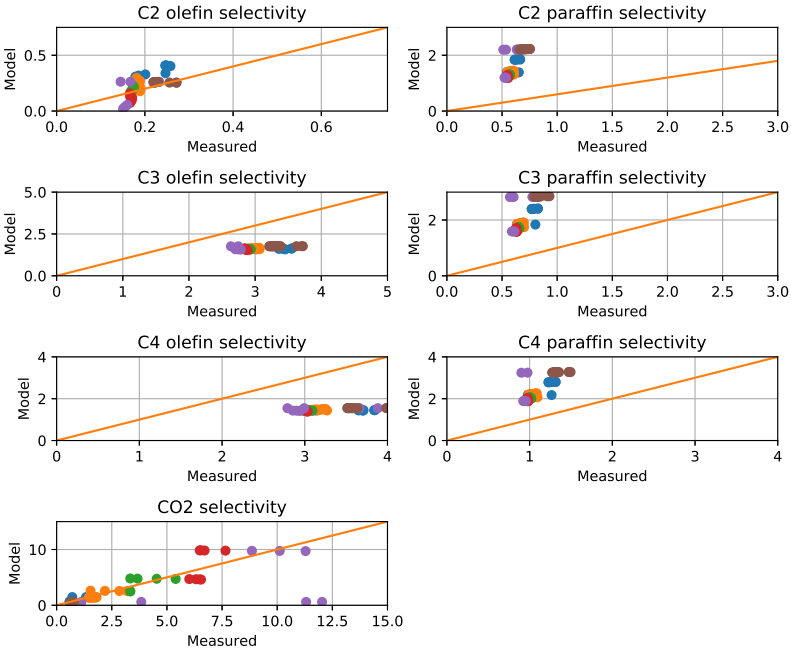

Figure 5.20: Parity plot of the C_2-C_4 paraffin and olefin selectivity, along with the CO_2-selectivity, for the commercial type catalyst with $H_2/CO = 1.12$. All periods shown in the figure are without water addition as the experimental data show some quite unusual behavior when water is fed to the reactor inlet. The blue dots correspond to period A, the orange to period B, the green to period C, the red to period D, the purple to period E, and brown to period F.

Figure 5.21 shows the trend plots for the main responses for the commercial type catalyst with $H_2/CO = 1.12$. The periods, A-F, shown in the trend plots are without the addition of water to the reactor inlet as when water was added to the system, some odd behaviors were observed experimentally, including a drop in C_{5+}-selectivity. The periods B-E are under reduced flow rate.

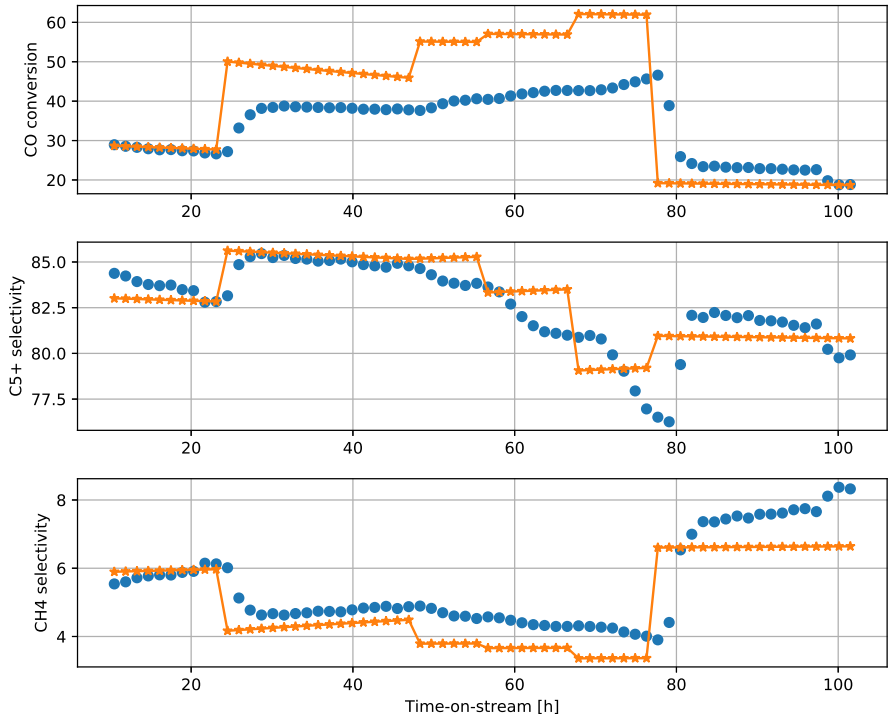

Figure 5.21: Trend plots of the conversion of CO, C_{5+}-selectivity, and CH_4-selectivity for the commercial type catalyst with $H_2/CO = 1.12$. No period with the addition of water is included when doing the model fitting as the experimental data show some unusual responses when water is added to the system.

6 Discussion

6.1 Catalysts C3, C10, C11, and C14

The proposed model, as outlined in Section 5, is overall quite capable of describing the data for the catalysts C3, C10, C11, and C14. The proposed model is based on the consorted vinylene mechanism as proposed by Rytter et al. [1]. As can be seen from the tables containing the model parameters and the respective absolute uncertainties for each catalyst, the uncertainties show that the estimated model parameters are all statistically significant. Additionally, the parity and trend plots also indicate that the proposed model is adequately describing the experimental data. As demonstrated very well in the parity plots and trend plots of the CO-conversion, the kinetic model can correctly account for the effect of water, even being able to show both positive and negative effects, as observed, for instance, for catalysts C10 and C14 in Figure 5.6 and Figure 5.12.
In the trend plots, some transient behavior can be observed experimentally, particularly at the beginning of each period (this transient behavior can be seen clearly in the trend plot for catalyst C14 shown in Figure 5.12), which are not captured by the model. However, as the conditions at the reactor inlet remain constant throughout each particular period, it is expected that the model, for one particular period, should predict a constant CO-conversion level. The only variations to the CO-conversion across a period are due to the catalyst deactivation.

To model the catalyst deactivation, a second order deactivation model including the effect of water, as displayed in Section 5, was found to adequately describe the deactivation of the catalyst. By including the partial pressure of water, the catalyst will deactivate faster as more water is fed to the reactor inlet or as more water is produced by the synthesis, and as such the correct behavior with respect to water is captured by the model. This behavior can readily be observed by considering the trend plots for the catalysts. On the other hand, it should be pointed out that as water plays important roles in both the reaction kinetics and catalyst deactivation, it can be a challenge to properly separate the two effects of water, particularly at the beginning of periods where water is added. When doing the modeling it was assumed that the initial response to water was (mostly) kinetic in nature, and so the parameters in the kinetic expression (mainly to r_1) were changed to capture these responses. As mentioned

in both Section 4 and Section 5, for catalysts C3, C10, C11, and C14, the initial period (period A with low CO-conversion) is not considered when doing the model fitting. For these catalysts, unusually large catalyst deactivations were observed in this particular period. In some cases, the initial deactivation caused a drop of nearly 10 % to CO-conversion. Due to this uncharacteristic catalyst deactivation, it was decided to not consider the period when fitting the model to the experimental data. It was believed that the periods B-E were more correctly representing the catalysts. As mentioned above, for periods B-E, the proposed deactivation model seems quite able to capture the catalyst deactivation.
At this point, it should be mentioned that in the deactivation model, no specific deactivation mechanism (such as sintering, re-oxidation, poisoning, etc.) is considered. Instead, the deactivation model describes only the loss of (relative) active sites on the catalyst surface over time.
When studying the catalyst deactivation over longer periods of time, it can appear as if the deactivation approaches some asymptotic offset as pointed out by Forzatti and Lietti [53]. Such a behavior is not included in the proposed catalyst deactivation model. In fact, with the current model, as the TOS tends to become very large, the relative number of active sites will tend toward zero as well. A modification to account for this asymptotic behavior has not been attempted. The proposed deactivation model has only been tested for relatively low TOS ($< \sim 160$ h).

To describe the product selectivities, the chain growth model, as outlined in Section 5, was found, for all catalysts, to be adequate at explaining the data, especially when considering the C_{5+}-selectivities. The proposed chain growth model is quite interesting as it is not containing the partial pressure of hydrogen, something several other proposed chain growth models do. From the consorted vinylene mechanism, it is reasoned that hydrogen is a part of both the propagation and the termination steps [1]. As such, the partial pressure of hydrogen is not directly a part of the chain growth model.
The effect of water is also well accounted for by the model, enhancing the C_{5+}-selectivity, an important behavior observed for C_{5+} as reported by several authors [14, 18, 19, 20, 21].
The α-model does, however, overpredict the C_{5+}-selectivity in the periods C and D for catalyst C11. When considering the experimental data, a lot of inherent noise appears to be present in the data. Particularly, it is difficult to see exactly how this catalyst responds to water (with respect to the C_{5+}-selectivity) as initially, it does not appear that the C_{5+}-selectivity increases when large amounts of water is added in period D. However, it appears as if the selectivity increases

after some time. Due to the noise, and uncertainty of some periods for catalyst C11, the effect of water is more difficult to estimate properly compared to the catalysts C3, C10, and C14.
As with the kinetics, some transient behavior is also observed in the selectivities. This is perhaps most notable in catalyst C3 where, in period B, the experimentally observed C_{5+}-selectivity falls from $\sim$ 80 % to $\sim$ 78.5 % over the period. The model predicts a near constant C_{5+}-selectivity over the same period. It is believed that the experimental points close to the end of the periods are near steady-state, and as such these points are in focus when doing the model fitting.

For the catalysts C3, C10, C11, and C14, the proposed methane formation model is adequately describing the CH_4-selectivities and is able to capture the effects of water on the selectivities, even though water is not actively a part of the formation rate expression. As water is added, the partial pressures of the other components in the system will decrease (keeping the total pressure constant), including the partial pressure of hydrogen, and as such, the expected responses are observed.
For the catalysts C10 and C11, the CH_4-selectivities are generally described very well by the methane formation model, though for these catalysts, the model systematically underpredicts the CH_4-selectivities in period E by $\sim$ 1 %. It is not clear why these deviations take place. Further, an alternative methane formation model in which the partial pressure of water is actively a part of the methane formation model is shown in Appendix D. This alternative model also underpredicts the CH_4-selectivities in the same way by approximately the same amount.

The secondary responses, namely the C_2-C_4 paraffin and olefin selectivities as well as the CO_2-selectivities, are explained reasonably well by the model. However, in general, the model systematically overpredicts the paraffin selectivities, while also systematically underpredicting the olefin selectivities. In general, the further polymerization reaction seems reasonable at describing the non-ASF behavior of ethene. With the inclusion of the further polymerization reaction of ethene, the ethene selectivities in the periods B and E are explained reasonably well by the model. However, the model also seems to systematically overpredict the ethene selectivities in the periods where water is added, namely in the periods C and D. This behavior is observed across all four catalysts. Seemingly, the effect of water on the ethene production is not correctly accounted for.
For the catalysts C3, C10, C11, and C14, the CO_2-selectivities are also very well explained across all periods by the introduction of the WGS reaction. Generally, the formation of CO_2 is quite small for these catalysts (at the most, the

CO_2-selectivity goes up to approximately 2 %). For catalyst C14, the selectivity of CO_2 is very small (significantly below 1 %) compared to the other catalysts.

As the catalysts have different characterizations, several of the model parameters can be plotted against, in this case, the cobalt dispersion to see how the model parameters change with the different catalysts. These plots can be seen in Figure 5.13, Figure 5.14, and Figure 5.15. In general, it appears that most model parameters follow linear trends with respect to the cobalt dispersions. One notable exception, however, is for the parameter f for catalyst C3 which significantly deviates from the general linear trend observed for the parameter, even though the other parameters used for catalyst C3, do follow the linear trend lines.
Interestingly, the parameter b, which is describing the coverage of hydrogen on the catalyst surface [1], does not appear to follow a linear trend, but rather seems to follow the olefin/paraffin ratios. In Figure 5.15, the average C_3 olefin/paraffin-ratio is plotted for each period, though similar trends are also observed for the C_2 and C_4 olefin/paraffin ratios. From the consorted vinylene mechanism, and also from what is generally understood as outlined at the beginning of Section 2, olefins are the primary products of the synthesis. The olefins can go through a hydrogenation step to form the corresponding paraffins, and it is observed variations in the olefin/paraffin ratios between different catalysts. It has been suggested that these variations are related to the activity of the olefin hydrogenation [54]. As such, it appears as though the model parameter b follows the olefin hydrogenation activity of the catalysts.

In general, the proposed model as outlined at the beginning of Section 5 works very well at describing the Fischer-Tropsch synthesis, being adept at account for the main responses including the effect of water.

6.2 Commercial type catalyst

The commercial type catalyst, as mentioned in Section 4, is a variant of catalyst C10. As such, several of the estimated parameters remain the same between the commercial type catalyst and catalyst C10. Some variations are expected as the catalyst performance is slightly different due to different productions. For the commercial type catalyst, two different H_2/CO-ratios of 2.1 and 1.12 are considered and shown in Section 5. A third H_2/CO-ratio of 1.72 is also considered and is shown in Appendix C. It should be noted that as the experimental data for this experiment seem rather inconsistent, several periods are not modeled

accurately. For the experiment with $H_2/CO = 1.72$, periods B and D are operated at the same flow rates corresponding to a CO-conversion of approximately 50 %, though in period B, the experimentally measured conversion overshoots at 60 %. It is not known why, however, one possibility is a change in temperature. A similar case is observed for the commercial type catalyst with $H_2/CO = 2.1$. Further, even when the CO-conversion increases from approximately 32 % in period A to 40 % in period C, the experimental data show a small drop in the C_{5+}-selectivity and a small increase in the CH_4-selectivity. This is contrary to the expected responses in which the C_{5+}-selectivity increases with increased conversion, while the CH_4-selectivity decreases with an increased conversion. Lastly, for this experiment, only the final period has water added to the reactor inlet. The remaining periods with added water were removed when doing the model fitting as experimentally the C_{5+}-selectivity was found to decline. As this particular dataset contains a significant amount of inconsistencies, the model fitted to these data is chosen to be shown in Appendix C.

As with catalysts C3, C10, C11, and C14, for the commercial type catalyst, a second order deactivation model including the effect of water was found to adequately describe the catalyst deactivation.
For the commercial type catalyst with $H_2/CO = 2.1$, the model used for catalyst C10 was found to also be adept at explaining the experimental data for this experiment, however, the model is not capable of describing the CH_4-selectivity when water is added to the reactor inlet. It should be noted that a few parameter values were changed, most notably the values for k_1, k_{CH_4}, k_α, and y. In general, the estimated absolute uncertainties show that all model parameters (with the exception of x) are statistically significant. The parameter x is a part of the methane formation model, and it can be seen in Figure 5.18 that the model presented at the beginning of Section 5 (referred to as *Model 1*) is unable to properly estimate the CH_4-selectivity when water is added. Model 1 only predicts a minor drop in the CH_4-selectivity when water is added to the reactor in the periods E and F. The observed behavior might be related to how water is fed to the system. For the catalysts C3, C10, C11, and C14, the total pressure is kept constant at 20 bar when water is added. As a result, the partial pressure of H_2 will drop with added water and thus the expected behavior is seen, even though water is not actively a part of the methane formation model.
On the other hand, for the commercial type catalyst, when water is added to the reactor inlet, the total pressure is increased to 22 bar - up from 20 bar when dry syngas is fed to the reactor. As water is added to obtain approximately 10 % water pressure at the reactor inlet, the partial pressure of hydrogen should

decrease accordingly, and a predicted drop in the CH_4-selectivity is observed, albeit very small. There is also a possibility that the increase in total pressure in the periods with added water causes the model to not properly capture the effect of water, as this would cause the partial pressure of hydrogen to again increase. The combination of the two effects, paired with a slight increase in CO-conversion explained above, could be the reason why the model only predicts a slight decrease in the CH_4-selectivity when water is first added to the reactor inlet in period E. As the experiment shows a significant response when water is added, it might indicate that the effect of water is kinetic by nature, as suggested by Ma et al. [20]. In light of this, an alternative model is also shown (referred to as *Model 2*) in which water is actively a part of the methane formation model. A part from the methane formation rate expression, the structure of Model 2 is identical to that of Model 1. The alternative model is shown in its entirety in Appendix D, and shown specifically for the commercial type catalyst with $H_2/CO = 2.1$ in Appendix D.5. The alternative model does seem to improve the CH_4-selectivity for the commercial type catalyst as shown in Figure 5.18. The alternative model is also fitted to the catalysts C3, C10, C11, and C14, and it appears that the alternative model is also explaining these experimental data to a satisfactory degree.
For the experiment run with $H_2/CO = 1.72$, while only a single period of water is considered, it can also be observed that the CH_4-selectivity responds significantly to water.

By studying the trend plots for the commercial type catalyst with $H_2/CO = 2.1$, it can be seen that the periods B and C, for the CO-conversion, are not captured by the model. Specifically, the model is systematically underestimating the CO-conversion in these particular periods. For period B, reportedly, the flow rate was adjusted to reach a conversion of approximately 50 %, though it can be seen that the conversion reaches nearly 55 %. While there might be several reasons the model is unable to adequately estimate the CO-conversion in these periods, one possibility is a change in temperature due to the exothermic nature of the Fischer-Tropsch synthesis. By making a small (4 K) change to the temperature in these periods, and introducing temperature dependencies of several model parameters, it is observed that the model can estimate the measured conversion levels in these periods way better. It should be noted that the activation energies required for the temperature dependencies are not estimated by the ODR, however, approximate values obtained from a previous project were used. In the previous project, data obtained for a CSTR were used and fitted to a model.

The results of making the changes to the temperature as described above for the commercial type catalyst with $H_2/CO = 2.1$ can be seen in Appendix B.

In general, both the kinetic model and the chain growth model seem adequate at describing the experimental data for the commercial type catalyst. The chain growth model does, however, systematically overestimate the C_{5+}-selectivity in period E. Exactly why the model is overestimating this period is uncertain, and as seen in Figure 5.18, both Model 1 and Model 2 predict roughly the same C_{5+}-selectivity. Additionally, it can be seen that the chain growth model is not properly accounting for the C_{5+}-selectivities for low CO-conversions (specifically periods D and G), though it should also be noted that these periods seem to have more noise compared to the other periods. A similar observation can also be noted for the CH_4-selectivities in the same periods.

As outlined in Section 4 and Section 5, for the commercial type catalyst with $H_2/CO = 1.12$, the periods with added water are not considered when doing the model fitting due to some unexpected, and inconsistent, behavior. Specifically, the C_{5+}-selectivity drops when water is first added to the system. As the periods with water are excluded, estimating the effect of water cannot be done in any significant way for this dataset. Further, by considering the trend plots shown in Figure 5.21, it appears as though the model is unable to correctly estimate the CO-conversion for this H_2/CO-ratio operated at reduced flows. It is expected that the theoretical maximum CO-conversion is at about 50 % as the stoichiometric hydrogen consumption coefficient is approximately 2 (a conservative estimate). This, too, seems to be the case as the experimental data slowly reaches CO-conversions close to 50 % under strictly reduced flow (corresponding to period E).
The model predicts that a CO-conversion level of 60 % is achievable. This model behavior could potentially be explained from the WGS reaction. As is noticed in Figure 5.20, the CO_2-selectivities become quite large (peaking at about ~ 12 % in period E). As the WGS also produces H_2, the corresponding production of hydrogen from the WGS will also be quite large when the CO_2-selectivity is large. It is possible that this additional H_2-production allows the model to convert even more CO through the Fischer-Tropsch synthesis, and thus the CO-conversion increases. While it appears as if the model breaks down under these extreme conditions, it should also be noted that the model remains consistent in the way that it never estimates any unphysical values, such as negative partial pressures, though the partial pressure of hydrogen becomes very close to zero in some instances.
As the model breaks down under these extreme conditions, the model can not

be expected to properly capture the product selectivities to a satisfactory degree either.

7 Conclusion

The proposed model is based on the consorted vinylene mechanism as proposed by Rytter et al. [1].
For the catalysts C3, C10, C11, and C14, the proposed model for the Fischer-Tropsch synthesis including the effect of water, is capable of predicting the main responses very nicely. This also includes the CH_4-selectivities although water is not actively a part of the methane formation model. The expected responses are still observed as an increase in the partial pressure of water causes a corresponding decrease to the partial pressure of hydrogen. For these catalysts, the CO-conversions are also very well estimated, with the model being able to correctly account for the various effects of water.
For all the catalysts under investigation in this thesis, a second order deactivation model including the effect of water was found to adequately describe the way the catalysts deactivate over time. The proposed deactivation model is able to account for an important behavior of the catalyst deactivation when water is added, namely that water increases the catalyst deactivation. It is believed that water enhances the effect of sintering [18].
Perhaps most interestingly, the proposed chain growth model is able to properly describe the product selectivities (especially the C_{5+}-selectivities) although this chain growth model does not contain the partial pressure of hydrogen, something most other proposed chain growth models do. The lack of the partial pressure of hydrogen is explained from the consorted vinylene mechanism where hydrogen is part of both the propagation and termination step. Furthermore, the effect of water is also well described by the chain growth model, and the correct behavior of the C_{5+}-selectivities are observed by the model.
By studying catalysts with different characterizations, it was found that most model parameters generally follow linear trends with respect to the cobalt dispersions. The most notable exception from these linear trends is the parameter b. This parameter describes the coverage of hydrogen on the catalyst surface, and it was observed that this parameter seems to follow the olefin hydrogenation activity of the catalysts.
By introducing the water-gas shift reaction, the CO_2-selectivities are also well explained by the model.

For the commercial type catalyst, a variant of the catalyst C10, the proposed model is also quite capable of describing the CO-conversion and the C_{5+}-selectivity, however, the model struggles to properly estimate the correct response for the CH_4-selectivity when water is added to the reactor inlet. In light

of these observations, an alternative model has been proposed in which water is actively a part of the methane formation model. This model does seem to perform significantly better concerning the CH_4-selectivities in the periods where water is added. The alternative model was also fitted to the experimental data for the catalysts C3, C10, C11, and C14, and both fitted models show the same performances for these particular catalysts.
It should also be pointed out that there are some experimental differences between the commercial type catalyst experiments, and the experiments carried out for the catalysts C3, C10, C11, and C14. For the experiments ran with the commercial type catalyst, when water is added to the reactor inlet, the total pressure is raised to 22 bar. In the periods where only dry syngas is fed to the reactor, the total pressure is kept at 20 bar. On the other hand, for the catalysts C3, C10, C11, and C14, the total pressure is always kept at 20 bar even when water is added. For the commercial type catalyst, the proposed model predict an expected decrease in the CH_4-selectivity, albeit only a very small drop is observed. This model behavior could be a combined result of the addition of water and increased total pressure. As the experimental data show a significant responses to water, it could also hint that water should actively be a part of the methane formation model, as shown in Appendix D. The alternative model captures the behavior with respect to water for the CH_4-selectivity of the commercial type better. However, to be able to draw definitive conclusions, more testing should be carried out.
For the commercial type catalyst with $H_2/CO = 1.12$, it is observed that the CO_2-selectivity becomes significant when operated at reduced flows. It appears as if the proposed model breaks down under these conditions, with the model predicting higher CO-conversion levels than the expected. As a result, it is difficult to properly estimate the product selectivities in this case. It should also be noted that, even though the model breaks down, the mode also remain consistent and never estimates any unphysical values, though the partial pressure of hydrogen under significantly reduced flow becomes very close to zero.

8 Future work

The proposed model seems overall to be quite good, though more testing should be done. The following bullet points should be considered moving forward with the model.

- The model should be tested for more datasets to see how the model is able to describe the data. Datasets with different catalyst characterization could help study the trends observed in this thesis.
- The model should be tested for even more H_2/CO-ratios. So far, only three such ratios of 2.1, 1.72, and 1.12 have been tested.
- The methane formation model should be looked more into, which will require to study the effect of water on the methane formation.
- The temperature dependency of the model parameters should be estimated. So far, only a single temperature of 210 °C, has been considered. The temperature dependency will be important as it is known that the temperature will affect the responses. To do this, data at different temperatures are required.
- The model could be expanded by introducing an energy balance as well. This would also require data at different temperatures.
- The model could also be expanded by using a heterogeneous model over a pseudo-homogeneous model (which is currently used). This would require a study of the heat- and mass transfer inside the catalyst particle.

List of Symbols

Symbol	Description	Unit
U_i	Stoichiometric coefficient for hydrogen consumption	-
$\nu_{i,j}$	Product stoichiometric coefficient	-
α	Chain growth propagation probability	-
y_n	Molar fraction of hydrocarbon with chain length n	-
ω_n	Weight fraction of hydrocarbon with chain length n	-
$\bar{n}_n$	Average carbon number	-
$\bar{n}_w$	Weight average carbon number	-
r_i	Reaction rate of reaction i	$\mathrm{kmol\,kg^{-1}\,h^{-1}}$
P_i	Partial pressure of component i	MPa
D	Deactivation of catalyst	-
W_{tot}	Total mass flow	$\mathrm{kg\,h^{-1}}$
$\tilde{R}_i$	Total reaction rate of component i	$\mathrm{kg\,kg^{-1}\,h^{-1}}$
$\hat{R}_i$	Total reaction rate of component i	$\mathrm{kmol\,kg^{-1}\,h^{-1}}$
ρ_{cat}	Catalyst density	$\mathrm{kg\,m^{-3}}$
ξ	Dimensionless volume	-
m_{cat}	Catalyst mass	kg
S_{C_i}	Selectivity of carbon i	-
Y_i	Observed measurement i	-
X_i	Independent variable i	-
$s_{\hat{\beta}_i}$	Estimated standard deviation of parameter $\hat{\beta}_i$	-
ε	Noise associated with measurement	-
δ	Noise associated with explanatory variable	-
σ	Standard deviation	-
ω_i	Weight used in ODR defined as $1/\sigma_{\varepsilon_i}$	-
d_i	Weight used in ODR defined as $\sigma_{\varepsilon_i}/\sigma_{\delta_i}$	-
χ	Conversion	-
T	Temperature	K

References

[1] Erling Rytter and Anders Holmen. "Consorted Vinylene Mechanism for Cobalt Fischer–Tropsch Synthesis Encompassing Water or Hydroxyl Assisted CO-Activation." In: *Topics in Catalysis* 61.9 (2018), pp. 1024–1034. URL: https://doi.org/10.1007/s11244-018-0932-3.

[2] Vadim S. Ermolaev, Kirill O. Gryaznov, Eduard B. Mitberg, Vladimir Z. Mordkovich, and Valentin F. Tretyakov. "Laboratory and pilot plant fixed-bed reactors for Fischer–Tropsch synthesis: Mathematical modeling and experimental investigation." In: *Chemical Engineering Science* 138 (2015), pp. 1 –8. URL: http://www.sciencedirect.com/science/article/pii/S0009250915005217.

[3] I. Puskas and R.S. Hurlbut. "Comments about the causes of deviations from the Anderson-Schulz-Flory distribution of the Fischer-Tropsch reaction products." English. In: *Catalysis Today* 84.1-2 (2003), pp. 99–109.

[4] A. Lillebø, E. Rytter, E. A. Blekkan, and A. Holmen. "Fischer–Tropsch Synthesis at High Conversions on Al2O3-Supported Co Catalysts with Different H2/CO Levels." In: *Industrial & Engineering Chemistry Research* 56 (2017), pp. 13281–13286. URL: https://doi.org/10.1021/acs.iecr.7b01801.

[5] Magne Hillestad. "Modeling the Fischer–Tropsch Product Distribution and Model Implementation." In: *Chemical Product and Process Modeling* 10 (Sept. 2015).

[6] Hamid Mahmoudi, Maedeh Mahmoudi, Omid Doustdar, Hessam Jahangiri, Athanasios Tsolakis, Sai Gu, and Miroslaw Lech Wyszynsk. "A review of Fischer-Tropsch synthesis process, mechanism, surface chemistry and catalyst formulation." In: *Biofuels Engineering* 2 (Mar. 2017).

[7] Cheryl K Rofer-DePoorter. "A comprehensive mechanism for the Fischer-Tropsch synthesis." In: *Chemical Reviews* 81.5 (1981), pp. 447–474.

[8] T. M. L. Wigley, R. Richels, and J. A. Edmonds. "Economic and environmental choices in the stabilization of atmospheric CO2 concentrations." In: *Nature* 379 (1996), pp. 240 –243. URL: https://doi.org/10.1038/379240a0.

[9] Hans Schulz. "Short history and present trends of Fischer–Tropsch synthesis." In: *Applied Catalysis A: General* 186.1 (1999), pp. 3 –12. URL: http://www.sciencedirect.com/science/article/pii/S0926860X9900160X.

[10] Peter McKendry. “Energy production from biomass (part 1): overview of biomass.” In: *Bioresource Technology* 83.1 (2002). Reviews Issue, pp. 37 –46. URL: http://www.sciencedirect.com/science/article/pii/S0960852401001183.

[11] Peter McKendry. “Energy production from biomass (part 2): conversion technologies.” In: *Bioresource Technology* 83.1 (2002). Reviews Issue, pp. 47 –54. URL: http://www.sciencedirect.com/science/article/pii/S0960852401001195.

[12] S. C. SAXENA. “Bubble Column Reactors and Fischer-Tropsch Synthesis.” In: *Catalysis Reviews* 37.2 (1995), pp. 227–309. eprint: https://doi.org/10.1080/01614949508007096. URL: https://doi.org/10.1080/01614949508007096.

[13] GERARD P. VAN DER LAAN and A. A. C. M. BEENACKERS. “Kinetics and Selectivity of the Fischer–Tropsch Synthesis: A Literature Review.” In: *Catalysis Reviews* 41.3-4 (1999), pp. 255–318. eprint: https://doi.org/10.1081/CR-100101170. URL: https://doi.org/10.1081/CR-100101170.

[14] Mohammad Ostadi, Erling Rytter, and Magne Hillestad. “Evaluation of kinetic models for Fischer–Tropsch cobalt catalysts in a plug flow reactor.” In: *Chemical Engineering Research and Design* 114 (2016), pp. 236 –246. URL: http://www.sciencedirect.com/science/article/pii/S0263876216302775.

[15] Mark E Dry. “The Fischer–Tropsch process: 1950–2000.” In: *Catalysis Today* 71.3 (2002). Fischer-Tropsch synthesis on the eve of the XXI Century, pp. 227 –241. URL: http://www.sciencedirect.com/science/article/pii/S0920586101004539.

[16] Øyvind Borg, Sigrid Eri, Edd A. Blekkan, Sølvi Storsæter, Hanne Wigum, Erling Rytter, and Anders Holmen. “Fischer-Tropsch synthesis over γ-alumina-supported cobalt catalysts: Effect of support variables.” In: *Journal of Catalysis* 248.1 (2007), pp. 89 –100. URL: http://www.sciencedirect.com/science/article/pii/S0021951707001042.

[17] Hessam Jahangiri, James Bennett, Parvin Mahjoubi, Karen Wilson, and Sai Gu. “A review of advanced catalyst development for Fischer–Tropsch synthesis of hydrocarbons from biomass derived syn-gas.” In: *Catal. Sci. Technol.* 4 (8 2014), pp. 2210–2229. URL: http://dx.doi.org/10.1039/C4CY00327F.

[18] Erling Rytter, Øyvind Borg, Nikolaos E. Tsakoumis, and Anders Holmen. "Water as key to activity and selectivity in Co Fischer-Tropsch synthesis: γ-alumina based structure-performance relationships." In: *Journal of Catalysis* 365 (2018), pp. 334 –343. URL: http://www.sciencedirect.com/science/article/pii/S0021951718302550.

[19] Wenping Ma, Gary Jacobs, Dennis E. Sparks, Robert L. Spicer, Burtron H. Davis, Jennifer L.S. Klettlinger, and Chia H. Yen. "Fischer–Tropsch synthesis: Kinetics and water effect study over 25%Co/Al2O3 catalysts." In: *Catalysis Today* 228 (2014). Natural Gas Conversion the Status and Potentials in the Light of NGCS-10, pp. 158 –166. URL: http://www.sciencedirect.com/science/article/pii/S0920586113004860.

[20] Wenping Ma, Gary Jacobs, Tapan K. Das, Cornelius Mduduzi Masuku, Jungshik Kang, Venkat Ramana Rao Pendyala, Burtron H. Davis, Jennifer L. S. Klettlinger, and Chia H. Yen. "Fischer–Tropsch Synthesis: Kinetics and Water Effect on Methane Formation over 25%Co/γ-Al_2O_3 Catalyst." In: *Industrial & Engineering Chemistry Research* 53.6 (2014), pp. 2157–2166. eprint: https://doi.org/10.1021/ie402094b. URL: https://doi.org/10.1021/ie402094b.

[21] C.E. Kliewer, S.L. Soled, and G. Kiss. "Morphological transformations during Fischer-Tropsch synthesis on a titania-supported cobalt catalyst." In: *Catalysis Today* 323 (2019). Special Issue Honoring Umit S. Ozkan: 2017 ACS Henry H. Storch Award Winner, pp. 233 –256. URL: http://www.sciencedirect.com/science/article/pii/S0920586118305911.

[22] Erling Rytter and Anders Holmen. "Deactivation and Regeneration of Commercial Type Fischer-Tropsch Co-Catalysts—A Mini-Review." In: *Catalysts* 5 (June 2015), pp. 478–499.

[23] Nikolaos E. Tsakoumis, Magnus Rønning, Øyvind Borg, Erling Rytter, and Anders Holmen. "Deactivation of cobalt based Fischer–Tropsch catalysts: A review." In: *Catalysis Today* 154.3 (2010). Eleventh International Symposium on Catalyst Deactivation , Delft(The Netherlands,) October 25-28, 2009., pp. 162 –182. URL: http://www.sciencedirect.com/science/article/pii/S0920586110002282.

[24] Andre P. Steynberg, Soumitra R. Deshmukh, and Heinz J. Robota. "Fischer-Tropsch catalyst deactivation in commercial microchannel reactor operation." In: *Catalysis Today* 299 (2018). Special Issue of Catalysis Today for NGCS 11 Tromsø., pp. 10 –13. URL: http://www.sciencedirect.com/science/article/pii/S0920586117303863.

[25] Øyvind Borg. "Role of Alumina Support in Cobalt Fischer-Tropsch Synthesis." PhD thesis. Norwegian University of Science and Technology, 2007.

[26] Rutger A. van Santen, Albert J. Markvoort, Minhaj M. Ghouri, Peter A. J. Hilbers, and Emiel J. M. Hensen. "Monomer Formation Model versus Chain Growth Model of the Fischer–Tropsch Reaction." In: *The Journal of Physical Chemistry C* 117 (Mar. 2013), pp. 4488–4504.

[27] E.W. Kuipers, I.H. Vinkenburg, and H. Oosterbeek. "Chain Length Dependence of α-Olefin Readsorption in Fischer-Tropsch Synthesis." In: *Journal of Catalysis* 152.1 (1995), pp. 137 –146. URL: http://www.sciencedirect.com/science/article/pii/S0021951785710688.

[28] Dieter Förtsch, Kyra Pabst, and Edwin Groß-Hardt. "The product distribution in Fischer–Tropsch synthesis: An extension of the ASF model to describe common deviations." In: *Chemical Engineering Science* 138 (2015), pp. 333 –346. URL: http://www.sciencedirect.com/science/article/pii/S0009250915004893.

[29] Jun Cheng, P. Hu, Peter Ellis, Sam French, Gordon Kelly, and C. Martin Lok. "A DFT study of the chain growth probability in Fischer–Tropsch synthesis." In: *Journal of Catalysis* 257.1 (2008), pp. 221 –228. URL: http://www.sciencedirect.com/science/article/pii/S0021951708001772.

[30] Branislav Todic, Wenping Ma, Gary Jacobs, Burtron H Davis, and Dragomir B Bukur. "Effect of process conditions on the product distribution of Fischer–Tropsch synthesis over a Re-promoted cobalt-alumina catalyst using a stirred tank slurry reactor." In: *Journal of Catalysis* 311 (2014), pp. 325–338.

[31] Akram Tavakoli, Morteza Sohrabi, and Ali Kargari. "Application of Anderson–Schulz–Flory (ASF) equation in the product distribution of slurry phase FT synthesis with nanosized iron catalysts." In: *Chemical Engineering Journal* 136.2 (2008), pp. 358 –363. URL: http://www.sciencedirect.com/science/article/pii/S138589470700277X.

[32] RB Anderson, RA Friedel, and HH Storch. "Fischer-Tropsch Reaction Mechanism Involving Stepwise Growth of Carbon Chain." In: *The Journal of Chemical Physics* 19.3 (1951), pp. 313–319.

[33] C Perego, R Bortolo, and R Zennaro. "Gas to liquids technologies for natural gas reserves valorization: The Eni experience." In: *Catalysis Today* 142.1-2 (2009), pp. 9–16.

[34] Sara Lögdberg, Matteo Lualdi, Sven Järås, John C. Walmsley, Edd A. Blekkan, Erling Rytter, and Anders Holmen. "On the selectivity of cobalt-based Fischer-Tropsch catalysts: Evidence for a common precursor for methane and long-chain hydrocarbons." In: *Journal of Catalysis* 274.1 (2010), pp. 84 –98. URL: http://www.sciencedirect.com/science/article/pii/S0021951710002125.

[35] Ian C Yates and Charles N Satterfield. "Intrinsic kinetics of the Fischer-Tropsch synthesis on a cobalt catalyst." In: *Energy & Fuels* 5.1 (1991), pp. 168–173.

[36] Gerard P Van der Laan and Antonie ACM Beenackers. "Intrinsic kinetics of the gas–solid Fischer–Tropsch and water gas shift reactions over a precipitated iron catalyst." In: *Applied Catalysis A: General* 193.1-2 (2000), pp. 39–53.

[37] Branislav Todic, Wenping Ma, Gary Jacobs, Burtron H. Davis, and Dragomir B. Bukur. "CO-insertion mechanism based kinetic model of the Fischer–Tropsch synthesis reaction over Re-promoted Co catalyst." In: *Catalysis Today* 228 (2014). Natural Gas Conversion the Status and Potentials in the Light of NGCS-10, pp. 32 –39. URL: http://www.sciencedirect.com/science/article/pii/S092058611300374X.

[38] Roberto Zennaro, Marco Tagliabue, and Calvin H Bartholomew. "Kinetics of Fischer–Tropsch synthesis on titania-supported cobalt." In: *Catalysis Today* 58.4 (2000), pp. 309–319.

[39] Mohsen Mansouri, Hossein Atashi, Ali Akbar Mirzaei, and Reza Jangi. "Kinetics of the Fischer-Tropsch synthesis on silica-supported cobalt-cerium catalyst." In: *International Journal of Industrial Chemistry* 4.1 (2013), p. 1.

[40] Luis M. Aparicio and James A. Dumesic. "Ammonia synthesis kinetics: Surface chemistry, rate expressions, and kinetic analysis." In: *Topics in Catalysis* 1.3 (1994), pp. 233–252. URL: https://doi.org/10.1007/BF01492278.

[41] Anders Nielsen, Jørgen Kjaer, and Bennie Hansen. "Rate equation and mechanism of ammonia synthesis at industrial conditions." In: *Journal of Catalysis* 3.1 (1964), pp. 68 –79. URL: http://www.sciencedirect.com/science/article/pii/0021951764900946.

[42] Jia Yang, Wenping Ma, De Chen, Anders Holmen, and Burtron H. Davis. "Fischer-Tropsch synthesis: A review of the effect of CO conversion on methane selectivity." In: *Applied Catalysis A: General* 470 (2014), pp. 250 –260. URL: http://www.sciencedirect.com/science/article/pii/S0926860X13006807.

[43] S. Storsæter, A. Borg, E.A. Blekkan, and A. Holmen. "Study of the effect of water on Fischer-Tropsch synthesis over supported cobalt catalysts." In: *Journal of Catalysis* 231.2 (2005), pp. 405 –419. URL: http://www.sciencedirect.com/science/article/pii/S002195170500059X.

[44] A.K. Dalai and B.H. Davis. "Fischer-Tropsch synthesis: A review of water effects on the performances of unsupported and supported Co catalysts." In: *Applied Catalysis A: General* 348.1 (2008), pp. 1 –15. URL: http://www.sciencedirect.com/science/article/pii/S0926860X08003803.

[45] David S. Newsome. "The Water-Gas Shift Reaction." In: *Catalysis Reviews* 21.2 (1980), pp. 275–318. eprint: https://doi.org/10.1080/03602458008067535. URL: https://doi.org/10.1080/03602458008067535.

[46] Branislav Todic, Tejas Bhatelia, Gilbert F. Froment, Wenping Ma, Gary Jacobs, Burtron H. Davis, and Dragomir B. Bukur. "Kinetic Model of Fischer–Tropsch Synthesis in a Slurry Reactor on Co–Re/Al2O3 Catalyst." In: *Industrial & Engineering Chemistry Research* 52.2 (2013), pp. 669–679. eprint: https://doi.org/10.1021/ie3028312. URL: https://doi.org/10.1021/ie3028312.

[47] Paul T Boggs and Janet E Rogers. "Orthogonal distance regression." In: *Contemporary Mathematics* 112 (1990), pp. 183–194.

[48] Zhengyou Zhang. "Parameter estimation techniques: A tutorial with application to conic fitting." In: *Image and vision Computing* 15.1 (1997), pp. 59–76.

[49] Paul T. Boggs, Clifford H. Spiegelman, Janet R. Donaldson, and Robert B. Schnabel. "A computational examination of orthogonal distance regression." In: *Journal of Econometrics* 38.1 (1988), pp. 169 –201. URL: http://www.sciencedirect.com/science/article/pii/0304407688900322.

[50] H. P. Helfrich and D. Zwick. "A trust region method for implicit orthogonal distance regression." In: *Numerical Algorithms* 5.10 (Oct. 1993), pp. 535–545. URL: https://doi.org/10.1007/BF02108668.

[51] Ronald E. Walpole, Raymond H. Myers, Sharon L. Myers, and Keying Ye. *Probability & Statistics for Engineers & Scientists*. Pearson Education International, 1998.

[52] Andreas Helland Lillebø. "Conversion of biomass derived synthesis gas into liquid fuels via the Fischer-Tropsch synthesis process: Effect of alkali and alkaline earth metal impurities and CO conversion levels on cobalt based catalysts." PhD thesis. Norwegian University of Science and Technology, 2014.

[53] Pio Forzatti and Luca Lietti. "Catalyst deactivation." In: *Catalysis today* 52.2-3 (1999), pp. 165–181.

[54] Øyvind Borg, Pascal D.C. Dietzel, Aud I. Spjelkavik, Erik Z. Tveten, John C. Walmsley, Spyridon Diplas, Sigrid Eri, Anders Holmen, and Erling Rytter. "Fischer-Tropsch synthesis: Cobalt particle size and support effects on intrinsic activity and product distribution." In: *Journal of Catalysis* 259.2 (2008), pp. 161 –164. URL: `http://www.sciencedirect.com/science/article/pii/S0021951708003187`.

A Residual plots

In the following section, the residual plots for catalysts C3, C10, C11, and C14 are shown. Additionally, the residual plots of the commercial type catalyst with $H_2/CO = 2.1$ and 1.12 are also shown here. The residual plots are constructed by plotting the difference between the measured responses and the model responses, $\varepsilon_i = Y_i - \hat{Y}_i$, against a particular parameter such as inlet H_2/CO-ratio, mass flow, pressure and so on.

A.1 Catalyst C3

In Figure A.1, the residual plots for the CO-conversion are shown for catalyst C3. In the residual plots, each experimental period B-E are also shown separately. The residuals of the CO-conversion are plotted against the catalyst mass, TOS, inlet H_2/CO-ratio, and mass flow. If the residuals appear randomly around zero, the model is said to be capable of describing the data well.

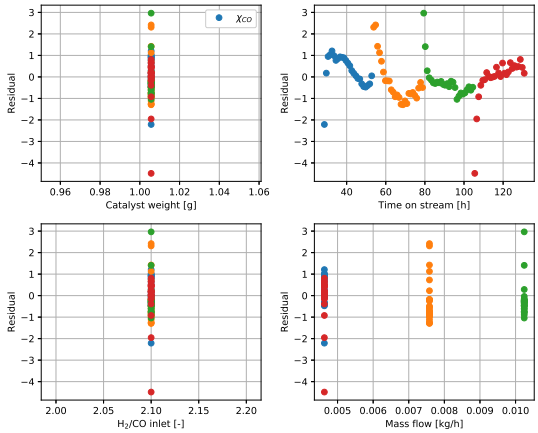

Figure A.1: Residual plots of the CO-conversion for catalyst C3. The residual $\varepsilon = \chi_{CO}^{exp} - \chi_{CO}^{model}$ is plotted against the catalyst mass, TOS, H_2/CO at reactor inlet, and mass flow. If the residuals appear randomly around zero, it is an indication that the model is able to describe the measurements well. In the residual plots, each period B-E are shown separately. The blue dots correspond to period B, the orange to period C, the green to period D, and the red to period E.

Figure A.2 shows the residual plots for the C_{5+}-selectivity for catalyst C3. In the residual plots, each experimental period B-E are shown separately, and the residuals are plotted against the catalyst mass, TOS, mass flow, α_1, partial pressure of CO, partial pressure of H_2, and partial pressure of H_2O. The blue dots correspond to period B, the orange to period C, the green to period D, and the red to period E.

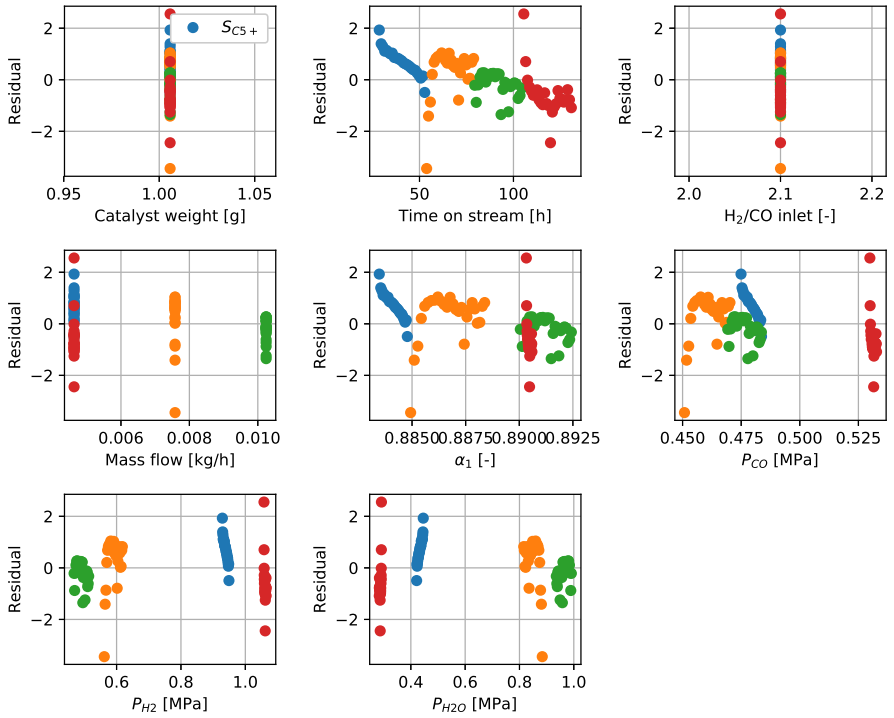

Figure A.2: Residual plots of the C_{5+}-selectivity for catalyst C3. The residual $\varepsilon = S^{exp}_{C_{5+}} - S^{model}_{C_{5+}}$ is plotted against the catalyst mass, TOS, H_2/CO-ratio at reactor inlet, mass flow, α_1, partial pressure of CO, partial pressure of H_2, and partial pressure of H_2O. The blue dots correspond to period B, the orange to period C, the green to period D, and the red to period E.

In Figure A.3, the residual plots for the CH_4-selectivity are shown for catalyst C3. In the residual plots, each experimental period B-E are shown separately. The residuals are plotted against the catalyst mass, TOS, H_2/CO-ratio at reactor inlet, mass flow, α_1, partial pressure of CO, partial pressure of H_2, and partial pressure of H_2O. The blue dots correspond to period B, the orange to period C, the green to period D, and the red to period E.

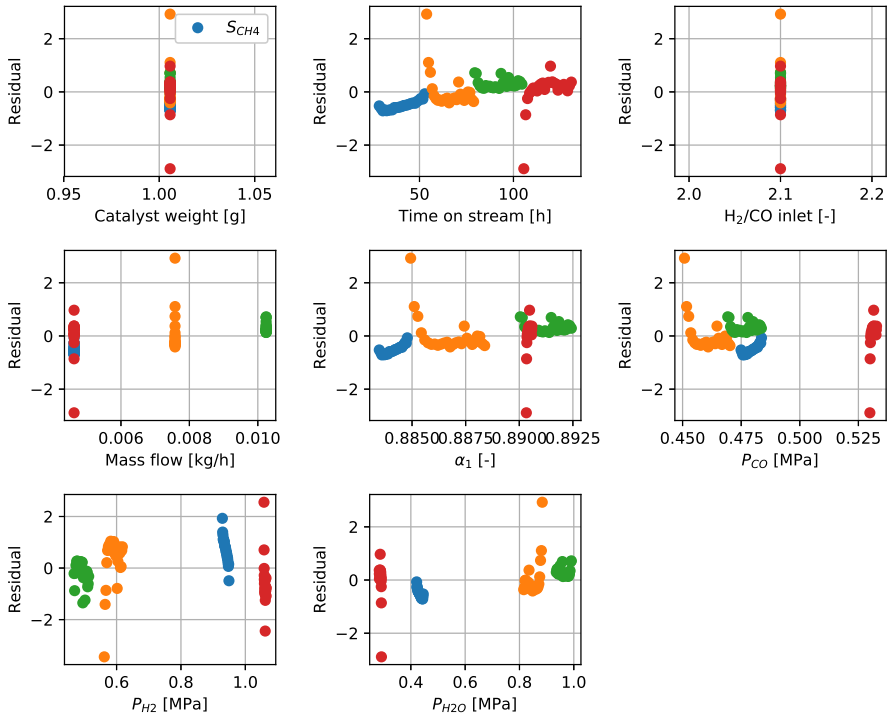

Figure A.3: Residual plots of the CH_4-selectivity for catalyst C3. The residual $\varepsilon = S^{exp}_{CH_4} - S^{model}_{CH_4}$ is plotted against the catalyst mass, TOS, H_2/CO-ratio at reactor inlet, mass flow, α_1, partial pressure of CO, partial pressure of H_2, and partial pressure of H_2O. The blue dots correspond to period B, the orange to period C, the green to period D, and the red to period E.

A.2 Catalyst C10

In Figure A.4, the residual plots for the CO-conversion are shown for catalyst C10. In the residual plots, each experimental period B-E are also shown separately. The residuals of the CO-conversion are plotted against the catalyst mass, TOS, inlet H_2/CO-ratio, and mass flow. If the residuals appear randomly around zero, the model is said to be capable of describing the data well. The blue dots correspond to period B, the orange to period C, the green to period D, and the red to period E.

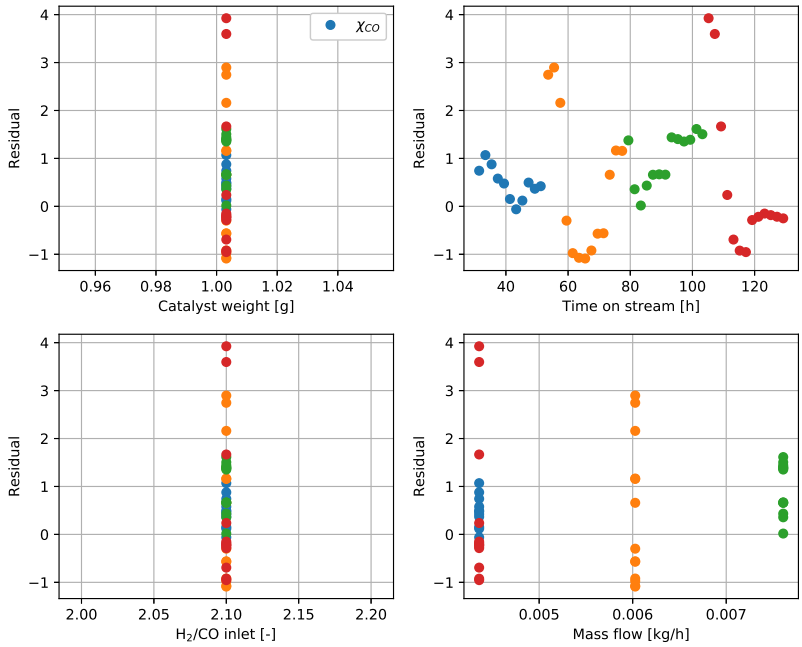

Figure A.4: Residual plots of the CO-conversion for catalyst C10. The residual $\varepsilon = \chi_{\mathrm{CO}}^{\mathrm{exp}} - \chi_{\mathrm{CO}}^{model}$ is plotted against the catalyst mass, TOS, H_2/CO at reactor inlet, and mass flow. If the residuals appear randomly around zero, it is an indication that the model can describe the measurements well. In the residual plots, each period B-E are shown separately. The blue dots correspond to period B, the orange to period C, the green to period D, and the red to period E.

Figure A.5 shows the residual plots for the C_{5+}-selectivity for catalyst C10. In the residual plots, each experimental period B-E are shown separately, and the residuals are plotted against the catalyst mass, TOS, mass flow, α_1, partial pressure of CO, partial pressure of H_2, and partial pressure of H_2O. The blue dots correspond to period B, the orange to period C, the green to period D, and the red to period E.

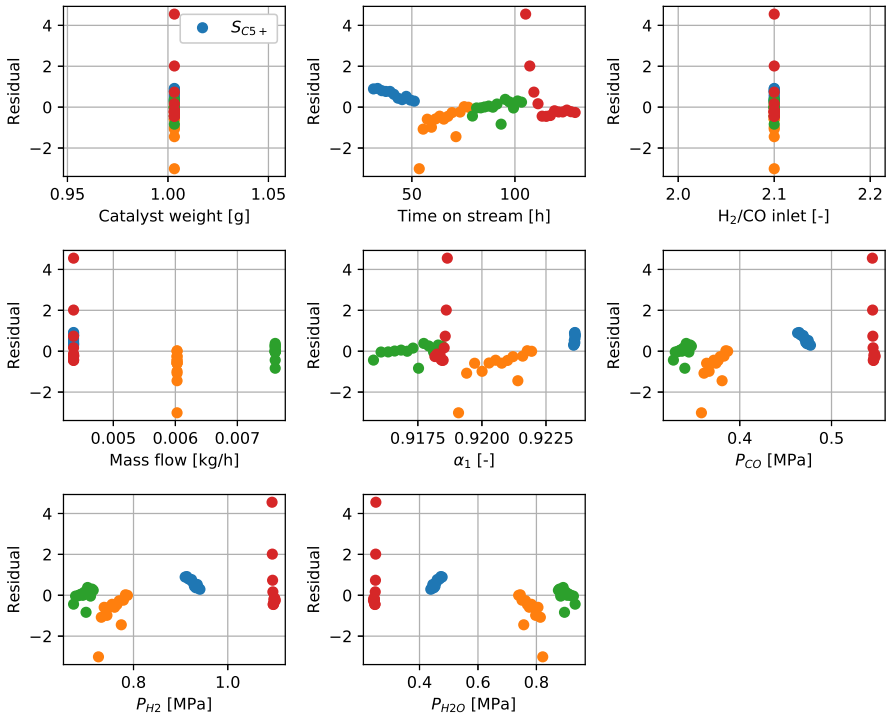

Figure A.5: Residual plots of the C_{5+}-selectivity for catalyst C10. The residual $\varepsilon = S^{exp}_{C_{5+}} - S^{model}_{C_{5+}}$ is plotted against the catalyst mass, TOS, H_2/CO-ratio at reactor inlet, mass flow, α_1, partial pressure of CO, partial pressure of H_2, and partial pressure of H_2O. The blue dots correspond to period B, the orange to period C, the green to period D, and the red to period E.

In Figure A.6, the residual plots for the CH_4-selectivity are shown for catalyst C10. In the residual plots, each experimental period B-E are shown separately. The residuals are plotted against the catalyst mass, TOS, H_2/CO-ratio at reactor inlet, mass flow, α_1, partial pressure of CO, partial pressure of H_2, and partial pressure of H_2O. The blue dots correspond to period B, the orange to period C, the green to period D, and the red to period E.

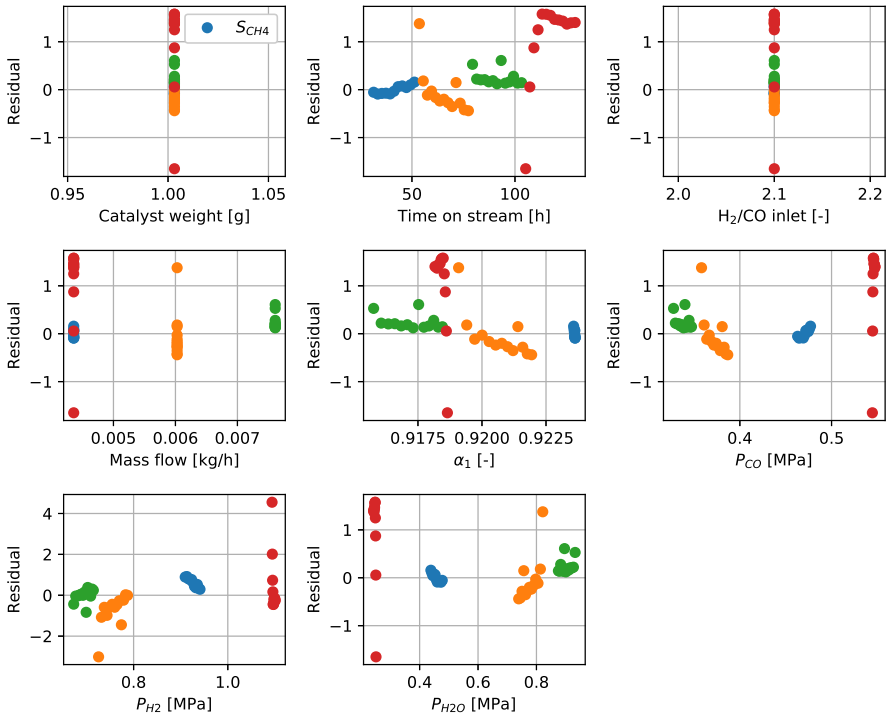

Figure A.6: Residual plots of the CH_4-selectivity for catalyst C10. The residual $\varepsilon = S^{exp}_{CH_4} - S^{model}_{CH_4}$ is plotted against the catalyst mass, TOS, H_2/CO-ratio at reactor inlet, mass flow, α_1, partial pressure of CO, partial pressure of H_2, and partial pressure of H_2O. The blue dots correspond to period B, the orange to period C, the green to period D, and the red to period E.

A.3 Catalyst C11

In Figure A.7, the residual plots for the CO-conversion are shown for catalyst C11. In the residual plots, each experimental period B-E are also shown separately. The residuals of the CO-conversion are plotted against the catalyst mass, TOS, inlet H_2/CO-ratio, and mass flow. If the residuals appear randomly around zero, the model is said to be capable of describing the data well. The blue dots correspond to period B, the orange to period C, the green to period D, and the red to period E.

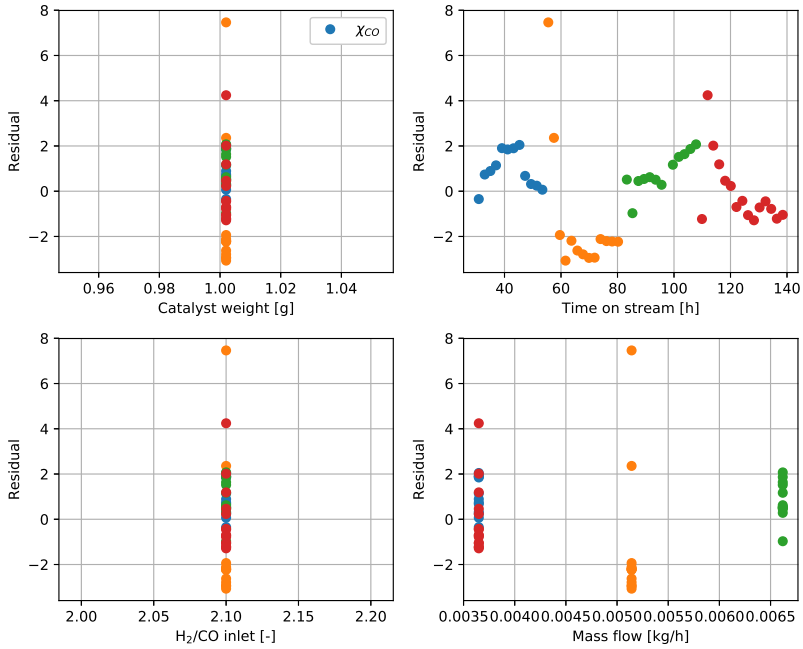

Figure A.7: Residual plots of the CO-conversion for catalyst C11. The residual $\varepsilon = \chi_{\mathrm{CO}}^{\mathrm{exp}} - \chi_{\mathrm{CO}}^{model}$ is plotted against the catalyst mass, TOS, H_2/CO at reactor inlet, and mass flow. If the residuals appear randomly around zero, it is an indication that the model is able to describe the measurements well. In the residual plots, each period B-E are shown separately. The blue dots correspond to period B, the orange to period C, the green to period D, and the red to period E.

Figure A.8 shows the residual plots for the C_{5+}-selectivity for catalyst C11. In the residual plots, each experimental period B-E are shown separately, and the residuals are plotted against the catalyst mass, TOS, mass flow, α_1, partial pressure of CO, partial pressure of H_2, and partial pressure of H_2O. The blue dots correspond to period B, the orange to period C, the green to period D, and the red to period E.

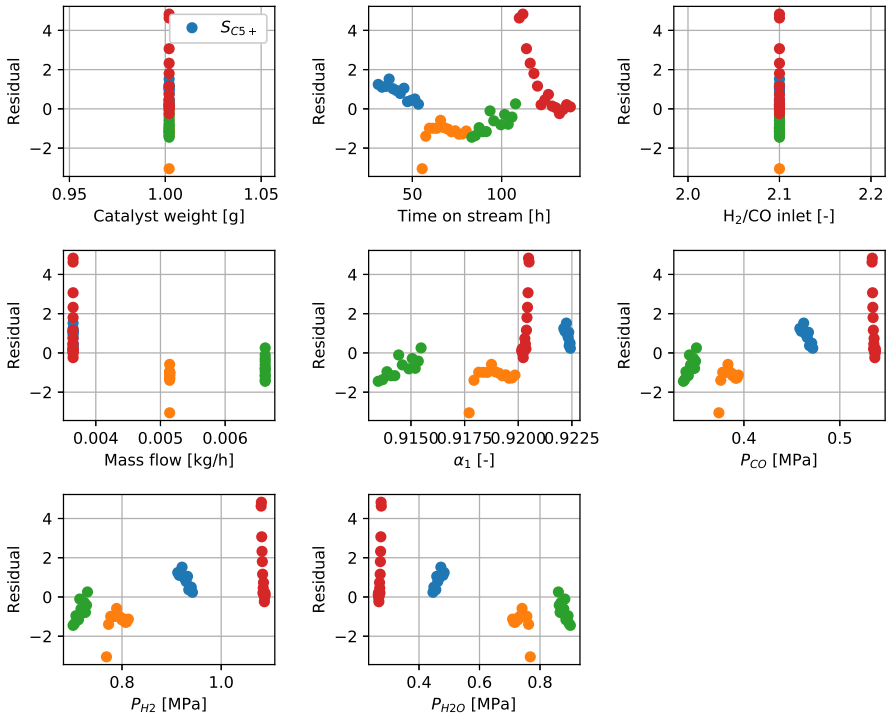

Figure A.8: Residual plots of the C_{5+}-selectivity for catalyst C11. The residual $\varepsilon = S^{exp}_{C_{5+}} - S^{model}_{C_{5+}}$ is plotted against the catalyst mass, TOS, H_2/CO-ratio at reactor inlet, mass flow, α_1, partial pressure of CO, partial pressure of H_2, and partial pressure of H_2O. The blue dots correspond to period B, the orange to period C, the green to period D, and the red to period E.

In Figure A.9, the residual plots for the CH_4-selectivity are shown for catalyst C11. In the residual plots, each experimental period B-E are shown separately. The residuals are plotted against the catalyst mass, TOS, H_2/CO-ratio at reactor inlet, mass flow, α_1, partial pressure of CO, partial pressure of H_2, and partial pressure of H_2O. The blue dots correspond to period B, the orange to period C, the green to period D, and the red to period E.

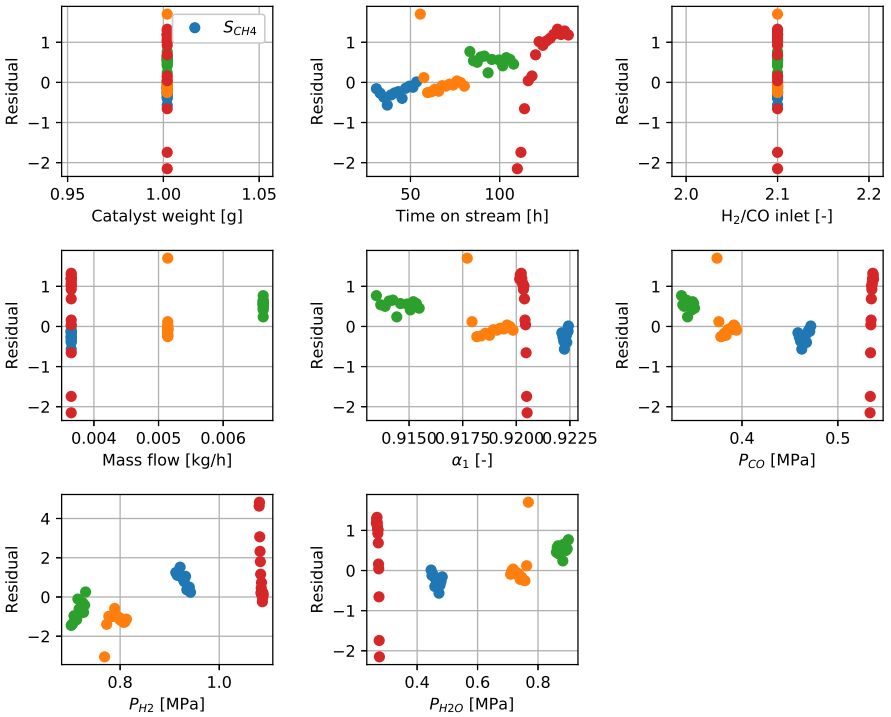

Figure A.9: Residual plots of the CH_4-selectivity for catalyst C11. The residual $\varepsilon = S^{exp}_{CH_4} - S^{model}_{CH_4}$ is plotted against the catalyst mass, TOS, H_2/CO-ratio at reactor inlet, mass flow, α_1, partial pressure of CO, partial pressure of H_2, and partial pressure of H_2O. The blue dots correspond to period B, the orange to period C, the green to period D, and the red to period E.

A.4 Catalyst C14

In Figure A.10, the residual plots for the CO-conversion are shown for catalyst C14. In the residual plots, each experimental period B-E are also shown separately. The residuals of the CO-conversion are plotted against the catalyst mass, TOS, inlet H_2/CO-ratio, and mass flow. If the residuals appear randomly around zero, the model is said to be capable of describing the data well. The blue dots correspond to period B, the orange to period C, the green to period D, and the red to period E.

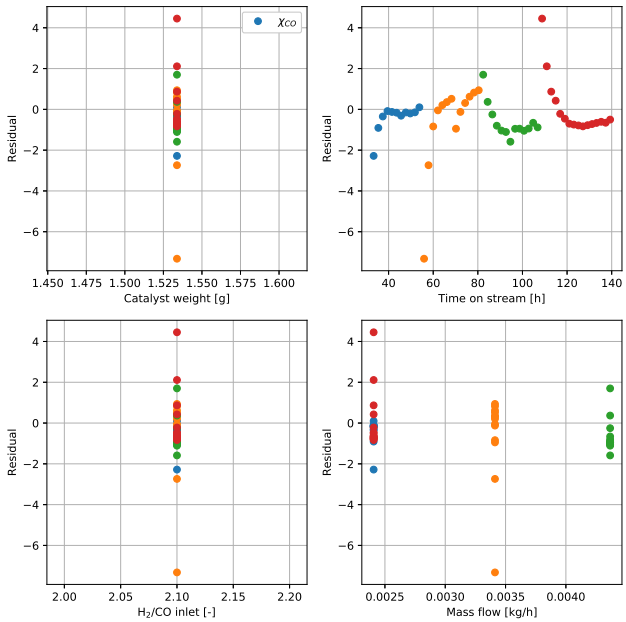

Figure A.10: Residual plots of the CO-conversion for catalyst C14. The residual $\varepsilon = \chi_{\mathrm{CO}}^{\mathrm{exp}} - \chi_{\mathrm{CO}}^{model}$ is plotted against the catalyst mass, TOS, H_2/CO at reactor inlet, and mass flow. If the residuals appear randomly around zero, it is an indication that the model can describe the measurements well. In the residual plots, each period B-E are shown separately. The blue dots correspond to period B, the orange to period C, the green to period D, and the red to period E.

Figure A.11 shows the residual plots for the C_{5+}-selectivity for catalyst C14. In the residual plots, each experimental period B-E are shown separately, and the residuals are plotted against the catalyst mass, TOS, mass flow, α_1, partial pressure of CO, partial pressure of H_2, and partial pressure of H_2O. The blue dots correspond to period B, the orange to period C, the green to period D, and the red to period E.

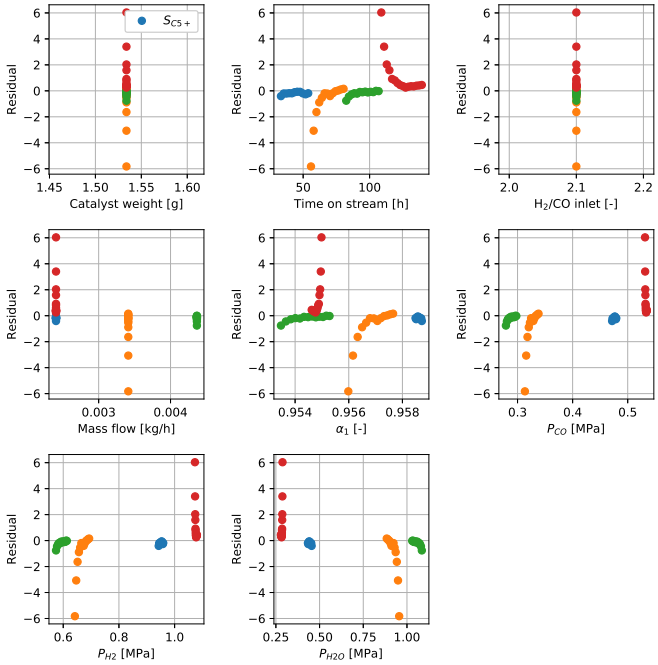

Figure A.11: Residual plots of the C_{5+}-selectivity for catalyst C14. The residual $\varepsilon = S^{exp}_{C_{5+}} - S^{model}_{C_{5+}}$ is plotted against the catalyst mass, TOS, H_2/CO-ratio at reactor inlet, mass flow, α_1, partial pressure of CO, partial pressure of H_2, and partial pressure of H_2O. The blue dots correspond to period B, the orange to period C, the green to period D, and the red to period E.

In Figure A.12, the residual plots for the CH_4-selectivity are shown for catalyst C14. In the residual plots, each experimental period B-E are shown separately. The residuals are plotted against the catalyst mass, TOS, H_2/CO-ratio at reactor inlet, mass flow, α_1, partial pressure of CO, partial pressure of H_2, and partial pressure of H_2O. The blue dots correspond to period B, the orange to period C, the green to period D, and the red to period E.

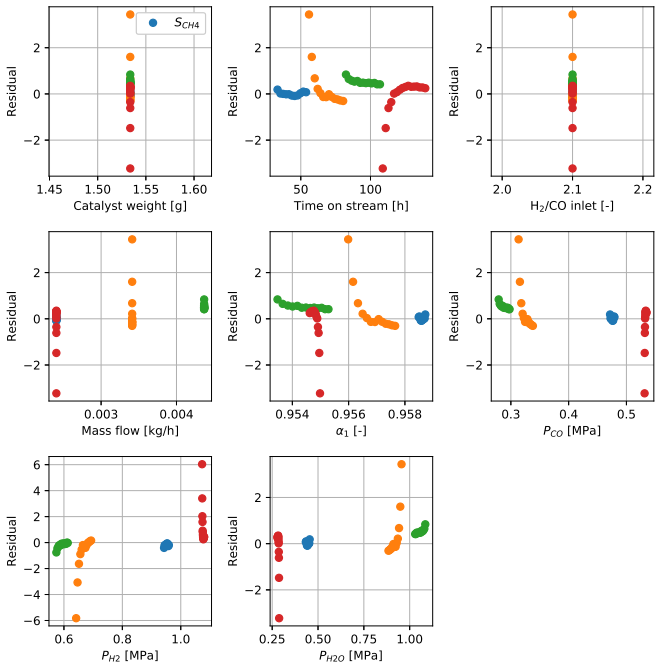

Figure A.12: Residual plots of the CH_4-selectivity for catalyst C14. The residual $\varepsilon = S^{exp}_{CH_4} - S^{model}_{CH_4}$ is plotted against the catalyst mass, TOS, H_2/CO-ratio at reactor inlet, mass flow, α_1, partial pressure of CO, partial pressure of H_2, and partial pressure of H_2O. The blue dots correspond to period B, the orange to period C, the green to period D, and the red to period E.

A.5 Commercial type catalyst, $H_2/CO = 2.1$

In Figure A.13, the residual plots of the conversion of CO are shown for the commercial type catalyst with $H_2/CO = 2.1$. In the residual plots, each experimental period A-G are also shown separately, and the residuals are plotted against the catalyst mass, TOS, H_2/CO-ratio at reactor inlet, mass flow, and temperature. If the residuals appear randomly around zero, the model is said to be able to describe the experimental data well. The blue dots correspond to period A, the orange to period B, the green to period C, the red to period D, the purple to period E, the brown to period F, and the pink to period G.

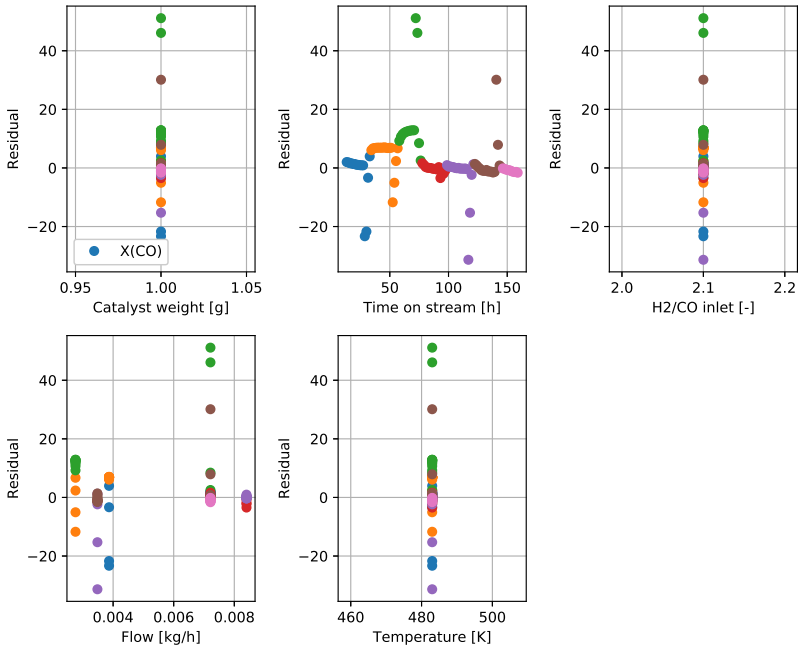

Figure A.13: Residual plots of the CO-conversion for the commercial type catalyst with $H_2/CO = 2.1$. The residual $\varepsilon = \chi_{CO}^{exp} - \chi_{CO}^{model}$ is plotted against the catalyst mass, TOS, H_2/CO-ratio at reactor inlet, mass flow, and temperature. Each period in the experimental run is shown separately. The blue dots correspond to period A, the orange to period B, the green to period C, the red to period D, the purple to period E, the brown to period F, and the pink to period G.

Figure A.14 shows the residual plots of the C_{5+}-selectivity for the commercial type catalyst with $H_2/CO = 2.1$. In the residual plots, each experimental period A-G are shown separately. The residuals are plotted against the catalyst mass, TOS, H_2/CO-ratio at reactor inlet, mass flow, α_1, P_{CO}, P_{H_2}, P_{H_2O} and temperature. The blue dots correspond to period A, the orange to period B, the green to period C, the red to period D, the purple to period E, the brown to period F, and the pink to period G.

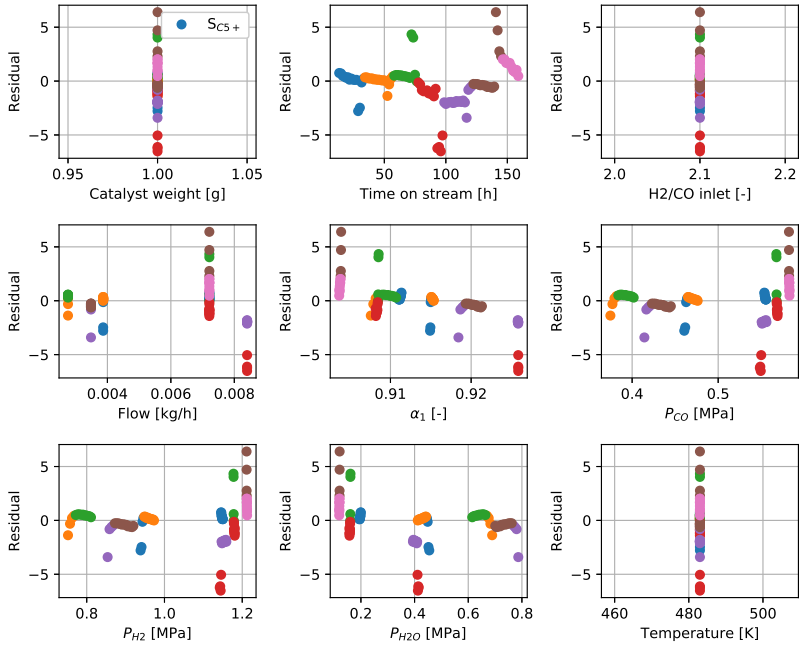

Figure A.14: Residual plots of the C_{5+}-selectivity for the commercial type catalyst with $H_2/CO = 2.1$. The residuals $S^{exp}_{C_{5+}} - S^{model}_{C_{5+}}$ are plotted against the catalyst mass, TOS, H_2/CO-ratio at reactor inlet, mass flow, α_1, partial pressure of CO, partial pressure of H_2, partial pressure of H_2O, and temperature. Each period in the experimental run is shown separately. The blue dots correspond to period A, the orange to period B, the green to period C, the red to period D, the purple to period E, the brown to period F, and the pink to period G.

In Figure A.15, the residual plots of the CH_4-selectivity for the commercial type catalyst with H_2/CO-ratio of 2.1 are shown. The residuals are plotted against the catalyst mass, TOS, H_2/CO-ratio at reactor inlet, mass flow, α_1, P_{CO}, P_{H_2}, P_{H_2O}, and temperature. The blue dots correspond to period A, the orange to period B, the green to period C, the red to period D, the purple to period E, the brown to period F, and the pink to period G.

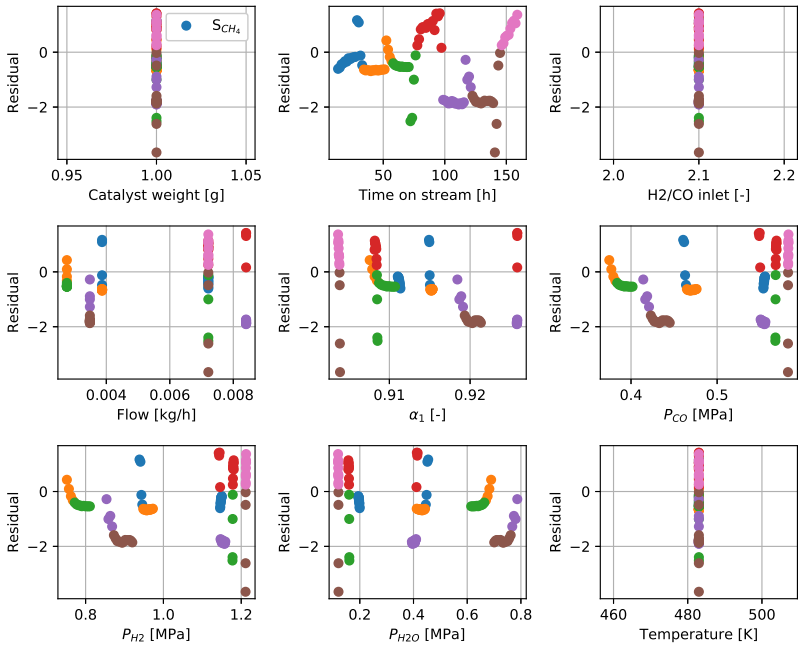

Figure A.15: Residual plots of the CH_4-selectivity for the commercial type catalyst with $H_2/CO = 2.1$. The residuals $S^{exp}_{CH_4} - S^{model}_{CH_4}$ are plotted against the catalyst mass, TOS, H_2/CO-ratio at reactor inlet, mass flow, α_1, partial pressure of CO, partial pressure of H_2, partial pressure of H_2O, and temperature. Each period in the experimental run is shown separately. The blue dots correspond to period A, the orange to period B, the green to period C, the red to period D, the purple to period E, the brown to period F, and the pink to period G.

A.6 Commercial type catalyst, $H_2/CO = 1.12$

In Figure A.16, the residual plots of the conversion of CO are shown for the commercial type catalyst with $H_2/CO = 1.12$. In the residual plots, each experimental period A-G are also shown separately, and the residuals are plotted against the catalyst mass, TOS, H_2/CO-ratio at reactor inlet, mass flow, and temperature. If the residuals appear randomly around zero, the model is said to be able to describe the experimental data well. The blue dots correspond to period A, the orange to period B, the green to period C, the red to period D, the purple to period E, and the brown to period F.

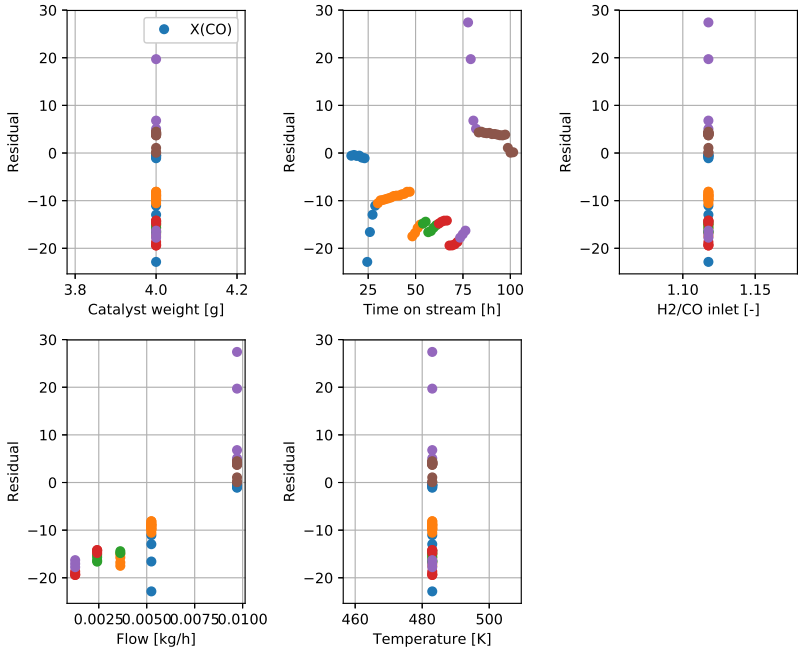

Figure A.16: Residual plots of the CO-conversion for the commercial type catalyst with $H_2/CO = 1.12$. The residual $\varepsilon = \chi_{CO}^{exp} - \chi_{CO}^{model}$ is plotted against the catalyst mass, TOS, H_2/CO-ratio at reactor inlet, mass flow, and temperature. Each period in the experimental run is shown separately. The blue dots correspond to period A, the orange to period B, the green to period C, the red to period D, the purple to period E, and the brown to period F.

Figure A.17 shows the residual plots of the C_{5+}-selectivity for the commercial type catalyst with $H_2/CO = 1.12$. In the residual plots, each experimental period A-G are shown separately. The residuals are plotted against the catalyst mass ,TOS, H_2/CO-ratio at reactor inlet, mass flow, α_1, P_{CO}, P_{H_2}, P_{H_2O} and temperature. The blue dots correspond to period A, the orange to period B, the green to period C, the red to period D, the purple to period E, and the brown to period F.

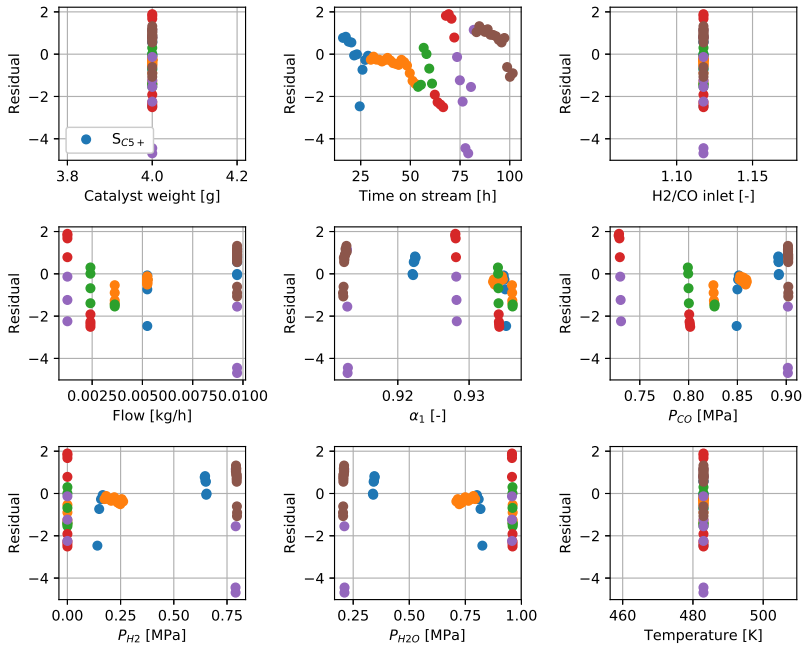

Figure A.17: Residual plots of the C_{5+}-selectivity for the commercial type catalyst with $H_2/CO = 1.12$. The residuals $S^{exp}_{C_{5+}} - S^{model}_{C_{5+}}$ are plotted against the catalyst mass, TOS, H_2/CO-ratio at reactor inlet, mass flow, α_1, partial pressure of CO, partial pressure of H_2, partial pressure of H_2O, and temperature. Each period in the experimental run is shown separately. The blue dots correspond to period A, the orange to period B, the green to period C, the red to period D, the purple to period E, and the brown to period F.

In Figure A.18, the residual plots of the CH_4-selectivity for the commercial type catalyst with H_2/CO-ratio of 1.12 are shown. The residuals are plotted against the catalyst mass, TOS, H_2/CO-ratio at reactor inlet, mass flow, α_1, P_{CO}, P_{H_2}, P_{H_2O}, and temperature. The blue dots correspond to period A, the orange to period B, the green to period C, the red to period D, the purple to period E, and the brown to period F.

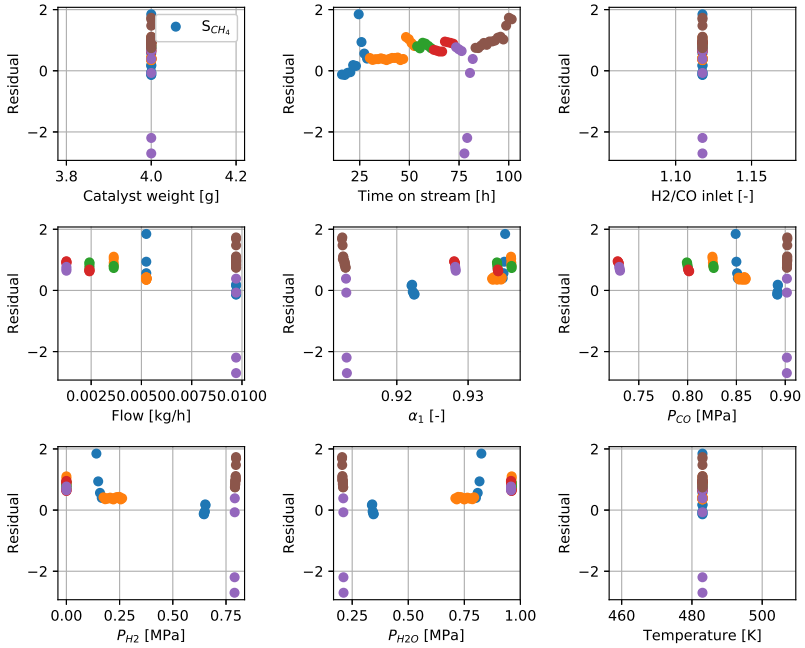

Figure A.18: Residual plots of the CH_4-selectivity for the commercial type catalyst with $H_2/CO = 1.12$. The residuals $S^{exp}_{CH_4} - S^{model}_{CH_4}$ are plotted against the catalyst mass, TOS, H_2/CO-ratio at reactor inlet, mass flow, α_1, partial pressure of CO, partial pressure of H_2, partial pressure of H_2O, and temperature. Each period in the experimental run is shown separately. The blue dots correspond to period A, the orange to period B, the green to period C, the red to period D, the purple to period E, and the brown to period F.

B Commercial type catalyst, temperature alteration

For the commercial type catalyst with $H_2/CO = 2.1$, it is observed in Figure 5.18 that periods B and C are not captured by the model. In the experiment, the flow rate in period B is reduced to a level such that the conversion of CO should reach 50 %. This is also predicted by the model as can be seen in the same figure. However, the experimental data show that the conversion reaches higher levels than what is predicted by the model. While there are several possibilities for these mismatches, one possibility is a change in temperature (due to higher conversion) in these periods as a result of the exothermic nature of the Fischer-Tropsch synthesis. To try to understand why the model predicts lower conversions in periods B and C, the temperature of these particular periods are manually set slightly above 483 K at 487 K. To account for this change in temperature, temperature dependencies of some parameters must be included. This is done by assuming the parameters follow an Arrhenius temperature dependency. The activation energies required in the temperature dependencies are not estimated by the ODR, however, some approximate values are used for the activation energies. These approximate values are obtained from a previous project (and adjusted somewhat here) in which the temperature dependencies of several parameters were estimated for data obtained for a continuously stirred tank reactor (CSTR).
When making these temperature alterations, only the model shown at the beginning of Section 5 (Model 1) is considered. The estimated parameters, and their respective absolute uncertainties in this case are given in Table B.1 below. Additionally, the trend plots of the CO-conversion, C_{5+}-selectivity, and CH_4-selectivity with changes in temperature in periods B and C are shown. Only these particular responses are chosen to be shown below as the impact of the temperature on the CO-conversion levels is the main observation considered in this case.

Parameter	Estimated value [a.u.]	Uncertainty [a.u.]
k_1	1.464	± 0.08328
E_1	104000	-
a	3.50	-
b	1.504	-
f	1.364	± 0.6564
g	1.523	-
β_o	0.10	-
k_{CH_4}	0.09013	± 0.01646
x	1.70	± 0.909
k_4	1.0	-
k_{wgs}	0.0010	-
k_d	0.01756	± 0.004933
k_α	0.03442	± 0.006594
E_α	882.75	-
y	0.2777	± 0.06511
c_{α_4}	0.70	-

Table B.1: Estimated parameters and their respective absolute uncertainties for the commercial type catalyst with $H_2/CO = 2.1$ and changed temperatures in periods B and C. The temperature in periods B and C are changed to 487 K. To account for the temperature changes, temperature dependencies are included for some parameters.

In Figure B.1, the trend plots of the conversion of CO, C_{5+}-selectivity, and CH_4-selectivity are shown for the commercial type catalyst with $H_2/CO = 2.1$. The temperatures are at 483 K, with the exceptions of periods B and C where the temperatures are set to 487 K as a test to see if this will help the model predict the overshoots observed in the experimental data.

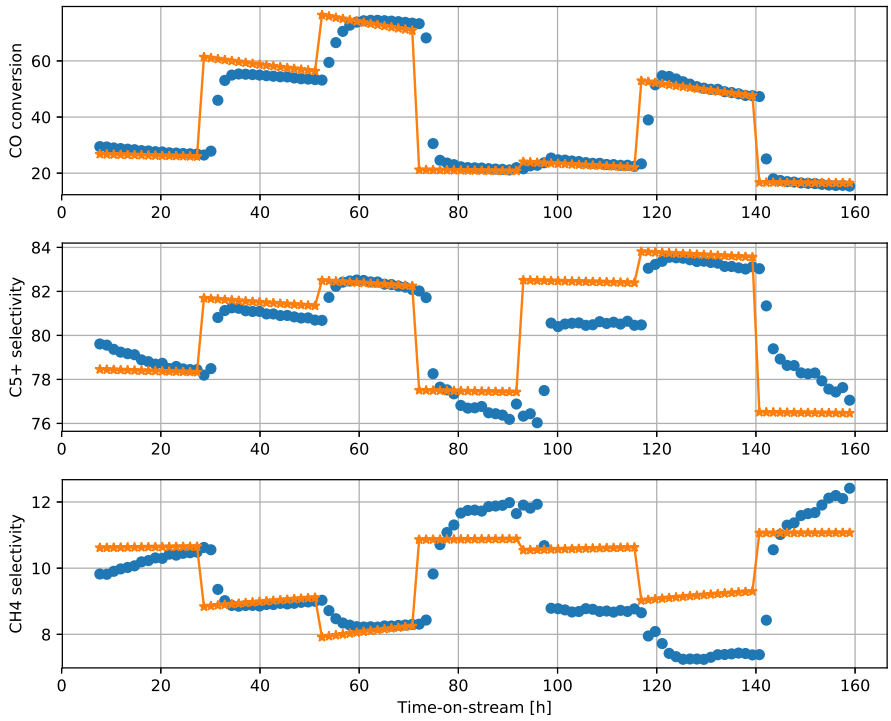

Figure B.1: Trend plots of the CO-conversion, C_{5+}-selectivity, and CH_4-selectivity for the commercial type catalyst with $H_2/CO = 2.1$, with changes in the temperature in periods B and C (487 K).

C Commercial type catalyst, $H_2/CO = 1.72$

For the commercial type catalyst with $H_2/CO = 1.72$, the estimated parameters and their respective absolute uncertainties are shown in Table C.1. The parameters that have no given uncertainty have been estimated manually through a trial-and-error process. As mentioned elsewhere in the report, as the commercial type catalyst is a variant of the catalyst C10, several of the estimated parameters remain the same between this catalyst and the catalyst C10. Some variations could be expected in terms of catalyst performance due to different productions. Between period A and C, it is experimentally measured that the C_{5+}-selectivity is decreased even when the conversion is increased, as such period A is weighted minimally when doing the model fitting.

Parameter	Estimated value [a.u.]	Uncertainty [a.u.]
k_1	1.353	± 0.1142
a	3.50	-
b	1.504	-
f	1.464	± 1.452
g	1.523	-
β_o	0.10	-
k_{CH_4}	0.09013	± 0.01669
x	1.70	± 2.00
k_4	0.90	-
k_{wgs}	0.0010	-
k_d	0.01756	± 0.01190
k_α	0.03920	± 0.01457
y	0.2477	± 0.1589
c_{α_4}	0.70	-

Table C.1: Estimated parameters and their respective absolute uncertainties for the commercial type catalyst with $H_2/CO = 1.72$. Parameters in which no given uncertainties are given have been estimated manually through a trial-and-error process.

To help evaluate the performance of the model, several parity plots are constructed; one for each response. The parity plots show the performance of each period as outlined in Section 4. It should be noted that the periods in this particular experimental run are not identical to the periods described earlier. The final two periods of the experimental run are not used, as some very strange

observations are seen experimentally, including a decrease in $S_{C_{5+}}$ when the conversion is increased to approximately 50 % with added water. The final period shown in the following figures for this catalyst is the only period in which water is added. All other periods are only changing the flow rate to obtain certain conversion levels.
Additionally, trend plots of the main responses (i.e. the CO-conversion, C_{5+}-selectivity, and CH_4-selectivity) are also constructed.

Figure C.1 shows the parity plots of the conversion of CO, C_{5+}-selectivity, and CH_4-selectivity for the commercial type catalyst with $H_2/CO = 1.72$. The periods A-G as described in short above are shown in each parity plot. The responses predicted by the model are plotted against the responses measured experimentally. A reference line is also included to see how well the model is capable of describing the experimental data.

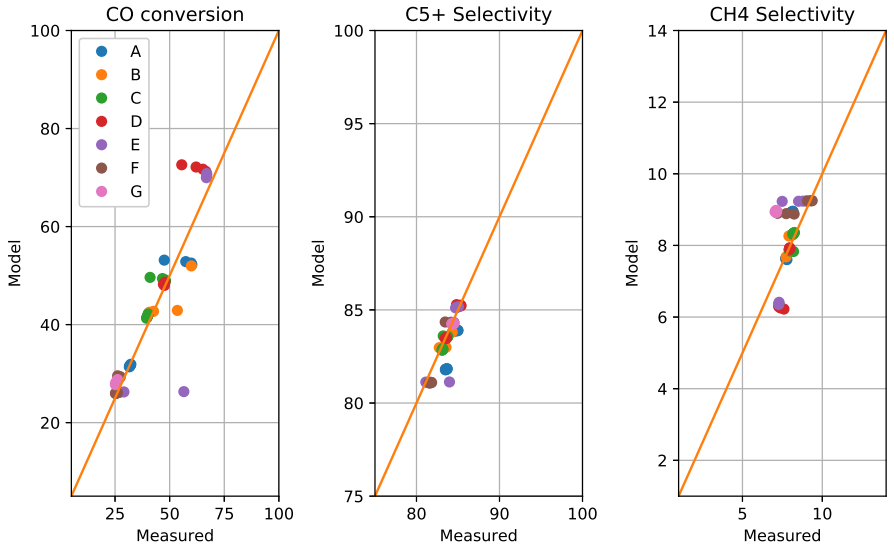

Figure C.1: Parity plots of the CO-conversion, C_{5+}-selectivity, and CH_4-selectivity for the commercial type catalyst with $H_2/CO = 1.72$. The periods A-G are shown in the plots. Only period G have water added to the reactor inlet.

In Figure C.2, the parity plots of the C_2-C_4 paraffin and olefin selectivities, along with the CO_2-selectivity, are shown for the commercial type catalyst with $H_2/CO = 1.72$. In each parity plot, the responses predicted by the model are plotted against the experimentally measured responses. A reference line is also included to see how well the model fits the experimental data. Only period G has water added to the reactor inlet. All other periods are run with dry syngas under various flow rates to achieve certain conversion levels.

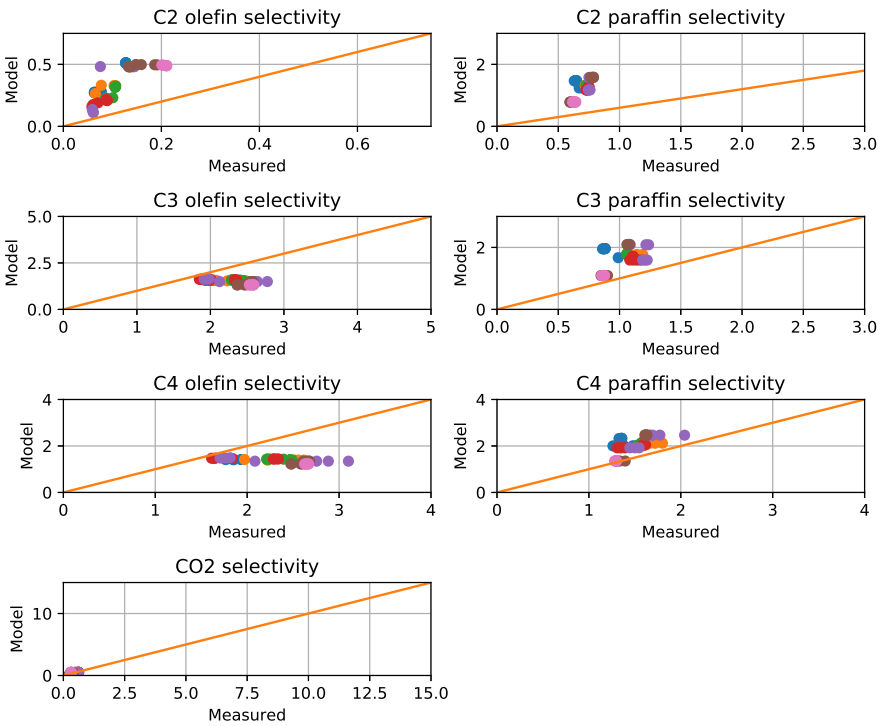

Figure C.2: Parity plots of the C_2-C_4 paraffin and olefin selectivities, as well as the CO_2-selectivity for the commercial type catalyst with $H_2/CO = 1.72$. The blue dots correspond to period A, the orange to period B, the green to period C, the red to period D, the purple to period E, the brown to period F, and finally the pink to period G.

Figure C.3, the trend plots of the CO-conversion, C_{5+}-selectivity, and CH_4-selectivity are shown for the commercial type catalyst with $H_2/CO = 1.72$. Only the final period, period G, is shown have added water to the reactor inlet. There are two more periods in the experimental run, however these periods are not used in the model fitting due to some rather strange observations; when the conversion is increased to approximately 50 % (and water is fed to the reactor inlet), the experimental data show a decline in the C_{5+}-selectivity. As a result, these two final periods are not included when doing the model fitting.

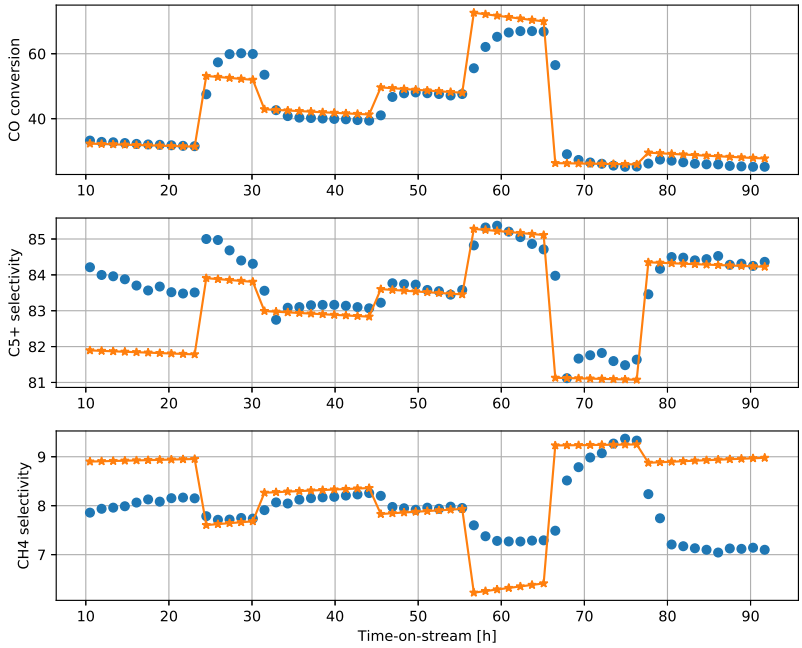

Figure C.3: Trend plots of the CO-conversion, C_{5+}-selectivity, and CH_4-selectivity for the commercial type catalyst with $H_2/CO = 1.72$. Only the final period, period G, has water added fed to inlet of the reactor. Two additional periods are included in the experimental run, but not considered when doing the model fitting as some unusual responses are observed, such as a decline in the C_{5+}-selectivity when the conversion is increased to approximately 50 % and with added water.

D Alternative methane formation model

An alternative mathematical model encompassing the reaction kinetics, product selectivities, and catalyst deactivation is also proposed. This alternative model is referred to as *Model 2* in Section 5. The main difference between this model and the one proposed in Section 5 is the expression for the methane formation. In the alternative model, water is included actively in the methane formation rate expression as described in Section 2. The alternative model is shown below.

$$r_1 = \frac{D\left(t, P_{\mathrm{H_2O}}\right) k_1' P_{\mathrm{CO}} P_{\mathrm{H_2}}^{0.5} \left(P^o + P_{\mathrm{H_2O}}\right)}{\left(1 + aP_{\mathrm{CO}} + bP_{\mathrm{H_2}}^{0.5} + fP_{\mathrm{H_2O}}\right)^2}, \quad k_1' = k_1 g, \quad P^o = g^{-1} \tag{D.1}$$

$$r_2 = \beta_o r_1 \tag{D.2}$$

$$r_3 = k_{\mathrm{CH_4}}' r_1 \left(\frac{P_{\mathrm{H_2}}}{1 + K_{\mathrm{CH_4}} P_{\mathrm{H_2O}}}\right)^x - \left(1 - \alpha_1\right)^2 r_1 - \left(1 - \alpha_2\right)^2 r_2 \tag{D.3}$$

$$r_4 = k_4 P_{\mathrm{C_2H_4}} P_{\mathrm{CO}} P_{\mathrm{H_2}}^2 \tag{D.4}$$

$$r_5 = k_{wgs} \left(P_{\mathrm{CO}} P_{\mathrm{H_2O}} - \frac{1}{K_{eq}} P_{\mathrm{CO_2}} P_{\mathrm{H_2}}\right) \tag{D.5}$$

$$K_{eq} = \exp\left(\frac{4577.8}{T} - 4.33\right) \tag{D.6}$$

$$\frac{\mathrm{d}D}{\mathrm{d}t} = -k_d D^n P_{\mathrm{H_2O}}^{\gamma}, \quad n = 2,\ \gamma = 1 \tag{D.7}$$

$$\alpha_1 = \frac{1}{1 + k_\alpha \left(\frac{1}{P_{\mathrm{CO}}}\right) \left(\frac{1}{P_{\mathrm{H_2O}}}\right)^y} \tag{D.8}$$

$$\alpha_2 = \alpha_1 \cdot e^{-0.27} \tag{D.9}$$

$$\alpha_4 = c_{\alpha_4} \cdot \alpha_1 \tag{D.10}$$

For each catalyst, the alternative model above is fitted to a corresponding set of experimental data. The results for each catalyst are presented in the following subsections. It should be noted that only the trend plots for this particular model are shown. Further, the commercial type catalyst with $\mathrm{H_2/CO} = 1.12$ is not fitted to this particular, alternative model as for those experimental data, no periods with added water are considered when doing the model fitting. As such, the effect of water on the methane formation can not be studied for these particular data.

D.1 Catalyst C3

For catalyst C3, the estimated parameters and their respective absolute uncertainties are shown for the alternative model in Table D.1. Estimated parameters with no given uncertainties have been estimated manually through a trial-and-error process.

Parameter	Estimated value [a.u.]	Uncertainty [a.u.]
k_1	1.928	± 0.07562
a	3.50	-
b	1.889	-
f	0.6760	± 0.1094
g	1.4282	-
β_o	0.10	-
$k'_{\mathrm{CH_4}}$	0.1211	± 0.006257
x	0.500	± 0.0982
$K_{\mathrm{CH_4}}$	1.20	-
k_4	1.20	-
k_{wgs}	0.00250	-
k_d	0.008503	± 0.001295
k_α	0.05792	± 0.003715
y	0.1170	± 0.03651
c_{α_4}	0.70	-

Table D.1: Estimated parameters and their respective absolute uncertainties for C3 with the alternative model. Parameters in which no given uncertainties are given have been estimated manually through a trial-and-error process.

Figure D.1 shows the trend plots of the CO-conversion, C_{5+}-selectivity, and CH_4-selectivity for catalyst C3 with the alternative model. As is the case for the results presented in Section 5, for catalyst C3, the period A is removed when doing the model fitting. As a result, only the periods B-E are shown.

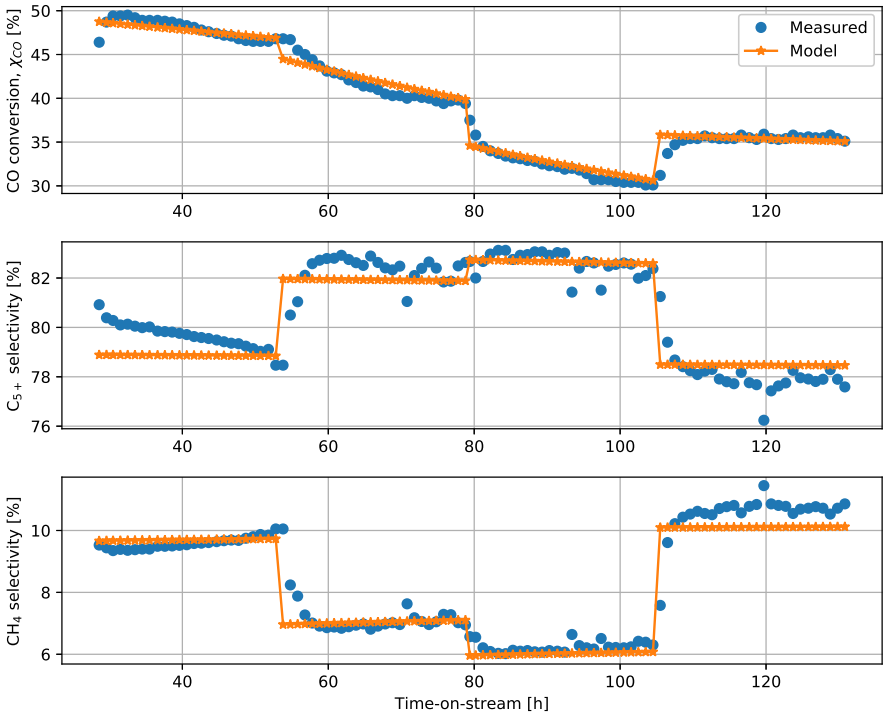

Figure D.1: Trend plots of the CO-conversion, C_{5+}-selectivity, and CH_4-selectivity for catalyst C3 with the alternative model. The periods B-E are shown in the plot. As before, period A is removed when doing the model fitting for reasons stated earlier.

D.2 Catalyst C10

For catalyst C10, the estimated parameters and their respective absolute uncertainties are shown for the alternative model in Table D.2. Estimated parameters with no given uncertainties have been estimated manually through a trial-and-error process.

Parameter	Estimated value [a.u.]	Uncertainty [a.u.]
k_1	1.815	± 0.1090
a	3.50	-
b	1.504	-
f	1.364	± 0.1936
g	1.523	-
β_o	0.10	-
$k'_{\mathrm{CH_4}}$	0.1151	± 0.01011
x	0.800	± 0.241
$K_{\mathrm{CH_4}}$	1.00	-
k_4	1.00	-
k_{wgs}	0.002155	-
k_d	0.01692	± 0.001348
k_α	0.02994	± 0.004919
y	0.3377	± 0.07133
c_{α_4}	0.70	-

Table D.2: Estimated parameters and their respective absolute uncertainties for C10 with the alternative model. Parameters in which no given uncertainties are given have been estimated manually through a trial-and-error process.

Figure D.2 shows the trend plots of the CO-conversion, C_{5+}-selectivity, and CH_4-selectivity for catalyst C10 with the alternative model. As is the case for the results presented in Section 5, for catalyst C1, the period A is removed when doing the model fitting. As such, only the periods B-E are shown in the figure.

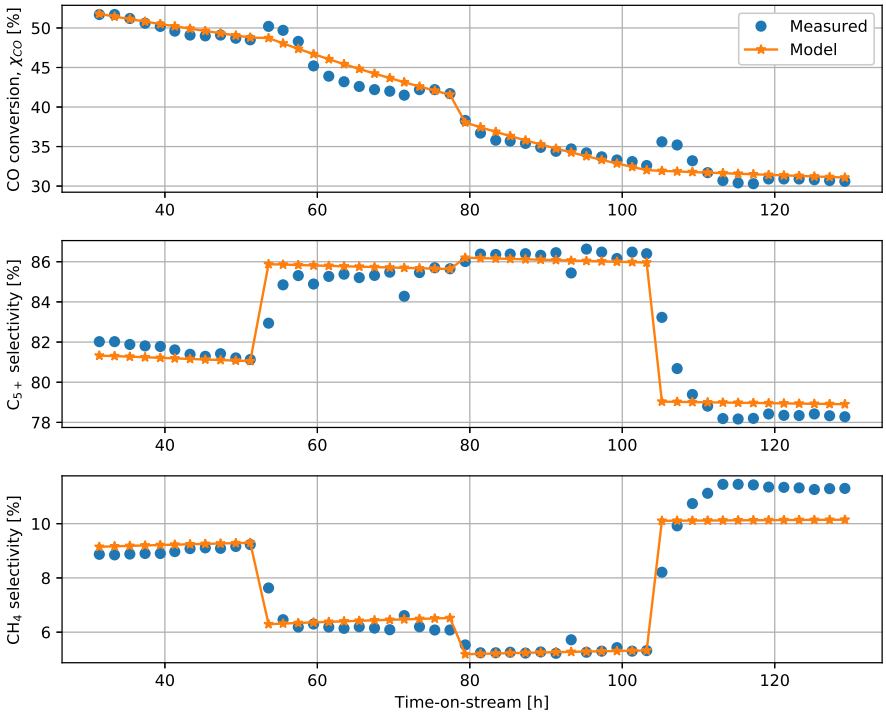

Figure D.2: Trend plots of the CO-conversion, C_{5+}-selectivity, and CH_4-selectivity for catalyst C10 with the alternative model. The periods B-E are shown in the plot. As before, period A is removed when doing the model fitting for reasons stated earlier.

D.3 Catalyst C11

For catalyst C11, the estimated parameters and their respective absolute uncertainties are shown for the alternative model in Table D.3. Estimated parameters with no given uncertainties have been estimated manually through a trial-and-error process.

Parameter	Estimated value [a.u.]	Uncertainty [a.u.]
k_1	1.448	$\pm$ 0.1745
a	3.50	-
b	1.152	-
f	1.897	$\pm$ 0.5616
g	1.070	-
β_o	0.10	-
$k'_{\mathrm{CH_4}}$	0.1100	$\pm$ 0.01922
x	0.510	$\pm$ 0.379
$K_{\mathrm{CH_4}}$	1.10	-
k_4	1.0	-
k_{wgs}	0.00215	-
k_d	0.001096	$\pm$ 0.006679
k_α	0.02727	$\pm$ 0.0081495
y	0.350	$\pm$ 0.130
c_{α_4}	0.70	-

Table D.3: Estimated parameters and their respective absolute uncertainties for C11 with the alternative model. Parameters in which no given uncertainties are given have been estimated manually through a trial-and-error process.

Figure D.3 shows the trend plots of the CO-conversion, C_{5+}-selectivity, and CH_4-selectivity for catalyst C11 with the alternative model. As is the case for the results presented in Section 5, for catalyst C11, the period A is removed when doing the model fitting. Only the periods B-E are shown in the figure as a result.

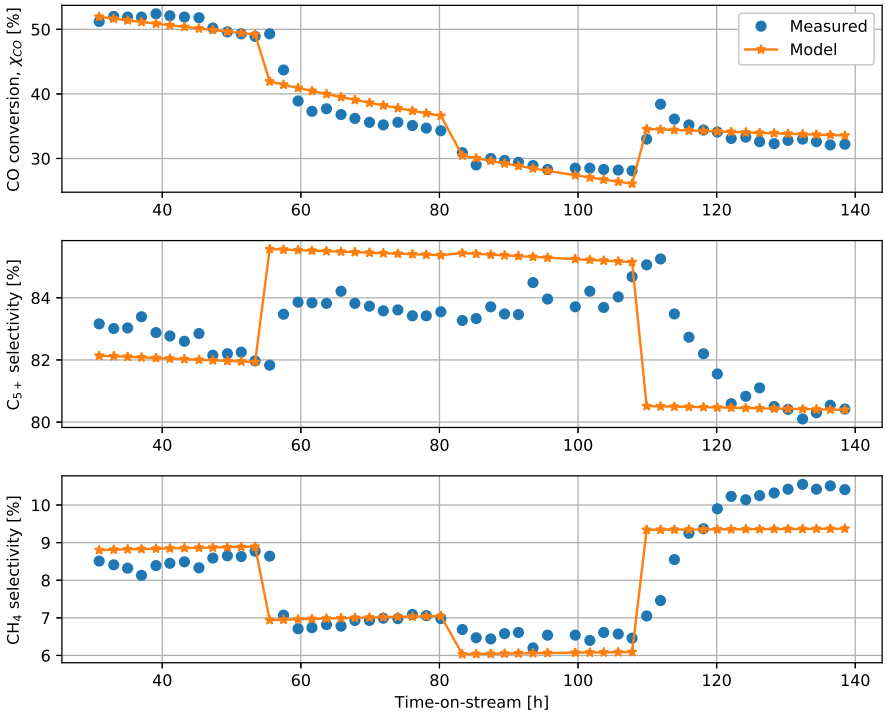

Figure D.3: Trend plots of the CO-conversion, C_{5+}-selectivity, and CH_4-selectivity for catalyst C11 with the alternative model. The periods B-E are shown in the plot. As before, period A is removed when doing the model fitting for reasons stated earlier.

D.4 Catalyst C14

For catalyst C14, the estimated parameters and their respective absolute uncertainties are shown for the alternative model in Table D.4. Estimated parameters with no given uncertainties have been estimated manually through a trial-and-error process.

Parameter	Estimated value [a.u.]	Uncertainty [a.u.]
k_1	0.5737	± 0.006066
a	3.50	-
b	1.669	-
f	1.170	± 0.3009
g	2.233	-
β_o	0.10	-
$k'_{\mathrm{CH_4}}$	0.09000	± 0.01197
x	0.900	± 0.365
$K_{\mathrm{CH_4}}$	0.90	-
k_4	0.450	-
k_{wgs}	0.000045	-
k_d	0.008140	± 0.003233
k_α	0.01462	± 0.007450
y	0.4500	± 0.2047
c_{α_4}	0.70	-

Table D.4: Estimated parameters and their respective absolute uncertainties for C14 with the alternative model. Parameters in which no given uncertainties are given have been estimated manually through a trial-and-error process.

Figure D.4 shows the trend plots of the CO-conversion, C_{5+}-selectivity, and CH_4-selectivity for catalyst C14 with the alternative model. As is the case for the results presented in Section 5, for catalyst C14, the period A is removed when doing the model fitting. Only the periods B-E are shown in the trend plots.

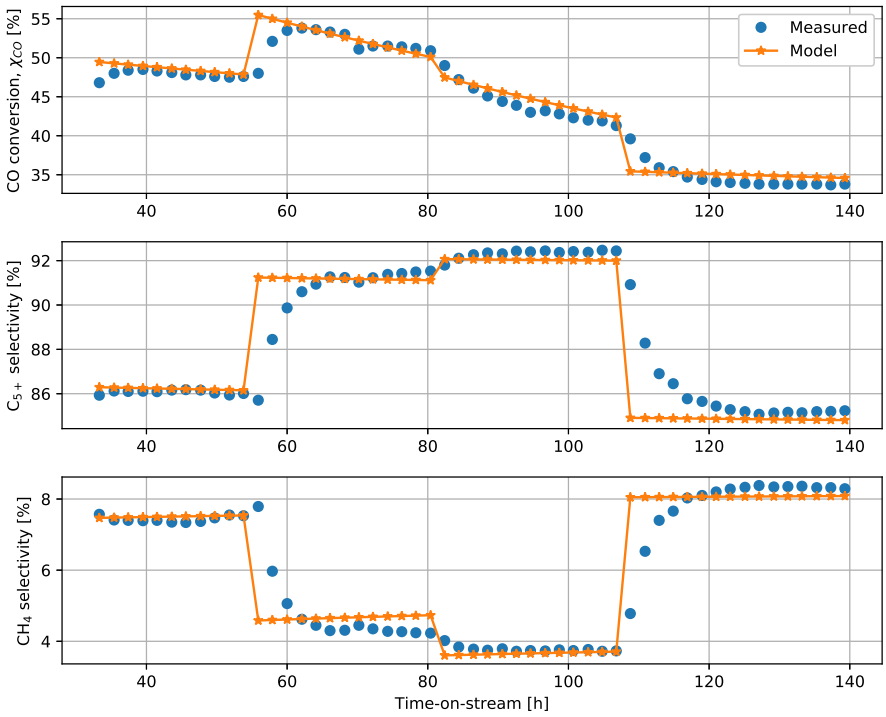

Figure D.4: Trend plots of the CO-conversion, C_{5+}-selectivity, and CH_4-selectivity for catalyst C14 with the alternative model. The periods B-E are shown in the plot. As before, period A is removed when doing the model fitting for reasons stated earlier.

D.5 Commercial type catalyst, $H_2/CO = 2.1$

For the commercial type catalyst with $H_2/CO = 2.1$, the estimated parameters and their respective absolute uncertainties are shown for the alternative model in Table D.5. Estimated parameters with no given uncertainties have been estimated manually through a trial-and-error process. It is to be noted that the temperature is set at 483 K across all the periods.

Parameter	Estimated value [a.u.]	Uncertainty [a.u.]
k_1	1.464	± 0.2184
a	3.50	-
b	1.504	-
f	1.364	± 1.490
g	1.523	-
β_o	0.10	-
k'_{CH_4}	0.1182	± 0.01647
x	0.800	± 0.850
K_{CH_4}	1.40	-
k_4	1.00	-
k_{wgs}	0.0010	-
k_d	0.01756	± 0.01224
k_α	0.04354	± 0.01665
y	0.2077	± 0.1450
c_{α_4}	0.70	-

Table D.5: Estimated parameters and their respective absolute uncertainties for the commercial type catalyst with $H_2/CO = 2.1$ and the alternative model. Parameters in which no given uncertainties are given have been estimated manually through a trial-and-error process.

Figure D.5 shows the trend plots of the CO-conversion, C_{5+}-selectivity, and CH_4-selectivity for the commercial type catalyst with $H_2/CO = 2.1$, and with the alternative model. It should be noted that in this case, the temperature is kept at 483 K across all periods.

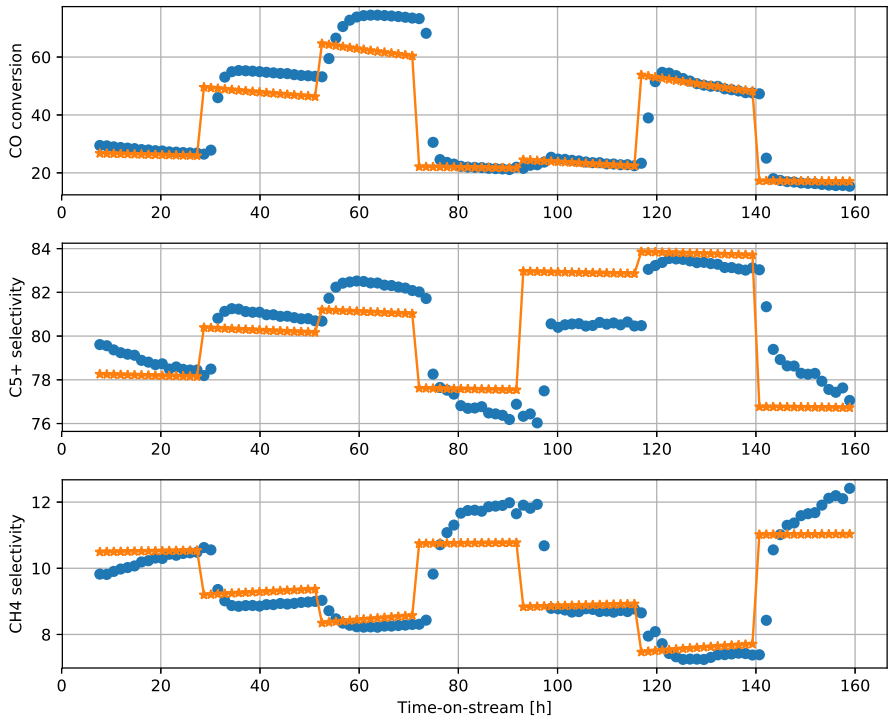

Figure D.5: Trend plots of the CO-conversion, C_{5+}-selectivity, and CH_4-selectivity for the commercial type catalyst with $H_2/CO = 2.1$, and with the alternative model. The temperature is kept at 483 K across all periods in the trend plots.

D.6 Commercial type catalyst, $H_2/CO = 1.72$

For the commercial type catalyst with $H_2/CO = 1.72$, the estimated parameters and their respective absolute uncertainties are shown for the alternative model in Table D.6. Any estimated parameters with no given uncertainties have been estimated manually through a trial-and-error process. Only the final period shown in the trend plots has water added to the reactor inlet.

Parameter	Estimated value [a.u.]	Uncertainty [a.u.]
k_1	1.353	± 0.09552
a	3.50	-
b	1.504	-
f	1.464	± 0.6720
g	1.523	-
β_o	0.10	-
k'_{CH_4}	0.1131	± 0.01555
x	0.800	± 0.645
K_{CH_4}	1.60	-
k_4	0.900	-
k_{wgs}	0.0010	-
k_d	0.01756	± 0.006454
k_α	0.04825	± 0.01496
y	0.1577	± 0.1467
c_{α_4}	0.70	-

Table D.6: Estimated parameters and their respective absolute uncertainties for the commercial type catalyst with $H_2/CO = 1.72$ and the alternative model. Parameters in which no given uncertainties are given have been estimated manually through a trial-and-error process.

Figure D.6 shows the trend plots of the CO-conversion, C_{5+}-selectivity, and CH_4-selectivity for the commercial type catalyst with $H_2/CO = 1.72$, and with the alternative model as described earlier. Only the final periods shown in the figure below has water added to the reactor inlet.

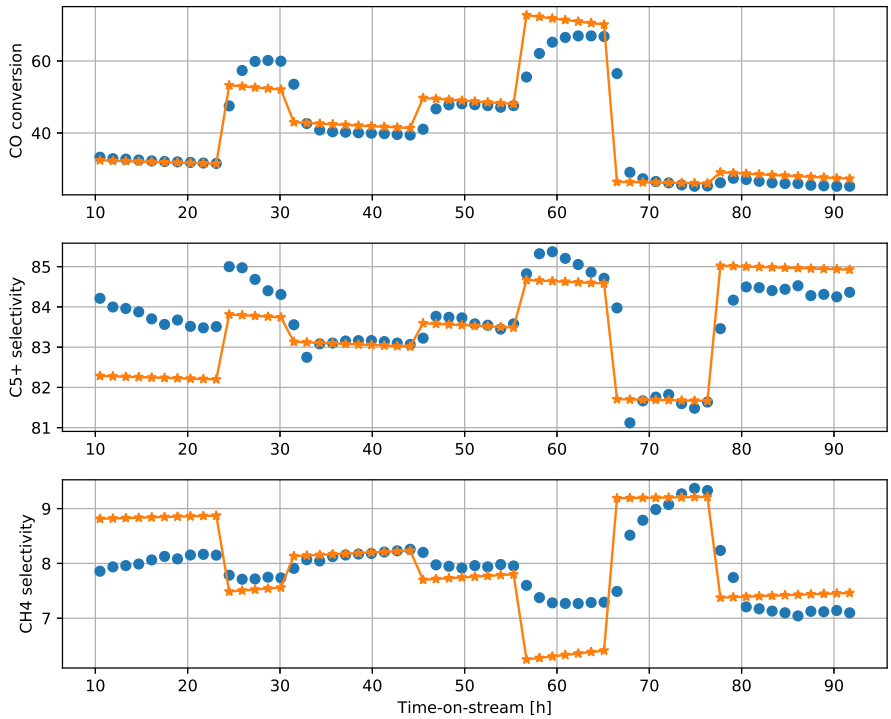

Figure D.6: Trend plots of the CO-conversion, C_{5+}-selectivity, and CH_4-selectivity for the commercial type catalyst with $H_2/CO = 1.72$, and with the alternative model.

E Reactor inlet calculations

To solve the reactor model, the `odeint`-solver needs a set of inlet conditions. The required inlet conditions include the weight fractions of all components in the system (most of which will be zero). The required inlet conditions that will typically be non-zero are the weight fractions of CO, H_2, N_2, and H_2O (the weight fraction of water at the reactor inlet will be non-zero when water is fed to the system). Further, the reactor model also requires the total mass flow at the inlet when it is defined on dimensionless form, which is the case as outlined in Section 2.4.

The experimental data report a flow (either the gas hourly space velocity (GHSV) or the volumetric flow), inlet H_2/CO-ratio, TOS, temperature, pressure, and catalyst mass. As a result, particularly the flow and H_2/CO-ratio must be used to calculate the total mass flow at the reactor inlet, as well as the weight fractions of the reactants and inert components.

The feed of CO, H_2, and N_2 come from premixed bottles with 3 % N_2 as the internal standard. The syngas bottles come at premixed H_2/CO-ratios of either 2.1 or 1.0. The volume of the bottle is 50 L.

In these cases, the volumetric fractions (which are assumed to be equal to the molar fractions, this assumption is valid under the assumption of ideal gas) can be calculated according to Equation (E.1) - Equation (E.3).

$$x_{\mathrm{N_2}} = 0.03 \tag{E.1}$$

$$x_{\mathrm{CO}} = \frac{1 - x_{\mathrm{N_2}}}{1 + r} \tag{E.2}$$

$$x_{\mathrm{H_2}} = \frac{r\,(1 - x_{\mathrm{N_2}})}{1 + r} \tag{E.3}$$

r is equal to the H_2/CO-ratio, and the following will hold true:

$$r = \frac{\mathrm{H_2}}{\mathrm{CO}} = \frac{F_{\mathrm{H_2}}}{F_{\mathrm{CO}}} = \frac{x_{\mathrm{H_2}}}{x_{\mathrm{CO}}} \tag{E.4}$$

If a premixed ratio is used, and additional hydrogen is added to obtain a higher H_2/CO-ratio, the following volumes can be used to calculate the volume fraction at the desired H_2/CO-ratio. Let r be as above.

$$V_{\mathrm{N_2}} = x_{\mathrm{N_2}} V_{tot} = 1.5 \tag{E.5}$$

$$V_{\mathrm{CO}} = 24.25 \tag{E.6}$$

$$V_{\mathrm{H_2}} = r \cdot 24.25 \tag{E.7}$$

In Equation (E.5) - Equation (E.7) above, a premixed H_2/CO-ratio of 1.0 is used as an example, however this method is also applicable for a premixed ratio of 2.1, though the volume 24.25 L should be replaced with 15.65 L. All volumes in the equations above are given in L.

As the volumetric flow at standard conditions (T_{std} = 273.15 K, P_{std} = 1 bar) are reported (or calculated from the GHSV, which is also reported at standard conditions), the volumetric flow at operating conditions can be calculated by Equation (E.8).

$$Q = Q_{std} \cdot \left(\frac{T_{operating}}{T_{std}} \right) \cdot \left(\frac{P_{std}}{P_{operating}} \right) \tag{E.8}$$

Once the volumetric flow at operating conditions is known, the molar flow of each component can be calculated using the ideal gas law as shown in Equation (E.9) below.

$$F_i = \frac{x_i P Q}{RT} \tag{E.9}$$

x_i is the molar fraction for component i and R is the universal gas constant. From the molar flows, the mass flows and corresponding weight fractions can easily be calculated using the molar masses of each component.

F Python code

```
#!/usr/bin/env python2
# -*- coding: utf-8 -*-
"""
Created on Tue Sep 25 13:07:53 2018

@author: andersrunningen
"""

"IMPORTING PACKAGES"
import time
import matplotlib.pyplot as plt
import numpy as np
from scipy import stats
from scipy.integrate import odeint
import scipy.odr
import xlrd
import warnings #Used to suppress warnings. Only use this when the code is working
"END IMPORT OF PACKAGES"

"DISABLING WARNINGS. ONLY INCLUDE ONCE CODE IS WORKING"
warnings.filterwarnings('ignore')

"INDEXING"
CO, CO2, H2, H2O, CH4, C2H6, C3H8, C4H10, C5P, C2H4, C3H6, C4H8, C5O, \
 N2, yC5P, zC5P, yC5O, zC5O = range(18)


"DEFINING ALL NECESSARY FUNCTIONS"
def xlread():
    "Function that extracts all data from the relevant Excel-file"
    "Input:     -"
    "Output:    matrix containing data"

    xl_workbook = xlrd.open_workbook('excel_docs/fts_borg_c10_data.xlsx')
    sheet_names = xl_workbook.sheet_names()
    xl_sheet = xl_workbook.sheet_by_name(sheet_names[0])
    data = [[xl_sheet.cell_value(r,col) for r in range(1,xl_sheet.nrows)]
\
              for col in range(xl_sheet.ncols)]
    return data

def coeff(i, alpha):
    """
    Function to calculate stoichiometric coefficients used in reactions
```

```
    Input:     carbon number i [-]
               alpha-value for n-parafin or 1-olefin reaction [-]

    Output:    stoichiometric coefficient, scalar [-]
    """
    return ((1.-alpha)**2)*alpha**(i-1)

def alpha(kac, Eac, Tk, pH2, pCO, pH2O, B0):
    """
    Function that calculates the alpha-value for the n-parafin reaction
    Input:      Correction factor, kac [-]
                Activation energy correction factor, Eac [-]
                Temperature, Tk [K]
                Partial pressure of H2, pH2 [MPa]
                Partial pressure of CO, pCO [MPa]
                Partial pressure of H2O, pH2O [MPa]

    Output:     alpha1, alpha-value for n-parafin reaction [-]
    """
    k1c, E1c, kac, Eac, ratio, alH2, alH2O, kdeac, Edeac, KB1, ECH4, OPar, \
    kcl, a4c, deac_power, coeff_water, KB2, KB3, aeq, kwgs, b, alr3 = B0
    ka = kac*0.0181*np.exp(-3291*Eac*(1./Tk - 1./483.))
    alpha1 = 1.0/(1.0 + ka*((1./pCO)**(alH2))*((1./pH2O)**(alH2O)))
    return alpha1

def partialpressure(y, M, Ptot):
    """
    Function that calculates the partial pressures of gaseous components
    Input:      Mass fraction of all components, y [-]
                Molecular weight of all components, M [kg/kmol]
                Total pressure, Ptot [bar]

    Output:     Partial pressures of CO, H2, H2O, and C2H4 [MPa]
    """
    #'Extracting' components assumed to be in gas phase
    omega_gas = y[[CO, CO2, H2, H2O, CH4, C2H6, C3H8, \
                   C4H10, C2H4, C3H6, C4H8, N2]]
    molecular_weight_gas = M[[CO, CO2, H2, H2O, CH4, C2H6, C3H8, \
                              C4H10, C2H4, C3H6, C4H8, N2]]

    y_gas = (omega_gas/molecular_weight_gas) / \
            (sum(omega_gas/molecular_weight_gas))
    pCO, pH2, pH2O, pC2H4, pCO2 = y_gas[[CO, H2, H2O, C2H4, CO2]]*Ptot*0.1
    return pCO, pH2, pH2O, pC2H4, pCO2

def catalyst_deactivation(a, TOS_deact, pH2O, pH2, Tk, B0):
    """
    Function to calculate the deactivation of the catalyst assuming
    higher order deactivation of the catalyst.
```

```
    Input:      Deactivation (unknown), a
                Time-on-stream, TOS [h]
                Partial pressure of steam, pH2O [bar]
                Temperature, Tk [K]
                List of initial parameters, B0 [-]

    Output:     Differental equation for deactivtion of catalyst, dadt
    """
    k1c, E1c, kac, Eac, ratio, alH2, alH2O, kdeac, Edeac, KB1, ECH4, OPar, \
    kcl, a4c, deac_power, coeff_water, KB2, KB3, aeq, kwgs, b, alr3 = B0
    k_deact = kdeac #*np.exp(-(104e03/8.314)*Edeac*(1./Tk - 1./483.))
    dadt = -k_deact*0.005*(a**deac_power)*(pH2O)**(1.0)
    return dadt

def rate(y, xhi, M, Tk, Ptot, Wtot, cat_weight, TOS, B0, TOS_array, a_array):
    """
    Function that calculates the rate expressions used in the PFR-model
    Input:      Mass fraction, y [-]
                Molecular weight, M [kg/kmol]
                Dimensionless reactor volume 'domain', xhi [-]
                Temperature, Tk [K]
                Total pressure, Ptot [bar]
                Total mass flow rate, Wtot [kg/s]
                Catalyst weight, cat_weight [g]
                Time on stream, TOS [h]
                List of initial guesses, B0 [-]

    Output:     Reaction rates [-] (due to model being dimensionless)
    """
    k1c, E1c, kac, Eac, ratio, alH2, alH2O, kdeac, Edeac, KB1, ECH4, OPar, \
    kcl, a4c, deac_power, coeff_water, KB2, KB3, aeq, kwgs, b, alr3 = B0
    R = np.zeros(14)
    v = np.zeros(21)

    pCO, pH2, pH2O, pC2H4, pCO2 = partialpressure(y, M, Ptot)


    TOS_deact = np.linspace(TOS_array[-2], TOS_array[-1], 2)
    a0 = a_array[-1]
    deac = odeint(catalyst_deactivation,  a0, TOS_deact, \
                  args=(pH2O, pH2, Tk, B0), atol=1.e-08, rtol=1.e-08)
    deact = np.float64(deac[-1])

    k1 = k1c*0.2696 #*np.exp(-(104e3/8.314)*E1c*(1./Tk - 1./483.))

    r1 = deact*k1*(pCO*(pH2**0.5)*(1+KB3*pH2O))/ \
        (1. + 3.50*KB1*pCO + 1.0*KB2*pH2**(0.5) + coeff_water*pH2O)**2
```

```
alpha1 = alpha(kac, Eac, Tk, pH2, pCO, pH2O, B0)
alpha2 = alpha1*np.exp(-0.27)
alpha4 = a4c*alpha1

r2 = OPar*r1

r3 = ratio*r1*(pH2)**alr3 - coeff(1,alpha1)*r1 - coeff(1,alpha2)*r2
#r3 = ratio*r1*(pH2/(1+b*pH2O))**alr3 \
        #- coeff(1,alpha1)*r1 - coeff(1,alpha2)*r2
r4 = kcl*pC2H4*(pH2**2)*pCO

Keq = np.exp(4577.8/Tk - 4.33)
r5 = kwgs*0.005*(pCO*pH2O-(1./Keq)*pCO2*pH2)

#Calculating the reaction rates of each component [kmol/kg*h]
R[CO] = -1.0*r1 -1.0*r2 -1.0*r3 -1.0*r4 -1.0*r5
R[H2] = -(3.-alpha1)*r1 -(2.+(1.-alpha2)**2)*r2 -3.0*r3 -2.0*r4 +1.0*r5
R[H2O] = 1.0*r1 +1.0*r2 +1.0*r3 +1.0*r4 -1.0*r5
R[CH4] = coeff(1,alpha1)*r1 +coeff(1,alpha2)*r2 +1.0*r3
R[C2H6] = coeff(2,alpha1)*r1
R[C3H8] = coeff(3,alpha1)*r1
R[C4H10] = coeff(4,alpha1)*r1
R[C5P] = ((1.-alpha1)*alpha1**4)*r1
R[C2H4] = coeff(2,alpha2)*r2 -(1.0-alpha4)*r4
R[C3H6] = coeff(3,alpha2)*r2 + coeff(1,alpha4)*r4
R[C4H8] = coeff(4,alpha2)*r2 + coeff(2,alpha4)*r4
R[C5O] = ((1.-alpha2)*alpha2**4)*r2 + ((1.-alpha4)*alpha4**2)*r4
R[CO2] = 1.0*r5
M[C5P] = 14.0*(5.+(alpha1/(1.-alpha1)))+2.0
M[C5O] = 14*(5.+(alpha2/(1.-alpha2)))
v[:14] = R*M*cat_weight/(Wtot*1000.*3600.)

#Calculating the weight average of the lumps etc.
#Number average of lumps
nnp = 5.+alpha1/(1.-alpha1)
nnq = 5.+alpha2/(1.-alpha2)

#Molar mass using the number average
Mnp = 14.*nnp+2.
Mnq = 14.*nnq
Mnpinv = 1./Mnp
Mnqinv = 1./Mnq

#Weight average of the lumps
Mwp = 14.*((4.+(1.+alpha1)/(1.-alpha1))*5 + \
           (1.+alpha1)*alpha1/(1.-alpha1)**2)/nnp + 2.
Mwq = 14.*((4.+(1.+alpha2)/(1.-alpha2))*5 + \
           (1.+alpha2)*alpha2/(1.-alpha2)**2)/nnq
```

```
    v[yC5P] =v[C5P]*Mnpinv
    v[zC5P] =v[C5P]*Mwp
    v[yC5O] =v[C5O]*Mnqinv
    v[zC5O] =v[C5O]*Mwq
    v[N2] = 0.0     #Inert gas in the system
    v[18] = deact
    v[19] = r1
    v[20] = r5

    return v

def objfun(B, X, M, B0, jj, normal):
    """
    Function that minimizes the objective function,
    namely error between model and experimental data
    """
    B0[jj] = B

    k1c, E1c, kac, Eac, ratio, alH2, alH2O, kdeac, Edeac, KB1, ECH4, OPar, \
    kcl, a4c, deac_power, coeff_water, KB2, KB3, aeq, kwgs, b, alr3 = B0

    n = X.shape[1]
    Ye = np.zeros((10,n))
    alfa1 = np.zeros((n))

    #Extracting data from input matrix (X)
    TOS = X[0,:]
    Tk = X[1,:]
    Ptot = X[2,:]
    omega_H2 = X[3,:]
    omega_CO = X[4,:]
    omega_N2 = X[5,:]
    omega_H2O = X[6,:]
    cat_weight = X[7,:]
    Wtot = X[8,:]

    #Defining dimensionless volume (of reactor) range
    xhi = np.linspace(0,1.0,2)

    #Initializing results
    XCO = np.zeros(n)
    SCH4 = np.zeros(n)
    SC2O = np.zeros(n)
    SC2P = np.zeros(n)
    SC3O = np.zeros(n)
    SC3P = np.zeros(n)
    SC4O = np.zeros(n)
    SC4P = np.zeros(n)
    SC5P = np.zeros(n)
```

```
SCO2 = np.zeros(n)
y0 = np.zeros(21)
Yout = np.zeros((n,21))
Yin = np.zeros_like(Yout)

TOS_array = np.array([])
a_array = np.array([])
TOS_array = np.append(TOS_array, 0.0)
a_array = np.append(a_array, 1.0)
r1_array = np.array([])
r5_array = np.array([])
pressure_matrix = np.zeros((3,n))

#Define objective function loop
for i in range(n):
    TOS_array = np.append(TOS_array, TOS[i])
    y0[CO], y0[H2], y0[N2], y0[H2O] =  \
                    omega_CO[i], omega_H2[i], omega_N2[i], omega_H2O[i]
    y = odeint(rate, y0, xhi, \
               args=(M, Tk[i], Ptot[i], Wtot[i],  cat_weight[i], \
                     TOS[i], B0, TOS_array, a_array), \
                     atol=1.e-7, rtol = 1.e-7)
    pCO, pH2, pH2O, pC2H4, pCO2 = partialpressure(y[-1,:-2],M,Ptot[i])
    pressure_matrix[0,i], pressure_matrix[1,i], \
    pressure_matrix[2,i] = pCO, pH2, pH2O
    Yout[i,:] = y[-1,:]
    Yin[i,:] = y0
    XCO[i] = (y[0,CO] - y[-1,CO])/(y[0,CO])*100.
    SCH4[i] = (y[-1,CH4] - y[0,CH4])/M[CH4] / \
                ((y[0,CO]-y[-1,CO])/M[CO])*100.
    SC2O[i] = (y[-1,C2H4]-y[0,C2H4])*2./M[C2H4] / \
                ((y[0,CO] - y[-1,CO])/M[CO])*100.
    SC2P[i] = (y[-1,C2H6]-y[0,C2H6])*2./M[C2H6] / \
                ((y[0,CO] - y[-1,CO])/M[CO])*100.
    SC3O[i] = (y[-1,C3H6]-y[0,C3H6])*3./M[C3H6] / \
                ((y[0,CO] - y[-1,CO])/M[CO])*100.
    SC3P[i] = (y[-1,C3H8]-y[0,C3H8])*3./M[C3H8] / \
                ((y[0,CO] - y[-1,CO])/M[CO])*100.
    SC4O[i] = (y[-1,C4H8]-y[0,C4H8])*4./M[C4H8] / \
                ((y[0,CO] - y[-1,CO])/M[CO])*100.
    SC4P[i] = (y[-1,C4H10]-y[0,C4H10])*4./M[C4H10] / \
                ((y[0,CO] - y[-1,CO])/M[CO])*100.
    SCO2[i] = (y[-1,CO2] - y[0,CO2])/M[CO2] / \
                ((y[0,CO]-y[-1,CO])/M[CO])*100.
    SC5P[i] = 100. - \
        (SCO2[i]+SCH4[i]+SC2O[i]+SC2P[i]+SC3O[i]+SC3P[i]+SC4O[i]+SC4P[i])
    alfa1[i] = alpha(kac, Eac, Tk[i], pH2, pCO, pH2O, B0)
    a_array = np.append(a_array, y[-1,-3])
    r1_array = np.append(r1_array, y[-1,-2])
```

```
        r5_array = np.append(r5_array, y[-1,-1])
    Ye[0,:] = (XCO)
    Ye[1,:] = (SCH4)
    Ye[2,:] = (SC2O)
    Ye[3,:] = (SC2P)
    Ye[4,:] = (SC3O)
    Ye[5,:] = (SC3P)
    Ye[6,:] = (SC4O)
    Ye[7,:] = (SC4P)
    Ye[8,:] = (SC5P)
    Ye[9,:] = (SCO2)

    if normal:
        return Ye
    else:
        return Ye, alfa1, Yin, Yout, TOS_array,  \
                a_array, r1_array, pressure_matrix, r5_array

"MAIN FILE"
if __name__ == '__main__':
    tic = time.time()

    data = xlread()
    data = np.array(data)

    M = np.zeros(14)
    M[[CO, H2, H2O, CH4, C2H6, C3H8, C4H10, \
    C2H4, C3H6, C4H8, N2, CO2]] = 28, 2, 18, 16, 30, 44, 58, 28, 42, 56, 28, 44

    "BORG DATA"
    cat_weight, TOS, H2CO_0 = data[0,:], data[1,:], data[3,:]
    Tk, Ptot, Ftot = data[8,:], data[9,:], data[19,:]
    Wtot, omega_CO, omega_H2, omega_N2, omega_H2O = data[24,:],  \
                    data[25,:], data[26,:], data[27,:], data[28,:]
    XCO = data[29,:]

    "Selectivities including CO2"
    SCH4, SC2O, SC2P = data[31,:], data[32,:], data[33,:]
    SC3O, SC3P, SC4O, SC4P = data[34,:], data[35,:], data[36,:], data[37,:]
    SC5P, SCO2 = data[39,:], data[30,:]

    ##Defining which points (of the total) to use
    ii = [i for i in range(cat_weight.size) if i > 13]

    n = len(ii)
    X = np.zeros((9,n))
    Y = np.zeros((10,n))
    Ye = np.zeros((10,n))
```

```
X[0,:] = TOS[ii]
X[1,:] = Tk[ii]
X[2,:] = Ptot[ii]
X[3,:] = omega_H2[ii]
X[4,:] = omega_CO[ii]
X[5,:] = omega_N2[ii]
X[6,:] = omega_H2O[ii]
X[7,:] = cat_weight[ii]
X[8,:] = Wtot[ii]

Y[0,:] = XCO[ii]
Y[1,:] = SCH4[ii]
Y[2,:] = SC2O[ii]
Y[3,:] = SC2P[ii]
Y[4,:] = SC3O[ii]
Y[5,:] = SC3P[ii]
Y[6,:] = SC4O[ii]
Y[7,:] = SC4P[ii]
Y[8,:] = SC5P[ii]
Y[9,:] = SCO2[ii]

param_names =  ['k1c', 'E1c', 'kac', 'Eac', 'ratio', 'alH2', 'alH2O', \
                'kdeac', 'Edeac', 'KB1', 'ECH4', 'OPar', 'kcl', 'a4c', \
                'deac_power','coeff_water','KB2','KB3', 'aeq', 'kwgs', \
                'b', 'alr3']
k1c, kac, ratio, kdeac, KB1, kcl, coeff_water, \
deac_power, KB2, KB3, kwgs, b, alr3 = [1.0]*13
E1c, Eac, alH2, alH2O, Edeac, ECH4, OPar, a4c, aeq = [0.0]*9

#Initial guesses
k1c = 6.7312744981272141
E1c = 1.0               #Set to 0 due to no temperature variation in data
kac = 1.6240748932455871
Eac = 1.0               #Set to 0 due to no temperature variation in data
ratio = 0.086128717240470429
alH2 = 1.0
alH2O = 0.35766744688143287
kdeac = 3.3840977439739421
Edeac = 0.0             #Set to 0 due to no temperature variation in data
KB1 = 1.0
ECH4 = 0.0              #Set to 0 due to no temperature variation in data
OPar = 0.10000000000000001
kcl = 1.0
a4c = 0.70
deac_power = 2.0
coeff_water = 1.364142283636681
KB2 = 1.5042745200000001
KB3 = 1.5230340273847351
aeq = 0
```

```
kwgs = 0.43092017477928968
b = 0.90000000000000002
alr3 = 1.7

#Arranging initial guesses and choose which to estimate
B_init = np.array([k1c, E1c, kac, Eac, ratio, alH2,  \
                   alH2O, kdeac, Edeac, KB1, ECH4, OPar, \
                   kcl, a4c, deac_power, coeff_water, KB2, \
                   KB3, aeq, kwgs, b, alr3])
B0 = np.array([k1c, E1c, kac, Eac, ratio, alH2, alH2O, \
               kdeac, Edeac, KB1, ECH4, OPar, kcl, a4c, \
               deac_power, coeff_water, KB2, KB3, aeq, kwgs, b, alr3])
BIN = [          1,   0,   1,   0,     1,     0,     1,   1, \
       0,    0,    0,   0,    1,   0,      0,      \
       1,      0,   0,   0,    0,  0,  1]

#Choosing all parameters that are to be estimated
jj = [i for i, kk in enumerate(BIN) if kk != 0]
B = np.array([B0[j] for j in jj])

#Setting uncertainties for input and outputs
X_err = X.copy()
X_err[0,:] = 0.01               #TOS
X_err[1,:] = 1.0                #Tk
X_err[2,:] = 0.01               #Ptot
X_err[3,:] = 0.00001            #omega_H2
X_err[4,:] = 0.0001             #omega_CO
X_err[5,:] = 0.0001             #omega_N2
X_err[6,:] = 0.0001             #omega_H2O
X_err[7,:] = 0.0001             #cat_weight (g)
X_err[8,:] = 1.e-08             #Wtot (kg/s)

Y_err = Y.copy()
Y_err[0,:] = 0.3                #X(CO)
Y_err[1,:] = 0.3                #S(CH4)
Y_err[2,:] = 0.3                #S(C2O)
Y_err[3,:] = 1.5                #S(C2P)
Y_err[4,:] = 3.0                #S(C3O)
Y_err[5,:] = 2.0                #S(C3P)
Y_err[6,:] = 3.3                #S(C4O)
Y_err[7,:] = 3.0                #S(C4P)
Y_err[8,:] = 0.3                #S(C5P)
Y_err[9,:] = 0.3

#Create model and solve
mymodel = scipy.odr.Model(objfun,extra_args=(M, B0, jj, True))
mydata = scipy.odr.RealData(X, Y, sx = X_err, sy = Y_err)
myodr = scipy.odr.ODR(mydata, mymodel, beta0 = B, maxit=10000)
m = myodr.run()
```

```
B = m.beta
B0[jj] = B
Ye, alfa1, Yin, Yout, TOS_array, a_array, r1_array, \
    pressure_matrix, r5_array = objfun(B, m.xplus, M, B0, jj, False)
p = len(jj)
tfence = stats.t.isf(0.025, n-p)

#Printing relevant output
for i in range(len(param_names)):
    print(i+1, param_names[i], '=', B_init[i])
print('---------------------------------------')
for i in range(p):
    print(i+1, jj[i], param_names[jj[i]], m.beta[i],  \
          '+-', tfence*m.sd_beta[i])
R_err = Ye - Y
R_err = R_err/Y_err
nr, mr = R_err.shape
R_err = np.reshape(R_err, (nr*mr))
MSE = np.dot(R_err,R_err)/(n-p)
print('MSE = ', MSE, 'se = ', np.sqrt(MSE))
print(m.stopreason)

k1c, E1c, kac, Eac, ratio, alH2, alH2O, kdeac, Edeac, KB1, ECH4, OPar, \
kcl, a4c, deac_power, coeff_water, KB2, KB3, aeq, kwgs, b, alr3 = B0

toc = time.time()
print('---------------------------------------')
print('Time elapsed = ', toc-tic, 'sec')
```

Anders Runningen

Fischer-Tropsch reaction kinetics: Mathematical modeling and model fitting

NTNU
Norwegian University of
Science and Technology